A SYNTHESIS APPROACH FOR DESIGN OF SEPTUM HORNS

By:

Arvind Subramani

A Thesis

Submitted to the Faculty of Graduate Studies

in Partial Fulfillment of the requirements

for the Degree of

Master of Science in Electrical Engineering

Department of Electrical and Computer Engineering

University of Manitoba

Winnipeg, Manitoba, Canada

THE UNIVERSITY OF MANITOBA

FACULTY OF GRADUATE STUDIES

*****

COPYRIGHT PERMISSION

A SYNTHESIS APPROACH FOR DESIGN OF SEPTUM HORNS

BY

Arvind Subramani

A Thesis/Practicum submitted to the Faculty of Graduate Studies of The University of Manitoba in partial fulfillment of the requirement of the degree

Of

MASTER OF SCIENCE

Acknowledgements

I would like to sincerely thank my advisor Prof L. Shafai for his undeniable support, time and patience. His guidance towards the completion of my Master's research is deeply appreciated. I am grateful for the opportunity to have worked under him and for the experience I have gained in his presence. I would like to deeply thank Prof ShivaKumar and Prof Barakat for their valuable time and support towards the completion of my Master's thesis.

I thank the almighty GOD for guiding me through every phase in my life and showing me the right path during testing times.

I would like to thank all the technical and support staff in the Department of Electrical and Computer Engineering for their help during my time at the department.

I thank my parents and family for making me the person I am today and letting me follow my dreams. I deeply appreciate my sister lavenya, my in-laws for their love and support.

I would like to thank the most important person in my life, my wife Shony. She being a constant source of inspiration and backbone of my life. I would like to thank my dear friend Suresh for his persistence and friendship. If not for him I would not be in Winnipeg.

Last but not the least, I would like to thank all my friends in Winnipeg and well-wishers back home for surrounding me with good spirits and encouragements.

Abstract

One of the simplest and probably the most widely used microwave antennas is the Horn Antenna. The function of Horn is to produce a uniform phase front with a large aperture than that of the waveguide and hence resulting in greater directivity. The horn is widely used as a feed element for large radio astronomy and communication dishes.

Corrugated horns are normally used in the above applications because of their properties of reduced edge diffractions and improved pattern symmetry. Their problem arises when high operating frequency is used (i.e.) the corrugations become too small that complicates building these types of structures. The septum horn investigated in this thesis has similar properties but has simpler geometry and advantages like low cost and high operating frequency.

The E-plane pattern of a conventional Rectangular horn has high sidelobes as a result of uniform amplitude distribution in the aperture. In septum horns, conducting plates are placed perpendicular to the E-plane of the horn aperture to alter the uniform distribution. This results in low sidelobes at the E-plane pattern. A Two-step Staircase distribution is introduced from the altered distribution. A synthesizing technique is developed using this distribution. This technique synthesizes complex distributions and provides optimum parameters to achieve desired sidelobes in the radiation pattern.

Based on this principle, a parametric study about the effect of the plates on the radiation pattern of pyramidal horn is investigated. The parameters of the Two-step Staircase distributions are correlated to the near field pattern of the septum pyramidal horn. An E-plane horn with movable conducting plates is fabricated and tested in the Antenna Laboratory at the University of Manitoba and its results are verified.

Table of Contents

List of Figures

List of Tables

Chapter 1

Introduction

1.1 Preface

The existence of the Horn antenna dates back to late 1800 but its revival began in the late 1930's during the period of World War 2. The horn is widely used as a feed element for large radio astronomy, satellite tracking and communication dishes. The horn has of course much greater utility than merely that of the feed for reflectors and lenses. It is a common element in phased array antennas, it is a reliable and accurate gain standard and, finally, it is a useful radiator in its own right. Its simplicity in construction and ease of excitation make the horn invaluable to engineers and scientists in a number of fields.

1.2 Objective of the Thesis:

This thesis deals with the study of a unique type of horn antenna. The need for this type of antenna has arised due to the increase in frequency of operations in communication systems. It is well known that the horn is used as the primary feed for a reflector antenna and therefore most commonly used in satellite communications. The operational frequency (>10 GHz) of this type of communication system has increased due to bandwidth requirements.

The corrugated horns are the most efficient horn feed used for these purposes. It has excellent radiation characteristics as Low Cross polarization and Low sidelobes. The only disadvantage for this type of antenna is, as the frequency of operation increases, the size of the horn reduces and respectively the size of the corrugations decreases. So, it becomes very expensive to manufacture such antennas with minor corrugations. In many current practical applications, the frequency of operation has increased to X-Band or Ku-Band. Therefore, to design corrugated horns for such frequency of operation becomes a very costly affair.

Therefore, it is essential for us to consider a practical alternative and the design studied in this thesis is a proposed alternative.

The design of this type of horn was first proposed by G.M. Peace and E.E.Swartz in 1964 and they termed it as "Amplitude Compensated Horn Antenna" [1]. The term amplitude compensated was given to this horn because they were trying to alter the uniform amplitude distribution of the horn to a tapered function. They used conductive plate's perpendicular across to the E-field inside a horn antenna. These plates distribute the electromagnetic field over the horn aperture to achieve desired tapered amplitude. Later, these types of horns were also termed as Septum horns, because the plates divide the horn aperture into many septums. With a 2-septum horn Peace and Swartz were able to achieve a side lobe level more than 30dB down. The study done by Peace and Swartz in their paper was on an E-plane sectoral horn. Further practical applications of this type of antenna were carried out by R.T.Nash [2] around the same time.

In this thesis, a detailed parametric study about the effect of the plates on the radiation pattern of a rectangular pyramidal horn is conducted. A synthesizing technique is developed to enable this parametric study. This technique helps us understand the significant parameters of the conductive plates, which alter the uniform distribution of the horn and provides its advantages. It also determines the optimum parametric values for achieving improved radiation characteristics.

Using the rectangular aperture theory [3-4], it is possible to simplify the amplitude distribution at the aperture of the horn and to compute its respective secondary patterns. By writing a program in MATLAB with the simplified secondary patterns a study is carried out to improve the Far-field radiation patterns of the horn. A Two-step Staircase distribution is introduced using the aperture theory and its effect on the secondary patterns is studied in detail. This in turn helped us in deducing the respective parametric values. The parameters which have the most significant effects on the field pattern are characterized. This study influenced the initial assumptions for the parametric simulation study of the pyramidal horn antenna with conductive plates.

A simple synthetic technique using the Staircase distribution is introduced to synthesize distributions like Cosine and Taylor. Secondary patterns are generated using the synthesized parameters. Also, the synthesized parameters are used in the designed horn to achieve the desirable field patterns.

The designed horns with plates are modeled and simulated using EM software Ansoft's HFSS. Using the simulations in HFSS it is possible to determine the Far-field and Near-field patterns of the design. The synthesis of amplitude distribution and the computed parametric simulation results will provide a deeper insight into the working principle for this type of antenna.

1.3 Organization of the Thesis:

The thesis is divided into four basic chapters. Chapter 1 gives a background literature of the horn antenna. The far-field radiation characteristics are derived for a pyramidal horn antenna. Also, in this chapter, different types of horn antennas and their important radiation parameters are discussed.

Chapter 2 presents the introduction of the new type of Staircase distribution. The background theory of the amplitude on the rectangular aperture is provided and simple equations are derived from them for the deduction of the secondary patterns. Using the software program written in MATLAB a detailed study about the effects of the parameter on the field pattern is carried out. Chapter 3 presents the synthesis of amplitude distribution using the Staircase distributions. Different amplitude distributions are synthesized using a synthesis technique.

Chapter 4 covers the simulation study of the pyramidal septum horn. The antenna performance is studied by the effects of the plate parameters and characterized. These field patterns are compared with the synthesized results from Chapter 3. An E-plane horn with plates is fabricated and measured in the anechoic chamber of the antenna laboratory at the University of Manitoba. The measured results are compared to the simulated ones. Finally, a conclusion of the thesis is given in Chapter 5.

1.4 Radiation characteristics:

Before we go on to derive the radiation fields for the horn antenna, let us first formulate the necessary components of a rectangular aperture as shown in Figure 1.1. This rectangular aperture is similar to the horn aperture at the radiating front. The aperture is assumed to lie on the x`-y` plane.

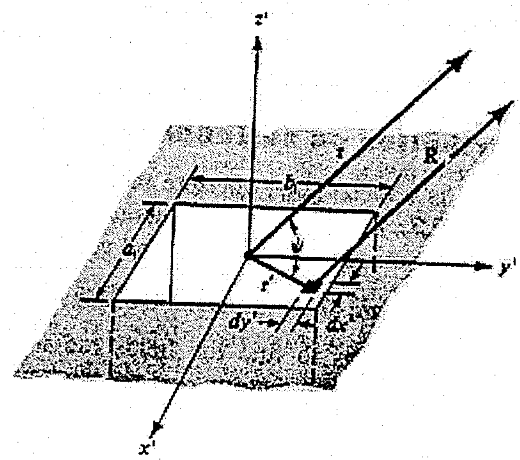

Figure 1.1: Rectangular aperture for antenna system analysis

The components of the equivalent electric and magnetic current densities for this aperture (x`-y` plane) are $J_{x'}, J_{y'}, M_{x'}, M_{y'}$ [17].

To derive the fields radiated by this antenna, the tangential components of the E or H fields over the aperture must be known, which provides the equivalent current J_s and M_s over the aperture. Using these Electric (J_s) and the Magnetic field (M_s) currents across the aperture, the E and H fields can be calculated from [4].

$$A = \frac{\mu}{4\pi} \iint_S J_s \frac{e^{-jkR}}{R} ds' \qquad F = \frac{\varepsilon}{4\pi} \iint_S M_s \frac{e^{-jkR}}{R} ds' \tag{1.1}$$

Where

$$J_s = \hat{n} \times H \qquad M_s = \hat{n} \times E$$

and $\hat{n}$ is the outward normal to the aperture. For far-field observations, R can be approximated as

$$R \approx r - r'\cos\psi \qquad \text{For phase variations}$$

$$R \approx r \qquad \text{For amplitude variations}$$

Where $r'\cos\psi = x'\sin\theta\cos\phi + y'\sin\theta\sin\phi$. This approximation is applicable to the phase variations in the field patterns of the antenna. The differential area is $ds' = dx'dy'$.

This gives equation (1.1) at far field as

$$A \cong \frac{\mu e^{-jkr}}{4\pi r} N \qquad\qquad F \cong \frac{\varepsilon e^{-jkr}}{4\pi r} L$$

In the far-field only the Θ and Φ components of the E and H-fields are dominant and are given in equation 1.2.

$$\begin{aligned}
&E_r \approx 0 && H_r \approx 0 \\
&E_\theta \approx -\frac{jke^{-jkr}}{4\pi r}\left(L_\phi + \eta N_\theta\right) && H_\theta \approx +\frac{jke^{-jkr}}{4\pi r}\left(N_\phi - \frac{L_\theta}{\eta}\right) \\
&E_\phi \approx +\frac{jke^{-jkr}}{4\pi r}\left(L_\theta - \eta N_\phi\right) && H_\phi \approx -\frac{jke^{-jkr}}{4\pi r}\left(N_\phi + \frac{L_\theta}{\eta}\right)
\end{aligned} \qquad (1.2)$$

Where $N_\theta, N_\phi, L_\theta \, and L_\phi$ according to the x'y' planes are

$$N_\theta = \iint_S \left[J_{x'} \cos\theta \cos\phi + J_{y'} \cos\theta \sin\phi \right] e^{+jkr'\cos\psi} dx' dy'$$

$$N_\phi = \iint_S \left[-J_{x'} \sin\phi + J_{y'} \cos\phi \right] e^{+jkr'\cos\psi} dx' dy'$$

$$L_\theta = \iint_S \left[M_{x'} \cos\theta \cos\phi + M_{y'} \cos\theta \sin\phi \right] e^{+jkr'\cos\psi} dx' dy' \qquad (1.3)$$

$$L_\phi = \iint_S \left[-M_{x'} \sin\phi + M_{y'} \cos\phi \right] e^{+jkr'\cos\psi} dx' dy'$$

Equation 1.2 gives the general radiation equations for a rectangular aperture as shown in figure 1.1.

The radiation characteristics of the widely used pyramidal horn are derived from the above equations. This horn is flared up in both directions (E and H) and is a combination of E and H-plane sectoral horns. Figure 1.2 shows a pyramidal horn [4] with flared out rectangular aperture lengths a_1 and b_1.

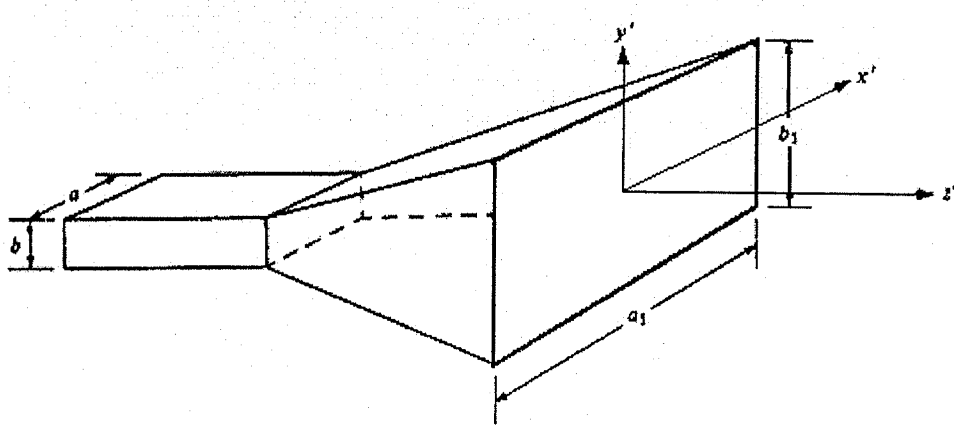

Figure 1.2: Geometry of pyramidal horn antenna

The tangential components of the E and H-fields over the aperture of the pyramidal horn are approximated by [4].

$$E'_y(x',y') = +E_o \cos\left(\frac{\pi}{a_1}x'\right) e^{-j\left[k(x'^2/\rho_2 + y'^2/\rho_1)/2\right]} \tag{1.4}$$

$$H'_x(x',y') = -\frac{E_o}{\eta}\cos\left(\frac{\pi}{a_1}x'\right) e^{-j\left[k(x'^2/\rho_2 + y'^2/\rho_1)/2\right]} \tag{1.5}$$

and their respective equivalent current densities are

$$J_y(x',y') = -\frac{E_o}{\eta}\cos\left(\frac{\pi}{a_1}x'\right) e^{-j\left[k(x'^2/\rho_2 + y'^2/\rho_1)/2\right]} \tag{1.6}$$

$$M_x(x',y') = +E_o \cos\left(\frac{\pi}{a_1}x'\right) e^{-j\left[k(x'^2/\rho_2 + y'^2/\rho_1)/2\right]} \tag{1.7}$$

The above expressions contains quadratic phase variations in both the x\` and y\` directions derived from [13]. The N_θ, N_ϕ, L_θ and L_ϕ from equation 1.3 are formulated after substituting equations 1.6 and 1.7 and J_x=0, M_y=0 into them. Equation 1.8 results after the substitutions [4].

$$\begin{aligned}
N_\theta &= -\frac{E_o}{\eta}\cos\theta\sin\phi I_1 I_2 \\
N_\phi &= -\frac{E_o}{\eta}\cos\phi I_1 I_2 \\
L_\theta &= E_o\cos\theta\cos\phi I_1 I_2 \\
L_\phi &= -E_o\sin\phi I_1 I_2
\end{aligned} \tag{1.8}$$

Where,

$$I_1 = \int_{-a_1/2}^{+a_1/2} \cos\left(\frac{\pi}{a}x'\right) e^{-jk\left[x'^2/(2\rho_1) - x'\sin\theta\cos\phi\right]} dx'$$

$$I_2 = \int_{-b_1/2}^{+b_1/2} e^{-jk\left[y'^2/(2\rho_1) - y'\sin\theta\sin\phi\right]} dy' \tag{1.9}$$

By rewriting $\cos\left(\frac{\pi}{a_1}x'\right)$ exponentially as $\cos\left(\frac{\pi}{a_1}x'\right) = \left[\frac{e^{j(\pi/a_1)x'} + e^{-j(\pi/a_1)x'}}{2}\right]$

A part of equation 1.9 can be expressed as

$$I_1 = I_1' + I_1'' \tag{1.10}$$

Where,

$$I_1' = \frac{1}{2}\sqrt{\frac{\pi\rho_2}{k}} e^{j(k_x'^2\rho_2/2k)} \{[C(t_2') - C(t_1')] - j[S(t_2') - S(t_1')]\}$$

$$t_1' = \sqrt{\frac{1}{\pi k\rho_2}}\left(-\frac{ka_1}{2} - k_x'\rho_2\right)$$

$$t_2' = \sqrt{\frac{1}{\pi k\rho_2}}\left(+\frac{ka_1}{2} - k_x'\rho_2\right) \tag{1.11}$$

$$k_x' = k\sin\theta\cos\phi + \frac{\pi}{a_1}$$

and

$$I_1''=\frac{1}{2}\sqrt{\frac{\pi\rho_2}{k}}e^{j(k_x''^2\rho_2/2k)}\{[C(t_2'')-C(t_1'')]-j[S(t_2'')-S(t_1'')]\}$$

$$t_1''=\sqrt{\frac{1}{\pi k\rho_2}}\left(-\frac{ka_1}{2}-k_x''\rho_2\right)$$
$$t_2''=\sqrt{\frac{1}{\pi k\rho_2}}\left(+\frac{ka_1}{2}-k_x''\rho_2\right) \qquad (1.12)$$
$$k_x''=k\sin\theta\cos\phi-\frac{\pi}{a_1}$$

Using equations1.10, 1.11 and 1.12, I_1 can be expressed as

$$I_1=\frac{1}{2}\sqrt{\frac{\pi\rho_2}{k}}\left(\begin{array}{l} e^{j(k_x'^2\rho_2/2k)}\{[C(t_2')-C(t_1')]-j[S(t_2')-S(t_1')]\} \\ +e^{j(k_x''^2\rho_2/2k)}\{[C(t_2'')-C(t_1'')]-j[S(t_2'')-S(t_1'')]\} \end{array}\right)$$

Using a similar process I_2 can be expressed as

$$I_2=\frac{1}{2}\sqrt{\frac{\pi\rho_1}{k}}e^{j(k_y^2\rho_1/2k)}\{[C(t_2)-C(t_1)]-j[S(t_2)-S(t_1)]\} \qquad (1.13)$$

Where,

$$k_y = k\sin\theta\sin\phi$$

$$t_1 = \sqrt{\frac{1}{\pi k\rho_1}}\left(-\frac{kb_1}{2} - k_y\rho_1\right)$$

$$t_2 = \sqrt{\frac{1}{\pi k\rho_1}}\left(\frac{kb_1}{2} - k_y\rho_1\right)$$

After substituting I_1 and I_2 in equation 1.8 and Combining equation 1.8 into equation 1.2, the far-zone E and H-field components are given as.

$$E_r = 0$$

$$E_\theta = -j\frac{ke^{jkr}}{4\pi r}\left[L_\phi + \eta N_\theta\right] = j\frac{kE_o e^{-jkr}}{4\pi r}\left[\sin\phi(1+\cos\theta)I_1 I_2\right]$$

$$E_\phi = +j\frac{ke^{-jkr}}{4\pi r}\left[L_\phi - \eta N_\theta\right] = j\frac{kE_o e^{-jkr}}{4\pi r}\left[\cos\phi(\cos\theta+1)I_1 I_2\right]$$

From the above equations we can refer that the principal E-plane pattern would be at $\phi=\pi/2$ and the H-plane pattern would be at $\phi=0$. Figure 1.3 gives the three dimensional field pattern of the pyramidal horn. The pattern of the pyramidal horn is very narrow in both principal E and H planes [4].

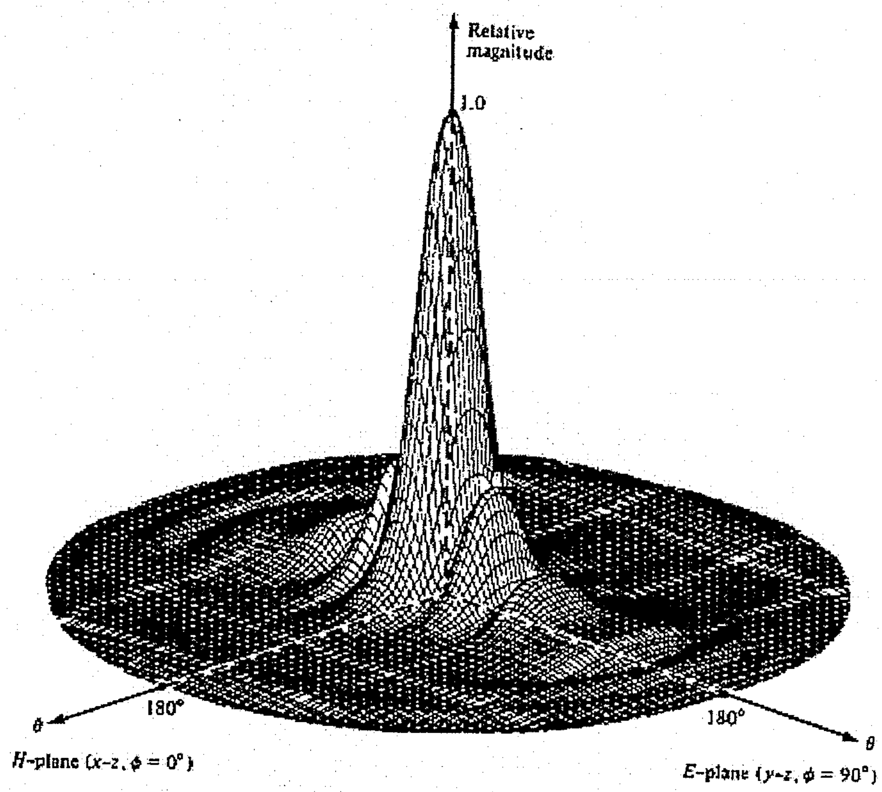

Figure 1.3: Three-dimensional Pattern of a Pyramidal Horn

1.5 Essential Horn Parameters:

a) Gain:

Horn is one of the most widely researched and analyzed microwave antennas. Many analysis and corrections to measure the accurate gain of the horn antenna has been devised [5-8]. It is the most significant parameter of the horn when it is used as a gain standard for other antennas. The gain of the antenna is mostly represented in dB. The typical gain for a horn ranges from 15 to 20 dB.

The paper by Braun [7] gives us an accurate gain for the horn antenna according to its H and E-plane aperture dimensions a, b and slant heights l_H and l_E(λ).

The value for G_E and G_H is found from a look up table in the paper and is formulated with respect to the values for A and B.

$$A = a\sqrt{\frac{50}{l_H}} \qquad B = b\sqrt{\frac{50}{l_E}}$$

$$g = \frac{G_E G_H}{10.1859\sqrt{50/l_H}\sqrt{50/l_E}}$$

Also, the general formula for measuring Gain for a standard horn can be determined by using the transmission loss versus separation between two identical standard horns. But this formula may introduce considerable error when the far-zone gain of pyramidal horn is measured at relatively short distances. Therefore to find the accurate gain, corrections are needed. Chu and Semplak [6] using the **near field power transmission formula** proposed one such correction from the ratio between the Fraunhofer and Fresnel gains. This correction with the power transmission formula predicts the gain accurately. The general gain formula is given by

$$G = \eta\frac{4\pi A}{\lambda^2}$$

Where,

A = Area of the aperture

η= Efficiency.

b) Directivity:

The directivity of a horn antenna can be expressed in terms of its effective aperture area. For a rectangular horn $A_p = a_E a_H$ and for a conical horn $A_p = \pi r^2$, where r is the aperture radius.

$$D = \frac{4\pi A_e}{\lambda^2} = \frac{4\pi \varepsilon_{ap} A_p}{\lambda^2}$$

Where, A_e = effective aperture

A_p = physical aperture

ε_{ap} = aperture efficiency = A_e/A_p

λ = Wavelength.

c) Side lobes:

Another important parameter of the horn radiator needed in most of its applications, is the sidelobe level. It is an important criterion in antenna range; anechoic chamber and standard gain applications because of its multipath considerations. In reflector illumination, it is an important factor that determines the main-beam efficiency and spurious wide-angle radiation effects.

The side lobes of a typical rectangular horn antenna are very high and are about –13 dB below the main lobe in the E-plane. This is mainly caused due to the wave diffractions at the edges of the horn. The need for low sidelobe level is very essential for many applications and in particular in its use as a feed for satellites and reflectors. Modifying the structure of the horn antennas at their edges can reduce these diffractions and result in a much better sidelobe level.

The corrugated horn, aperture-matched horn, septum horns and dielectric-loaded horns are widely used as feed horns because of their low level side lobes. This will be the most prominent parameter discussed in this thesis.

d) Effect of Flare angle and horn length on Field patterns :

The field patterns of the E and H-plane of a typical rectangular horn antenna as a function of flare angle and horn length is given in figure 1.4. In part (a) of figure1.4 the patterns in the E and H plane are compared as a function of the radial length of the horn R. Both E and H plane are set for a flare angle of 20°. The E-plane patterns have minor lobes and narrow beams between 4λ and 8λ The H-plane patterns have practically no side lobes.

In part (b) of figure 1.4, measured patterns for horns with R=8λ are compared as a function of flare angle. θ_E gives the E-plane flare angles in the upper row and θ_H gives the H-plane fare angles in the lower row respectively. Consider the case of θ_H and $\theta_E = 50°$, the E-plane pattern is split because of the phase shift at the aperture in the E-plane, whereas the H-plane pattern is not because the field goes to zero at the edges of the aperture in the H-plane, therefore the phase near the edges are relatively less important. When θ_H and θ_E is from 10 to 20°, the E-field patterns have narrow beams. In the particular case of θ_H and $\theta_E = 20°$, the E-field pattern is very similar to the H-field pattern. In such cases, the antenna will have low cross-polarization properties.

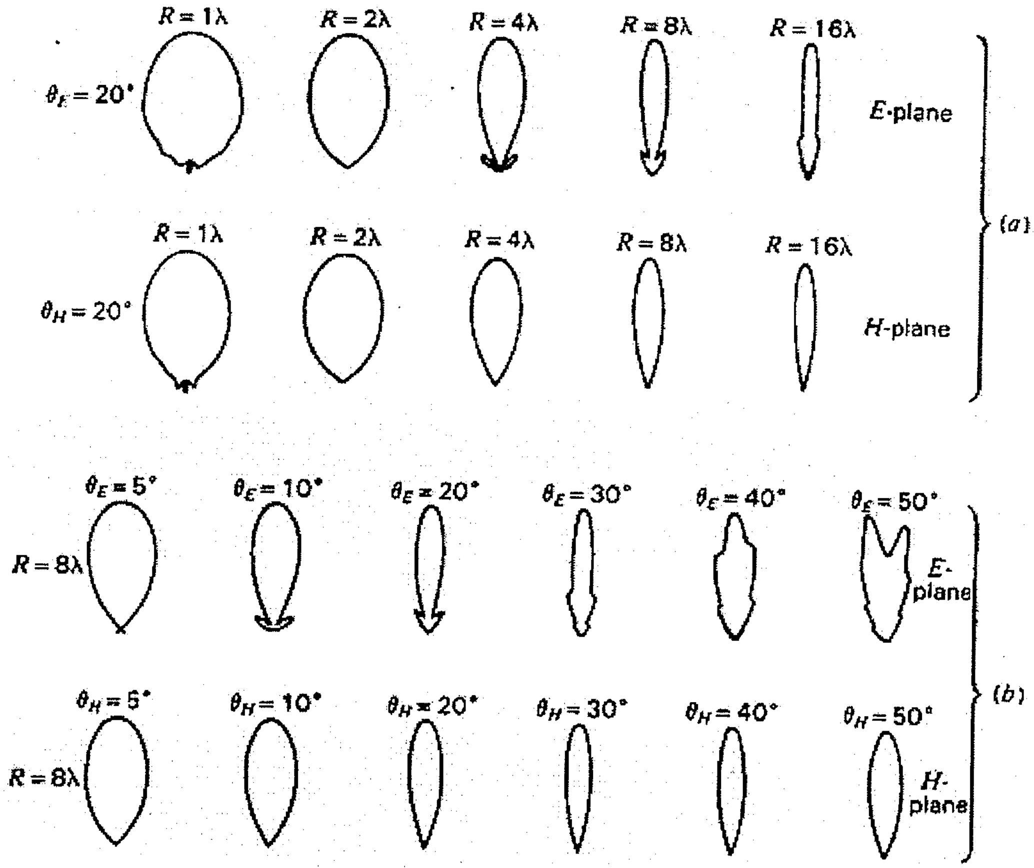

Figure 1.4: Measured E and H-plane patterns of rectangular horns as a function of horn flare angle and horn length [9]

e) Spill-over efficiency:

This is an important parameter to be considered when the horn is used as a feed to the Reflector antenna. Spillover energy can be defined as the energy, which is radiated from the feed but does not reach the reflector surface. Therefore, to achieve an efficient reflector antenna illumination, the spillover loss must be minimized.

They can be minimized using dielectric loaded horn antennas. The dielectric cone antennas are designed in such a way that they do not allow the energy to flow outside the reflector surface and therefore minimize the spillover loss. Other factors like using lenses and dielectric structures before the horn can also minimize the spillover loss.

f) Cross-polarization:

Polarization is the direction of the electric field transmitted by the antenna. Polarization of an antenna in a given direction is defined [4] as "the polarization of the wave transmitted (radiated) by the antenna. Note: When the direction is not stated, the polarization is taken to be the polarization in the direction of maximum gain." The cross-polarization factor is considered during the practical usage of antennas as a radiating and receiving element.

Cross-polarization is the state orthogonal to the reference co-polarization. If the signal is transmitted in the x-direction than the cross-polarization signal is in the y-direction. They can also be defined as two antennas in a transmit-receive configuration that are so polarized that no signal is received are said to be cross polarized. This occurs when both their polarization do not match at all. For a good design, the cross-polarization should be zero practically but it is not possible especially if you have circularly polarized radiation. Anything below –20 dB in cross-pol pattern compared to the co-pol pattern is considered to be an excellent feed antenna for the reflectors.

Corrugated horns, integrated horns, and septum horns have good low cross-polarizations properties.

1.6 Different types of horns:

a) Ridge horn:

Horn antennas have high aperture efficiencies but have limited operating bandwidths. To increase the operating bandwidth, ridges can be added to the waveguide and flared sections of the horns. A central ridge loads a waveguide and increases its useful bandwidth by lowering the cutoff frequency of the dominant mode. To increase the bandwidth, we can use the double-ridge structure, which is continuing from the waveguide into the pyramidal horn as in the figure below. A rectangular waveguide with a double ridge is a common design.

The only problem arising in this type of the horn is that the ridges must be terminated within the flared section therefore the horn aperture must be at least half a wavelength or more in width at the lowest frequency to permit propagation at the TE_{10} mode. Therefore, when wide bandwidths are considered large phase errors occur at high frequency unless the horn is extremely long. This phase error can be reduced to a minimum by using dielectric lens [10].

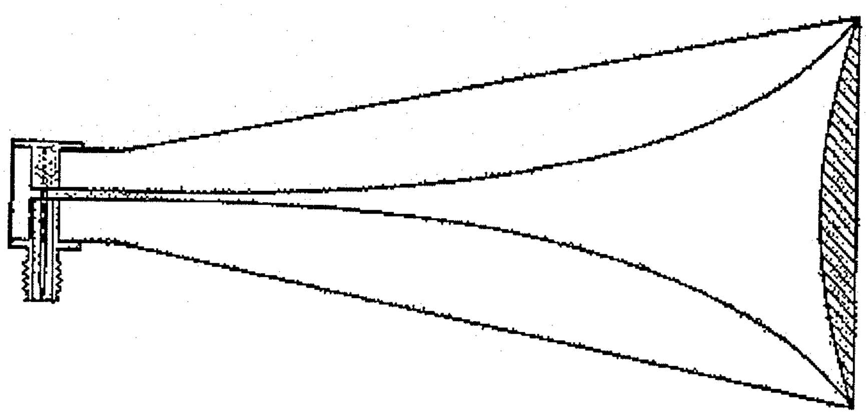

Figure 1.5: Geometry of Typical Ridge horn antenna

b) Diagonal Horn:

This is an unusual form of horn antenna but it has very desirable properties. All the cross-sections through this horn are square, including the aperture. For small flare angles, the mode of propagation within the horn is such that the electric vector is parallel to one of the diagonals. The resulting diagonal polarization of the aperture field has given rise to the name 'diagonal horn'.

The resulting radiation pattern in the far-field possesses almost perfect circular symmetry so that the 3, 10 and 20 dB beam widths are very closely equal, not only in the principal E and H planes, but also in the 45° and 135° planes. Sidelobes in the principal planes are observed to be at least 30dB down. In the ±45° planes, first side lobes have been observed to lie between 23 and 27dB down. Although cross-polarized lobes appear at about 16dB down in the ±45° planes, the horn efficiency remains high [12].

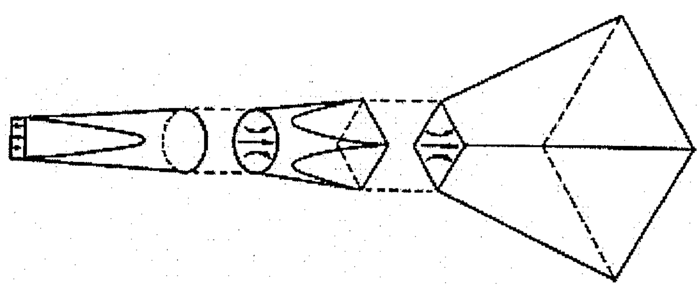

Figure 1.6: Diagonal horn antenna

c) Corrugated Horn:

Horn antennas are commonly used as a feed to large reflector. Therefore, there was a large emphasis placed on the horn antenna to reduce its spillover efficiency and cross-polarization losses. In a typical horn, the antenna pattern structure in the back lobe region is strongly influenced by diffractions from the edges; especially from those that are perpendicular to the E-field at the horn aperture. These diffractions lead to undesirable radiation not only in the back lobes but also in the main lobe and the side lobes.

The basic idea was to prevent illumination at the E-plane edges. Therefore, to decrease these diffractions two methods were proposed, Deep chokes and corrugated walls were introduced inside the horn surface. The corrugated horn was more successful than the choke slots horn because the choke slots introduced frequency sensitive propagation. A corrugated surface has 10 or more slots per wavelength. These slots are known as corrugations. Corrugated horns can provide reduced edge diffraction, improved pattern symmetry and reduced cross-polarization.

The analysis of an infinite corrugated surface may be simplified considerably by making the following assumptions.

- The slot walls (teeth) are vanishingly thin.
- Only the TEM mode in the slots is reflected from the base of the slots. The higher order modes are attenuated before reaching the base.

Using the second assumption, for such a surface the reactance is given as [11].

$$X = \frac{g}{g+t}\sqrt{\frac{\mu}{\varepsilon}}\tan k_o d$$

Where,

g = slot width

d = slot depth and

$g/g+t \cong 1$

This condition is satisfied if $t \leq g/10$ and the second assumption are valid for $g \leq \lambda/10$. Also, in order to prevent illumination of the E-plane edges, the surface reactance of the corrugated surface must be capacitive. Thus, we require $\lambda/4 < d < \lambda/2$.

The presence of the corrugations near the waveguide-horn junction can affect the impedance and the VSWR of the antenna. Therefore, the corrugations begin at a small distance away from the junction, which leads to low VSWR over a broad band. The corrugated horn antenna is very expensive to manufacture (especially if you consider physically small size horns). The E-plane pattern of a large control horn and a large corrugated horn having a flare angle of 34°, a slant height of 15.85 inches and a 9.7-inch square aperture is shown below.

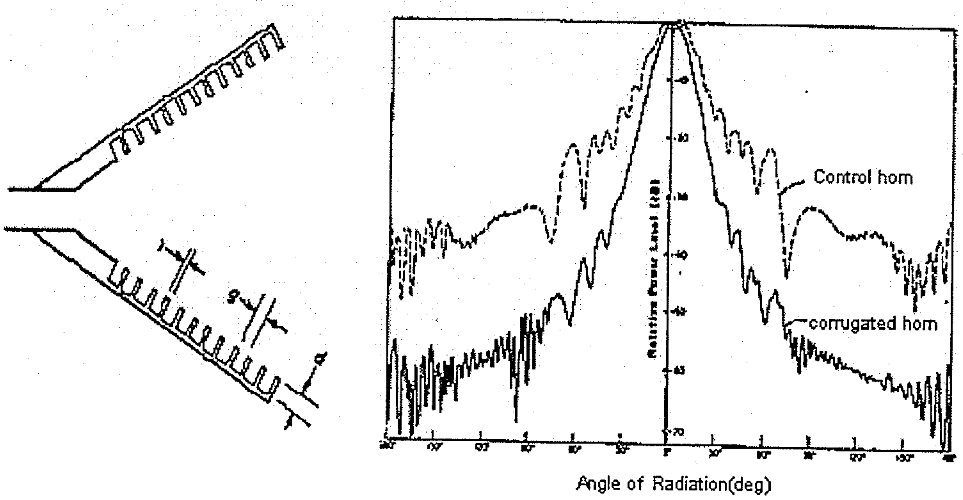

Figure 1.7: Corrugated horn antenna with comparison Field Patterns [11].

d) Aperture-matched Horn:

There is a significant improvement in the pattern; impedance and bandwidth characteristics of the horn by attaching a smooth curved surface section to the outside of its aperture edge. The curved surface section reduces the diffraction's that occur at the sharp edges of the aperture and provides smooth matching section between the horn modes and the free-space radiation. The shape of the rolled edge is not critical but its radius of curvature should be at least $\lambda/4$. This type of horn is very inexpensive and simple to construct.

The VSWR of the corresponding aperture-matched horn are much superior to those of the conventional horn because both the throat and aperture reflections are very minimal. The basic design of the aperture-matched horn can be extended to include corrugations to its inside surface. This type of design enjoys the advantages presented by both the aperture-matched and the corrugated horns with cross-polarized components of less that –45 dB over a significant part of the bandwidth. This type of horn is used as a reference and for frequency reuses applications in both satellite and terrestrial applications.

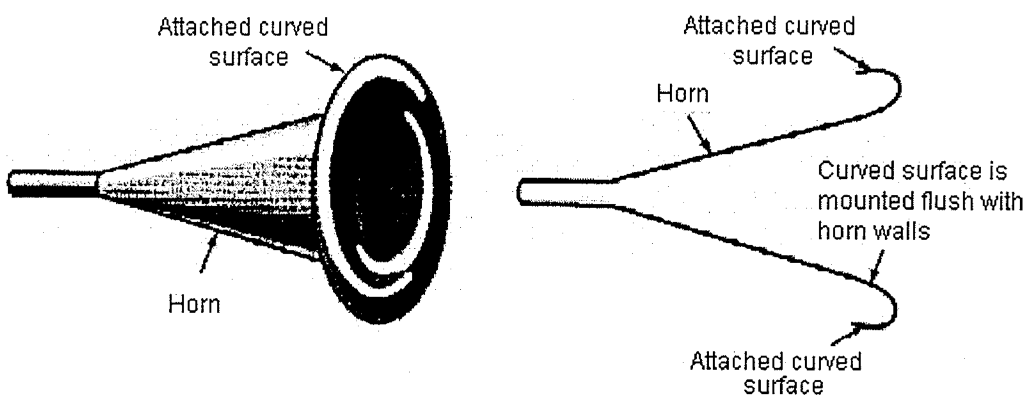

Figure 1.8: Geometry of an Aperture Matched horn [4].

e) Horn with lens:

To shield against stray radiation from the source side of a lens, a metallic enclosure may be used. This enclosure forms an electromagnetic horn of wide flare angle with a lens at the aperture. Without the lens an optimum horn of the same aperture would be much longer. The fact that the lens permits a much shorter structure for the same size aperture is the principal advantage of a lens-horn combination over a simple horn antenna. The type of lenses may be divided into two distinct types [9].

- Delay lenses, in which the electrical path length is increased by the lens medium. In delay lenses the wave is retarded by the lens medium. Dielectric lenses and H-plane metal –plate lenses are of the delay type.
- Fast lenses, in which the electrical path length is decreased by the lens medium. E-plane metal-plate lenses are the fast type.

f) Integrated horn antenna:

The integrated horn antenna is used for sub millimeter-wave applications with a Gaussian coupling efficiency of 75-80%. The main limitation of the standard integrated horn is caused because of its large flare angle of 70° caused due to the anisotropic etching of silicon. This limits the gain to 13dB and restricts its 10-dB beam width to 90°. But the new quasi-integrated horn antenna has improved pattern symmetry and higher gain. The quasi-integrated horn consists of a flared machined section attached to a standard integrated horn antenna to form a multimode horn.

The minimum dimension of the machined section is about 1.4λ, which permits the fabrication of the quasi-integrated horn up to 1.5 THz. The abrupt change in the flare angle at the junction on the integrated and the machined section of the horn, acts as a mode-converter. It excites mainly the TE_{10}, TE_{12}/TM_{12} and TE_{30} modes. These modes are subsequently properly phased on the radiating aperture by selecting the length and the flare angle of the machined section. This results in symmetrical patterns with low side lobe-level and low cross-polarization properties. Since the machined section transforms the 1.35 λ-square aperture of the standard integrated horn to a larger 3.56λ-square radiating aperture yielding a gain of 20dB. The calculated field patterns are given in the other figure where we can see that the pattern symmetry is excellent down to –20dB.

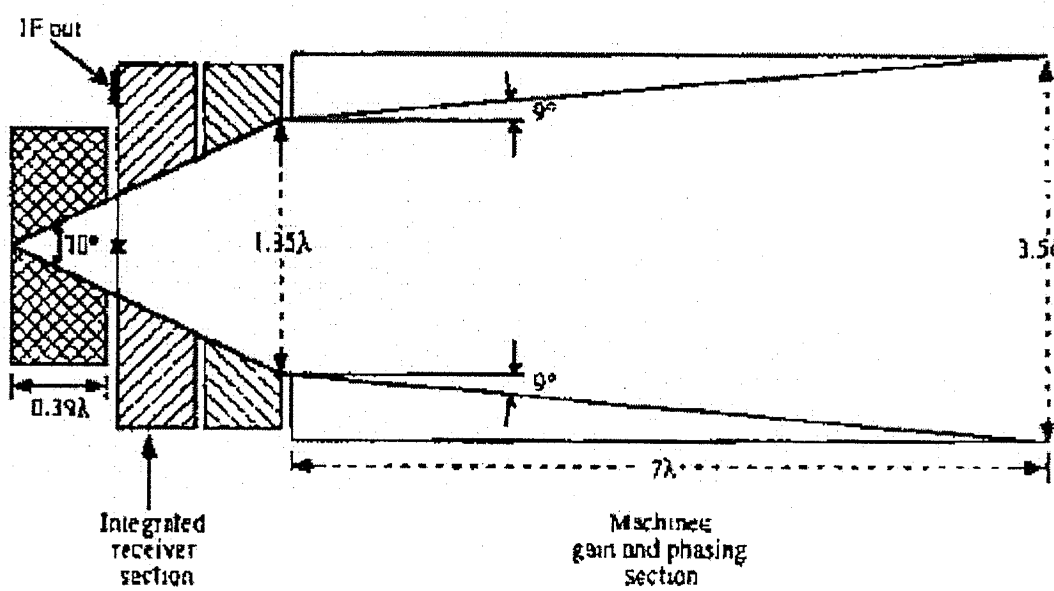

Figure 1.9: 20dB Quasi- Integrated horn antenna

g) Dielectric-Loaded horn:

A new approach has been developed which tends to eliminate the requirement for compromise between the uniform illumination and amount of energy lost in spillover between the horn feed and the reflector. Dielectric guided structures are placed between the primary feed and reflector. They are known as Dielguides. These guiding structures utilize the phenomenon of Total Internal Reflection, which is a property of the boundary between dielectric media, to reduce spillover and provide a more uniform reflector illumination. This technique is simple and inexpensive to implement. They are most commonly used in the Cassegrain reflector antenna. It also provides a broadband, highly efficient and low-noise antenna feed.

Another method that has been used to control the radiation pattern of electromagnetic horns is to insert totally within them various shapes of dielectric material like slabs, wedges, etc. to control in a predictable manner not only the phase distribution over the aperture, as is usually done by using classical parabolic lenses, but also to change the amplitude distribution over the aperture. This is useful to design low side lobe antenna patterns.

The figure below is a dual mode dielectric-loaded conical horn antenna. The thin dielectric band inside the horn excites a series of higher modes and therefore results in a symmetrical main beam with low side lobes [5].

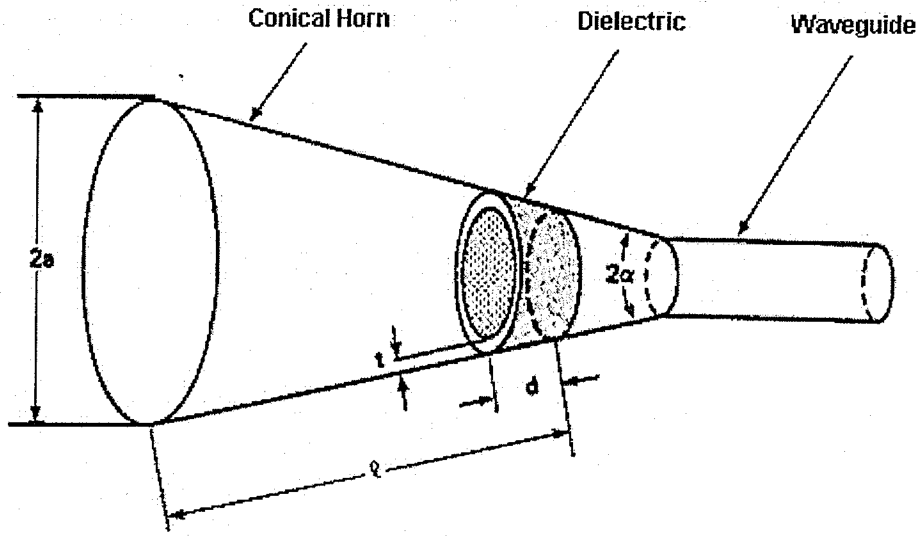

Figure 1.10: Dielectric Loaded horn

1.7 Motivation:

The major application of the horn is a feed for the reflector. In that case, the corrugated horn is the most successful one of the above cases. It has excellent radiation characteristics and low side lobe level.

Due to increase in operating frequency, different type of horns can be considered to replace the corrugated horns for these applications. The factors in choosing the horns are easy to design, low cost, high frequency operation. The septum horn is an excellent candidate. The septum horn is very similar to the normal E-Plane, H-plane and Pyramidal Horn except they have better radiation pattern with Low Side lobe level. To look at the reason behind this change, let us compare it to a rectangular pyramidal horn.

The electric field in the H-plane of a pyramidal horn tends to zero at the edges and results in a tapered distribution and reduced sidelines. But the electric field in the E-plane is close to uniform amplitude at the edges, resulting in high sidelobes (-13.5dB). Therefore, by altering this uniform amplitude distribution to a tapered function we can reduce these sidelobes. This change in distribution is possible by placing symmetric conductive plates perpendicular to the E-field inside the horn antenna. These plates distribute the electromagnetic field over the horn aperture to achieve the desired tapered amplitude on the aperture surface. These plates divide the horn into septums therefore the name septum horns.

It was established experimentally that the plates should be located in a manner which provides binomial distribution such that the center aperture between the plates includes half of the overall horn aperture area [1]. Also, the number of plates utilized should be kept to a minimum to preserve the bandwidth characteristics of the horn.

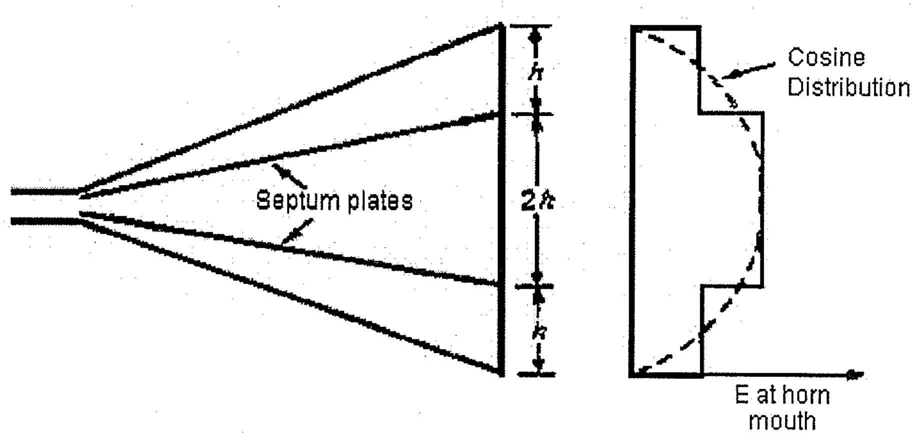

Figure 1.11: Principle of Septum horn antenna

1.8 Summary:

In this chapter an introduction to horn antenna was given and the need for septum horn antenna was established. The background theory of a rectangular pyramidal horn and its far field radiation characteristics were derived. Many important parameters of the antenna were discussed and also different types of horns were compared and studied.

Chapter 2

Parametric study of Two-step Staircase Distribution

2.1 Introduction:

The geometry under study is based on rectangular horns in the E-plane. There exists a uniform amplitude distribution and causes high side lobe in its respective far field pattern. This far field pattern can be improved by altering the uniform distribution in the Near-field of the aperture. This is done by introducing conductive plate's perpendicular to the E-field of the rectangular aperture.

Therefore, it is essential here to study the Near-field characteristics in detail for this kind of aperture. Step functions are used to obtain similar altered distribution due to the effect of the plates. A Two-step Staircase distribution is introduced. It is possible to deduce the far field pattern using the field study.. A MATLAB program is written using these simplified field equations, and a parametric study is carried out. This parametric study helps in understanding the septum horn design and its working principle.

2.2 Field Analysis for Rectangular Aperture:

The geometry of a typical rectangular horn antenna is shown in figure 1.2 from Chapter 1. The beam width and side-lobe characteristics are related to the Near-field distributions along the aperture. The rectangular aperture has width a_1 and height b_1 represented in terms of λ.

The general field over the aperture is given by [3].

$$F(x',y') = A(x',y')e^{-j\psi(x',y')} \tag{2.1}$$

Where, $A(x',y')$ represents the amplitude distribution and $\psi(x',y')$ is the phase distribution across the aperture.

Some important definitions to be noted for the study are the primary pattern (field along the aperture) and the secondary pattern (the far field pattern). The primary pattern would be the field distribution along the aperture or the near field i.e. $F(x',y')$ given in equation 2.1. The secondary pattern is the far field $g(\theta,\phi)$ of the antenna as shown in eq 2.2. The secondary pattern depends only on the relative distribution over the aperture. In this chapter, the study of secondary pattern would be more investigated as it would provide us a better insight into the important horn parameters (mainly the side lobes). The secondary pattern for the rectangular aperture is given as [3].

$$g(\theta,\phi) = \int_{-a_1/2}^{a_1/2} \int_{-b_1/2}^{b_1/2} F(x',y')e^{jk\sin\theta(x'\cos\phi + y'\sin\phi)}dx'.dy' \tag{2.2}$$

Assuming $F(x',y')=1$ in both plane for a uniformly illuminated aperture with uniform phase and amplitude, the secondary amplitude pattern from equation 2.2 can be simplified and express as.

$$g(\theta,\phi) = A\left[\frac{\sin\left(\frac{\pi a_1}{\lambda}\sin\theta\cos\phi\right)}{\frac{\pi a_1}{\lambda}\sin\theta\cos\phi}\right]\cdot\left[\frac{\sin\left(\frac{\pi b_1}{\lambda}\sin\theta\sin\phi\right)}{\frac{\pi b_1}{\lambda}\sin\theta\sin\phi}\right] \tag{2.3}$$

The patterns in the principal planes (XZ and XY) are of particular interest. Therefore, for the XZ- plane when $\phi=0$, equation 2.3 can be further simplified to

$$g(\theta,\phi) = g(\theta) = A\frac{\sin\left(\frac{\pi a}{\lambda}\sin\theta\right)}{\frac{\pi a}{\lambda}\sin\theta} \tag{2.4}$$

For the YZ-plane when $\phi=\pi/2$; the pattern in this plane is similar to eq (2.4) but a_1 is replaced by b_1. From the above expression, when we replace $u=\frac{\pi a_1}{\lambda}\sin\theta$, we get the patterns in a general form.

$$g(u) = \frac{\sin(u)}{u} \tag{2.5}$$

The secondary pattern characteristics for various types of aperture distributions have been extensively studied in [3]. The patterns for uniform, cosine distributions have been well established and charted in Appendix A. Using these well examined secondary pattern characteristics as comparisons, we will try to investigate the working principle of the thesis design. A MATLAB program can be written with this simplified secondary pattern in equation 2.5 and parametric study can be carried out.

2.3 Phase error effects:

In the above topic, an expression was derived for the secondary pattern when a uniform amplitude distribution was assumed at the aperture. The effects caused by phase variations on the secondary pattern were not considered. The phase variations on the fields over the aperture of the horn will have a significant effect on the final radiation pattern of the antenna.

Assuming the field being uniform in the Y-direction and if phase error exists in the X-direction only equation (2.2) can be rewritten as

$$g(\theta) = \int_{-a_1/2}^{a_1/2} F(x').e^{jkx'\sin\theta} dx' \qquad (2.7)$$

The phase error term $\psi(x)$ is introduced in equation 2.7 at the exponential $e^{jkx'\sin\theta}$.The phase error distribution can be separated into three basic forms.

- Linear error: $\psi(x) = \beta x$
- Quadratic error: $\psi(x) = \beta x^2$
- Cubic error: $\psi(x) = \beta x^3$

The linear phase error will cause a tilt in the main beam of the antenna. The quadratic phase error will lead to a reduction of directivity and an increase in sidelobe level on either side of the main lobe. The quadratic phase errors would naturally occur in a rectangular horn antenna due to phase variations at the aperture. This type of error can cause the disappearance of nulls and blending of the minor lobes in the pattern. The cubic errors cause asymmetrical patterns and increase in magnitude of one side of the minor lobes.

2.4 Two-step Staircase distribution:

It is known that the aperture of a general rectangular horn antenna has uniform amplitude distribution from the previous topics. Commonly, the uniform amplitude distribution can be represented as a step function [3]. It is also evident from the theory on the rectangular apertures; that the secondary pattern of step functions will be a form of sinc function with respect to the dimensions of the rectangular aperture equation 2.5.

This would be the typical field pattern for any rectangular horn antenna and can be represented as a step function with $F(x',y')=1$. Equation 2.5 is linear therefore superposition is possible by varying two step functions of different length when assuming uniform phase.

The significant contribution of the step functions in this study is

- The most important aspect of having step functions in this study is that the respective secondary pattern will be a form of sinc function. This simplifies the computation for the secondary pattern considerably (equation 2.5).
- Step functions can be added to form another function (like Two-step Staircase functions). It is simpler to find the respective secondary pattern for this new function.
- It is possible to synthesize any type of distribution in the primary pattern using these functions. By adding different combinations and sizes of the step functions, it is possible to achieve any respective distribution (Cosine, Taylor etc).

Therefore, using the sinc functions it is possible to do a parametric study of uniform distributions by computing the resultant secondary pattern. The main objective here is to study the effect of the near field using step functions and to depict its limitations. This study will provide us a clear insight about the working of the thesis design.

The parametric analysis of the amplitude distribution using step functions in done basically in two ways.

First, since conduction plates are introduced plates into the rectangular aperture in the thesis design, the horn aperture will be bifurcated or separated into many divisions. Let us consider the case of introducing two conduction plates into the horn aperture. These plates separate the horn into three apertures. According to the placing of the plates near the waveguide, the power flowing into the horn structure from the waveguide is controlled. When the position of the plate is nearer to the horn flare at the waveguide, more power will flow into the centre aperture than the other two apertures near it. As the plates are moved away from the horn flare, power flow into the center aperture is reduced. Therefore, by introducing these plates the uniform amplitude distribution of the horn aperture is altered.

This principle forms the first part of the synthesis. The altered amplitude distribution is shown in figure 2.1 using step functions. The distribution in figure 2.2 would be the added form of two step functions of different lengths. Since it looks similar to a staircase and is obtained by combining two step functions, let us name it as Two-step staircase distribution.

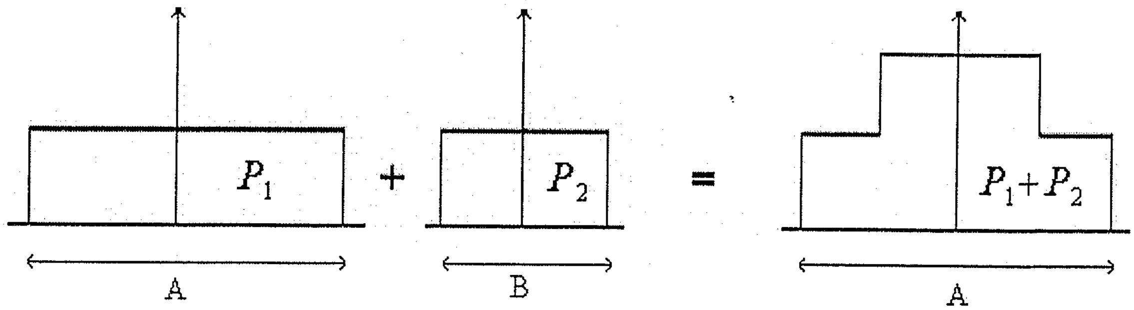

Figure 2.1: Formation of Two-step Staircase distribution using step functions

Step functions P_1 and P_2 are added together to form the resultant step function P_1+P_2. The secondary patterns of P_1 and P_2 can be determined from equation 2.5 and due to linearity their respective secondary patterns can be added together. Let g_1 and g_2 be the secondary patterns of P_1 and P_2 from equation 2.5 and the resultant secondary pattern g_{res} will be

$$g_{res}=g_1+g_2=\frac{\sin(u_A)}{u_A}+\frac{\sin(u_B)}{u_B}$$

A MATLAB program is written to add these respective sinc functions, respective to the lengths A and B, to obtain the resultant far field pattern. The far field patterns are analyzed significantly and its results are tabulated. The patterns provide information about important characteristics of the horn and its radiation properties.

2.5 Essential Parameters for the Parametric Study:

This study is based on the principle of step functions or staircase distributions. Therefore the parameters used in this study are derived from a similar distribution as in figure 2.2. Let us define the essential parameters in which this parametric study will be based on. The essential parameters are B, $\alpha 1$ and $\alpha 2$. Where

1. A is the length of the rectangular aperture give in terms of λ and is in accordance to the aperture design. A will remain as the assumed aperture length throughout the analysis.
2. B is the distance or the length between the two conducting plates on the horn aperture and can be varied when the plates are moved across the aperture (central aperture). It is also represented in terms of λ.
3. $\alpha 1$ and $\alpha 2$ are the respective heights of the two step functions to be added. They will be used as a ratio in the parametric study. These parameters will represent the placing of the plates near the waveguide and the plate length.

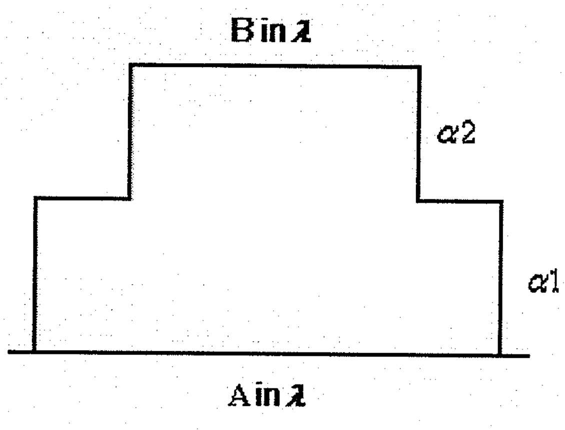

Figure 2.2: Parameters of a typical Two-Step Staircase distribution

Using the above defined essential parameters, the analysis of the amplitude distribution is carried out. Throughout the study, the parameters A and B are assumed to be in terms λ and parameters $\alpha 1$ and $\alpha 2$ to be numerical constants. $\alpha 1$ and $\alpha 2$ will be analyzed by using them as the 'ratio' parameter $\alpha 1 / \alpha 2$.

2.6 Parametric Study of Two-step Staircase Distribution:

For the first part of our analysis, parameter B will be varied, keeping A, $\alpha 1$ and $\alpha 1$ constant. A is assumed to be 4.7λ.This design size is similar to the rectangular aperture of the horn antenna which is to be simulated and compared. $\alpha 1$ and $\alpha 2$ are assumed to be 0.5 for this part of the study.

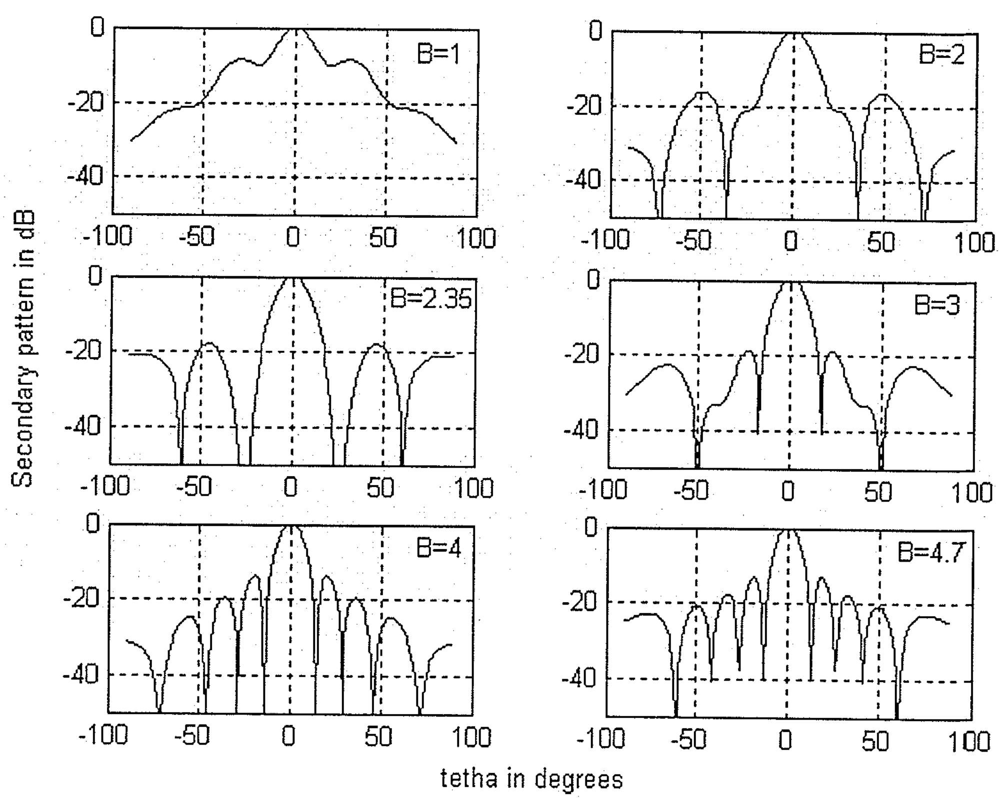

Figure 2.3: Generated Secondary Patterns for parametric changes in B from 1 to 4.7λ, $A=4.7\lambda$, $\alpha 1 = \alpha 2 = 0.5$.

The generated plots of the MATLAB program are shown in figure 2.3. The resultant secondary patterns occur when parameter B is changed from 1 to 4.7 λ.

From figure 2.3, it is evident that when the parameter B is between 2 and 3 λ, the secondary field pattern has side lobes around -20 dB and exhibits better characteristics than a uniform distribution of -13dB. Therefore, it is necessary here to have a closer look at the patterns between these ranges.

Also, when B=4.7 λ, the radiation pattern is similar to a horn antenna with uniform amplitude distribution (= -13 db in the first side lobe). This is because here both the parameters A and B are 4.7 λ, that is the length between the two plates coincides with the aperture length and hence a uniform distribution will result across the horn aperture.

Now, let us have a closer look when B varies from 2 to 3 λ, their respective generated MATLAB plots are shown in figure 2.4.

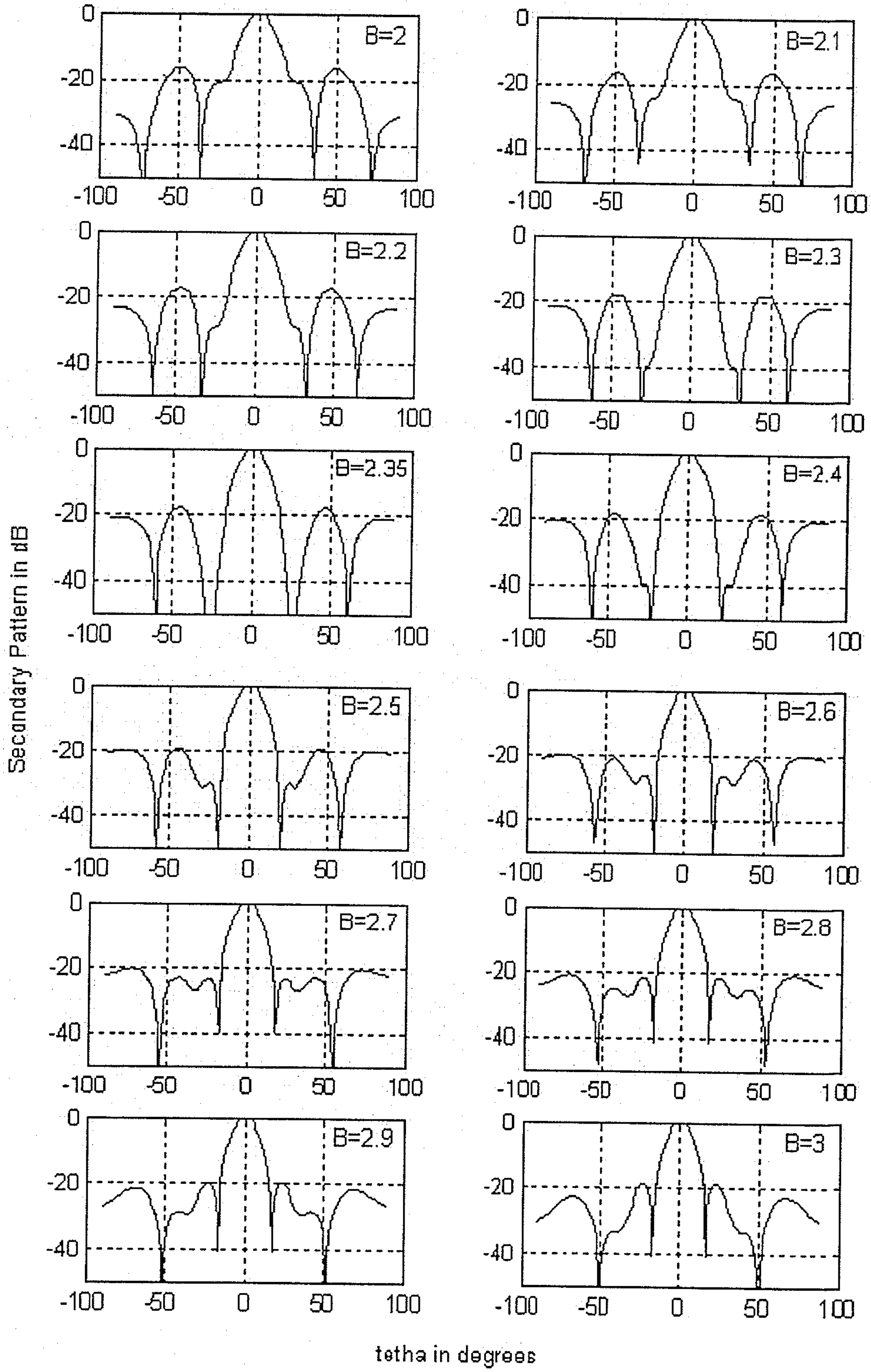

Figure 2.4: Generated Secondary Patterns for parametric changes in B from 2 to3 in λ, $A=4.7\lambda$, $\alpha 1=\alpha 2=0.5$

The far field patterns within this range have excellent characteristics. At B=2.2 λ, the first side lobe level is suppressed to about -30 dB and mostly remains less that -20 dB until B increases to 3 λ. After considering different cases in figure 2.4, we can select the patterns at B=2.35 λ and 2.7 λ for further analysis. The main reason for these conclusion are because of the occurrence of null at the first side lobe for the case when B=2.35 λ. Though their second and third sidelobes are very high, it will be interesting to see what happens to the null in the second part of the parametric study. Also for the case when B=2.7 λ the sidelobe envelope is well below -20dB.

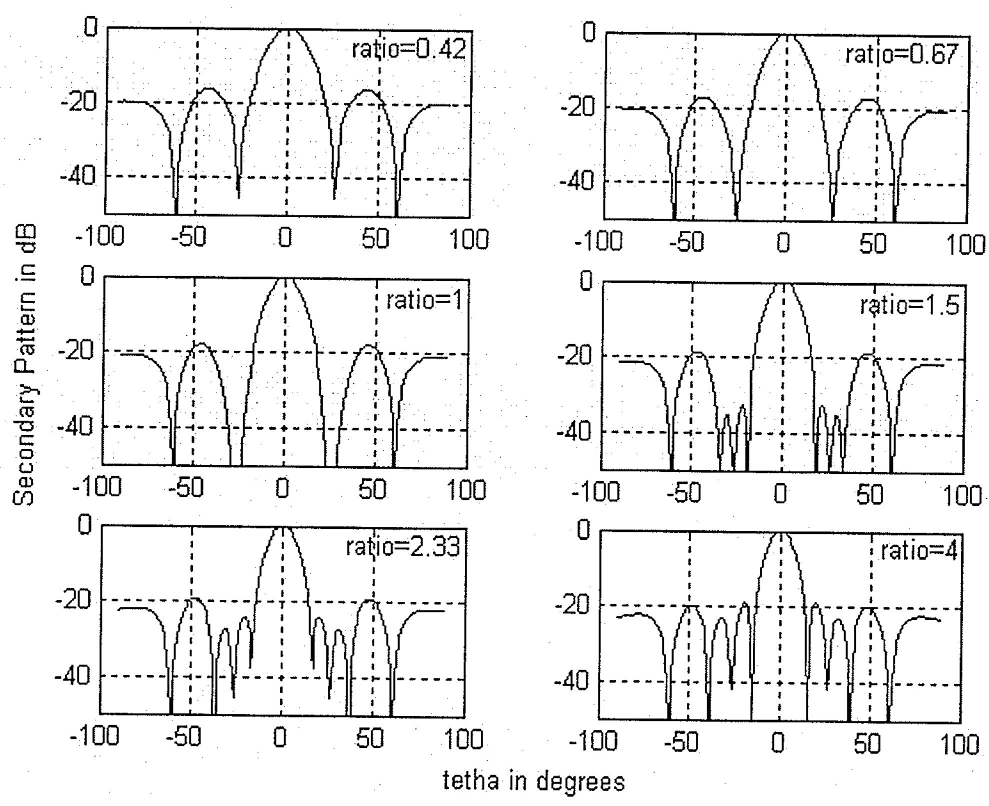

Figure 2.5: Generated Secondary Patterns for the parametric changes in the ratio of $\alpha 1$ *and* $\alpha 2$ *when B=2.35* λ, *A=4.7* λ, $\alpha 1 + \alpha 2 = 1$.

For the next part of the study, parameters $\alpha 1$ and $\alpha 2$ are varied as a ratio for the selected patterns. The value of the parameter A will remain the same (4.7λ). The generated plot in figure 2.5 shows the effect of changes in the far field due to parametric changes of $\alpha 1/\alpha 2$ represented as 'ratio'

In figure 2.5, for the case when the ratio is 1, we obtain a similar pattern as the one in the previous parametric study in figure 2.4 when B=2.35λ. As we increase the ratio from 1, minor side lobes arise and are well below -30dB. Though the sidelobes are very low they are not beneficial because of high third and fourth sidelobes. The minor side lobes increase has the ratio is incremented slowly. They gradually increment to about -25dB when their ratio is just greater than 2. Later, the first side lobe increases to -13dB has the ratio is increased more than 4.this pattern is similar to that of a typical rectangular horn.

The generated plots in figure 2.6 depict a similar study but for the case when B=2.7λ. For the entire parametric study, the first sidelobe lies mostly around -20dB. The entire sidelobe envelope lies around -20dB and gradually increases to -13dB when ratio is increased more than 4.

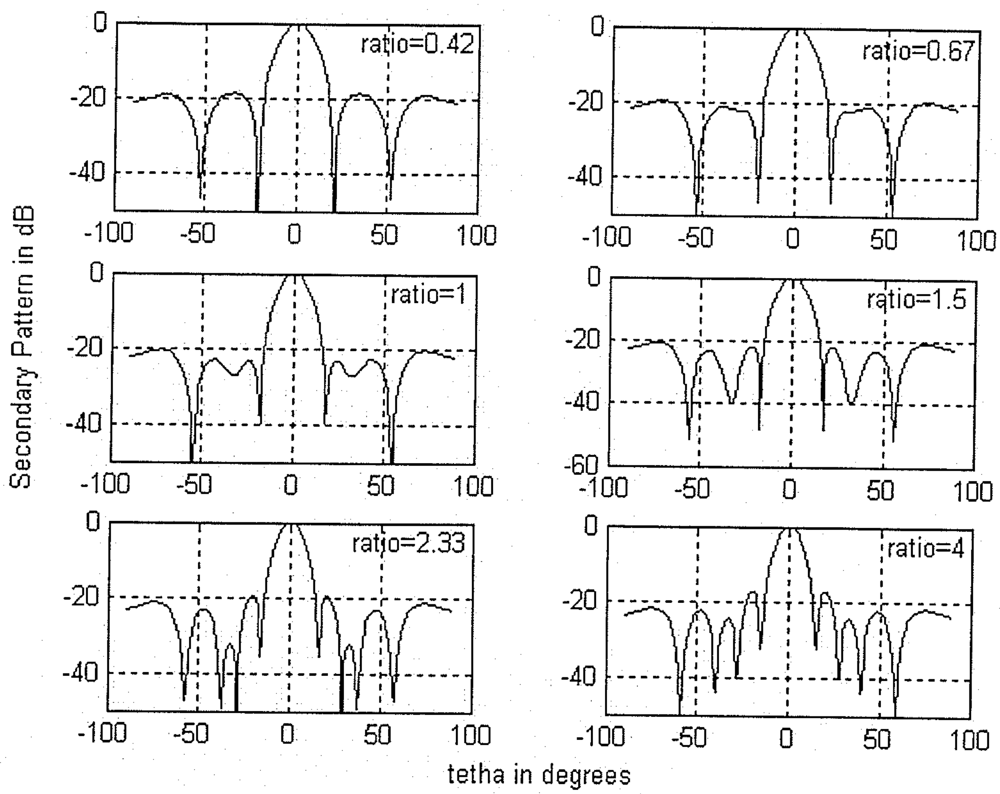

Figure 2.6: Generated Secondary Patterns for the parametric changes in the ratio of $\alpha 1$ and $\alpha 2$ when $B=2.7\lambda$, $A=4.7\lambda$, $\alpha 1+\alpha 2=1$.

It is also possible to study the phase error effects on these cases. This is done by introducing the phase factor into the Sinc function of the secondary pattern.

2.7 Summary:

A parametric study of the effect of Two-step Staircase distribution on the Far-field pattern of the antenna was carried out in this chapter. Simplified equations for the secondary pattern were derived using the rectangular aperture theory and these equations were significantly used in the MATLAB program for the parametric study and to generate their respective secondary patterns. This study gives us an insight into the placement of the plates across the horn aperture and its effect on the secondary pattern.

The first part of the parametric study has provided us significant information regarding the placement of the plates on the horn aperture. Assuming the horn aperture has the length 4.7 λ, we can conclude that improved field patterns are obtained when the plates are placed in such a way at the horn aperture that the length between them is from 2.35 λ to 2.7 λ.

The parametric study of ratio provides us information regarding the length of the conducting plates and its placing near the waveguide. This study also provides us correlated information of parameters $\alpha 1$ and $\alpha 2$ in the Two-step Staircase distribution to provide improved patterns in the far field.

A sidelobe envelope of about -20dB was achieved by altering the uniform amplitude distribution to a Two-step Staircase distribution. This is an improvement of 7dB in the far field patterns. The parametric study provides useful information regarding the use and placing of conductive plates in the horn aperture. Also, provides the optimum range of parameters which would be beneficial in the far field patterns.

- B (central aperture) between 2.35 λ and 2.7 λ, when A= 4.7 λ .
- Ratio ($\alpha 1/\alpha 2$) between 0.4 and 1.5.

Chapter 3

Synthesis of Amplitude Distributions

3.1 Introduction:

The rectangular horn has uniform amplitude distribution and this causes diffractions in the edges, which in turn results in a first sidelobe level of –13dB[4]. By introducing two conducting plates, the uniform distribution along the rectangular aperture is altered to a Two-step Staircase distribution. The horn aperture is bifurcated by the plates and the power flow into the aperture is controlled by its placement near the waveguide.

The parametric study in Chapter 2 helped us understand the effect of the plates on the radiation pattern and using that study optimum parameters for the placement of the plates on the horn aperture was determined. Considerable improvement in the first sidelobe level from -13dB of a normal rectangular horn (uniform distribution) to -20dB for a Two-step staircase distribution horn was obtained.

In this chapter a simple synthetic technique is introduced to synthesize different types of distribution using the Two-step Staircase distribution. It is well known [3-4] that for Cosine, Taylor distribution in the primary pattern, the far field patterns are much better than the uniform distribution. The first side lobe occurs at -23dB for the Cosine, it is even better for a Cosine-square distribution (about -32dB).

Using different combinations of step functions (generally some form of staircase distributions with correlation with the thesis design) the above discussed distributions can be synthesized. These distributions will be analyzed in accordance to the respective thesis design aperture length in terms of λ. The synthesis technique is carried out on cosine, Taylor and other distributions. Using the synthesized parameters and the MATLAB program from chapter 2, their respective secondary patterns can be generated.

For reasons to be discussed later the aperture size for the Cosine distributions as shown in figure 3.1, is selected to be 5 λ.

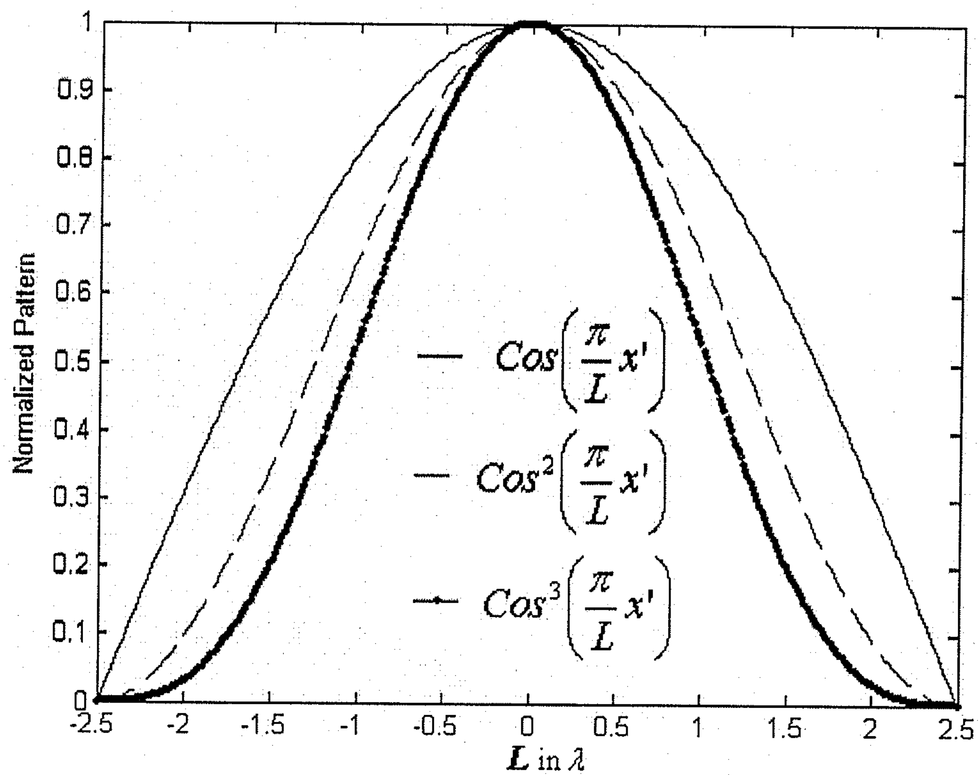

Figure 3.1: Cosine Distributions for L=5 λ

To synthesize the required distribution using the Two-step Staircase distribution, the parameter values of B, $\alpha 1$ and $\alpha 2$ have to be varied accordingly. It is also evident here that it is not possible to exactly synthesize the required distribution and therefore there will be some limitations. The resultant synthesized far field patterns will be secondary to the original distribution patterns in some cases but there will be an undisputable improvement when compared to the uniform distribution.

Also, when more number of staircases is used in synthesizing to achieve the desired distribution, better synthesized field patterns are achieved. But in the physical design this practically means more numbers of plates have to be introduced into the horn aperture. These plates will cause impedance problems near the waveguide of the horn and this will result in phase errors and gain reduction in the field patterns. Therefore, it is beneficial to limit the number of staircases. Hence, in our synthesis technique, we will limit the staircase distribution to a maximum of three staircases (Three-step Staircase distribution).

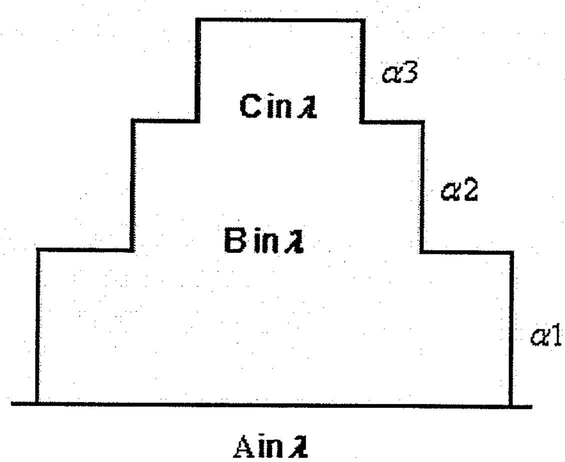

Figure 3.2: Three-step Staircase distribution and its parameters

The synthesis of the amplitude distributions will be carried out in two ways. First, amplitude distributions like Cosine and Taylor functions as shown in figure 3.1 and figure 3.18 will be considered with respect to the aperture length. These distributions will be synthesized using the Two-step Staircase distribution similar to the one shown in figure 2.2 and Three-step Staircase distribution as in figure 3.2.

Different combinations of Two-step Staircase distributions are possible to synthesize the needed distribution. The combinations of the parameters of the Two-step Staircase distributions which fit the needed distributions will be tabulated. Also, using these synthesized parameters their respective secondary patterns can be generated using the MATLAB program from the parametric study in Chapter 2. The synthesis technique generates parameters to achieve low sidelobes in the radiation pattern. This process is repeated again for the Three-step Staircase distribution. Finally, the generated results of the secondary pattern for both these synthesized parameters will be tabulated and compared to the original pattern from their respective distributions [Appendix A].

3.2 Cosine Distribution

As an example of the synthesis a cosine distribution over 5λ aperture is considered in this section. Let us take a closer look at synthesizing technique for synthesizing this distribution using the Two-step Staircase distribution. Though many ways are possible to synthesize the cosine distribution using the Two-step Staircase distribution, let us consider the one shown in figure 3.3 for explanation.

The parameters for the Two-step Staircase distribution $\alpha 1, \alpha 2$ and B are chosen accordingly in order to fit the required cosine distribution. The darker shaded regions are the Two-step Staircase distribution in figure 3.3 and try to fit the Cosine distribution. The synthesized parameters of the Cosine distribution using a Two-step Staircase distribution in figure 3.3 are $\alpha 1$=0.5, $\alpha 2$=0.4 and B=2λ. Using these parameters, their secondary patterns are generated from the MATLAB program in Chapter 2.

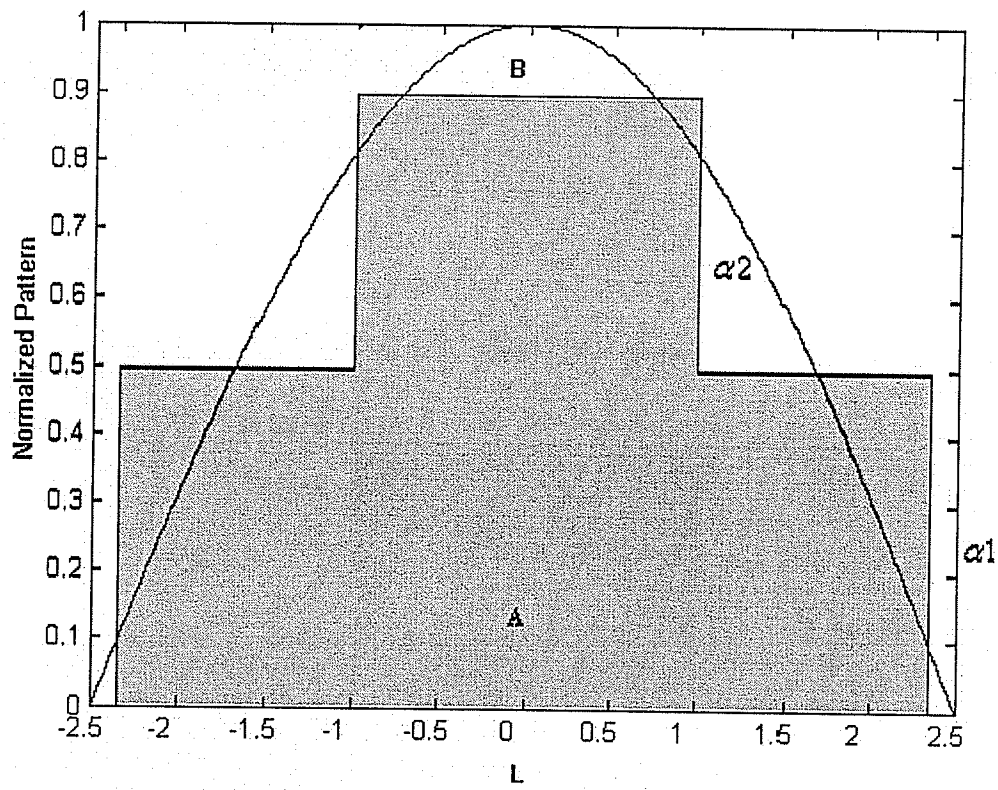

Figure 3.3: Synthesizing the Cosine Distribution of Base L=5λ, with Two-step distribution A=4.7λ, B=2λ, $\alpha 1$=0.5, $\alpha 2$=0.4.

A closer look at figure 3.3 would provide the fact that $\alpha 1+\alpha 2$=0.9, A=4.7λ. The synthesis procedure is repeated again for cases when $\alpha 1+\alpha 2$ are equal to 1 and 0.8 to characterize optimum results. The far field patterns with respect to the synthesized parametric values are generated and tabulated in Table (1) for the case when $\alpha 1+\alpha 2$=1.

It is also evident from figure 3.3 that the Cosine distribution can be synthesized using different parameters of Two-step Staircase distributions. Therefore, by repeating a similar process with different parameters of $\alpha 1$, $\alpha 2$ and B, the cosine distribution is synthesized using Two-step distributions and their respective parametric values are tabulated.

Table 1: Synthesis of Cosine Distribution using Two-Step Staircase Distribution $\alpha 1+\alpha 2=1$, $L=5\lambda$, $A=4.7\lambda$. B, $\alpha 1$, $\alpha 2$ are variables.

Parametric values					SSL1 (dB)	SLL2 (dB)
Case	**B(λ)**	$\alpha 1$	$\alpha 2$	$\alpha 1/\alpha 2$		
1	2.5	0.3	0.7	0.43	-17	-19
2	2.7	0.5	0.5	1	-23	-22
3	1.5	0.5	0.5	1	-13	-19
4	1	0.6	0.4	1.22	-10	-22

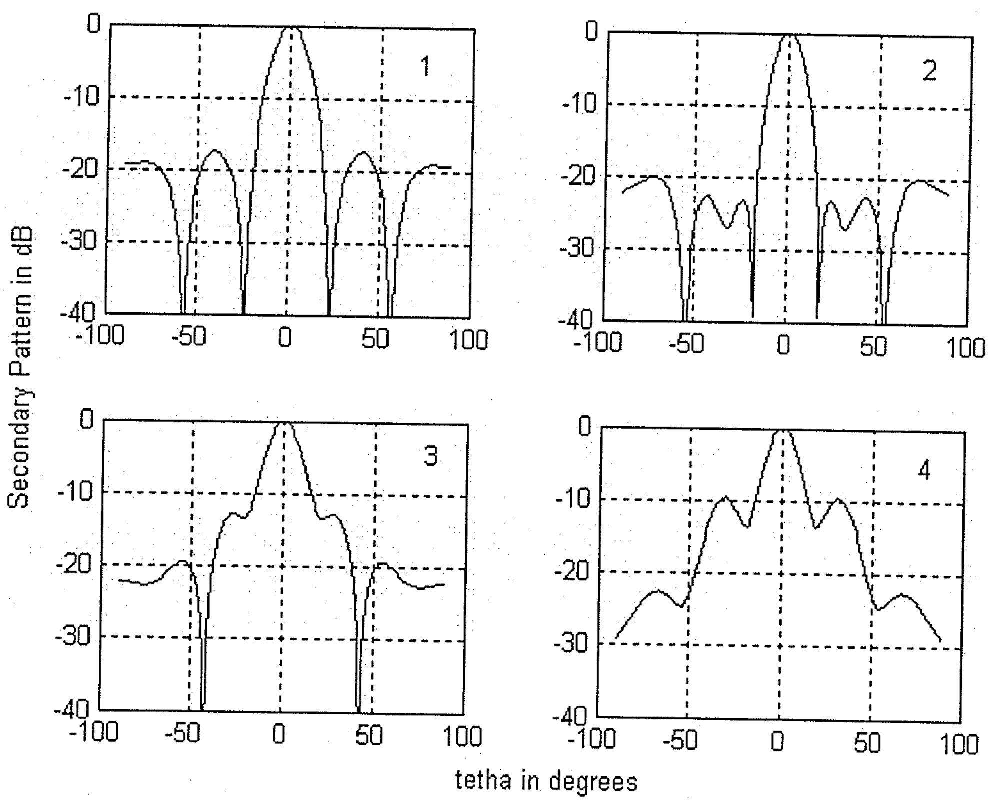

Figure 3.4: Generated Secondary Patterns for the synthesized parameters from Table1 using Two-step distribution for $\alpha 1+\alpha 2=1$, $L=5\lambda$ and $A=4.7\lambda$. B, $\alpha 1$, $\alpha 2$ are variables.

Table (1) and figure 3.4 show the tabulated and the generated secondary patterns according to the synthesized parameters. The first sidelobe level SLL1 and Second sidelobe level SLL2 in Table (1) are tabulated from the generated secondary patterns in figure 3.4.

Before analyzing the tabulated results given above, let us also synthesize the cosine distribution with the Three-step staircase distribution. This process is very similar to the Two-step staircase distribution, the only difference being the extra parameters involved in the synthesis. The extra parameters $\alpha 3$ and C will occur due to the use of the third step function as shown in figure 3.5. Here, also the shaded dark regions represent the Three-step Staircase Distribution and try to fit the Cosine Distribution.

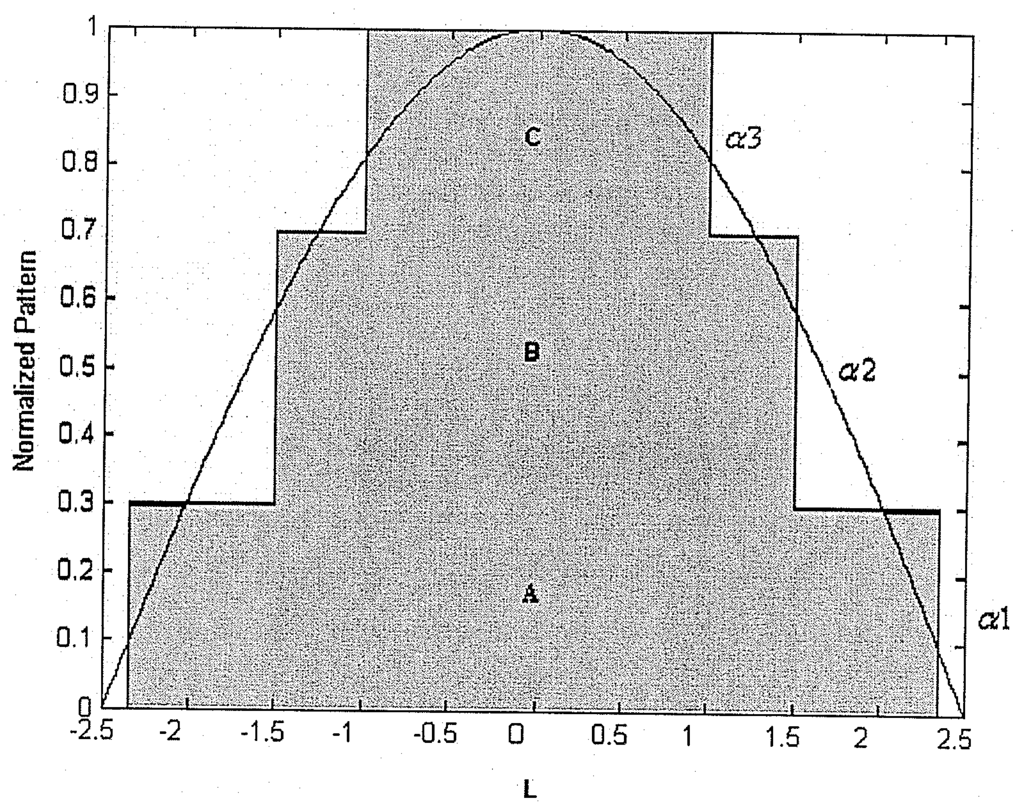

Figure 3.5: Synthesizing the Cosine Distribution with Three-step Staircase distribution $L=5\lambda$, $A=4.7\lambda$, $B=3\lambda$, $C=2\lambda$, $\alpha 1=0.3$, $\alpha 2=0.4$, $\alpha 3=0.3$.

Table 2: Synthesis of Cosine Distribution with Three-Step Staircase Distribution $\alpha1+\alpha2+\alpha3=1$, $L=5\lambda$, $A=4.7\lambda$. B, C, $\alpha1$, $\alpha2$, $\alpha3$ are variables.

Parametric values						SSL1 (dB)	SLL2 (dB)
Case	**B(λ)**	**C(λ)**	$\alpha1$	$\alpha2$	$\alpha3$		
1	3	2	0.3	0.4	0.3	-18	-21
2	3	1.5	0.3	0.3	0.4	-27	-22
3	3	1.5	0.2	0.6	0.2	-27	-28
4	3	1	0.4	0.3	0.3	-15	-21
5	2.5	1	0.4	0.3	0.3	-14	-21
6	2	1	0.5	0.3	0.2	-14	-26

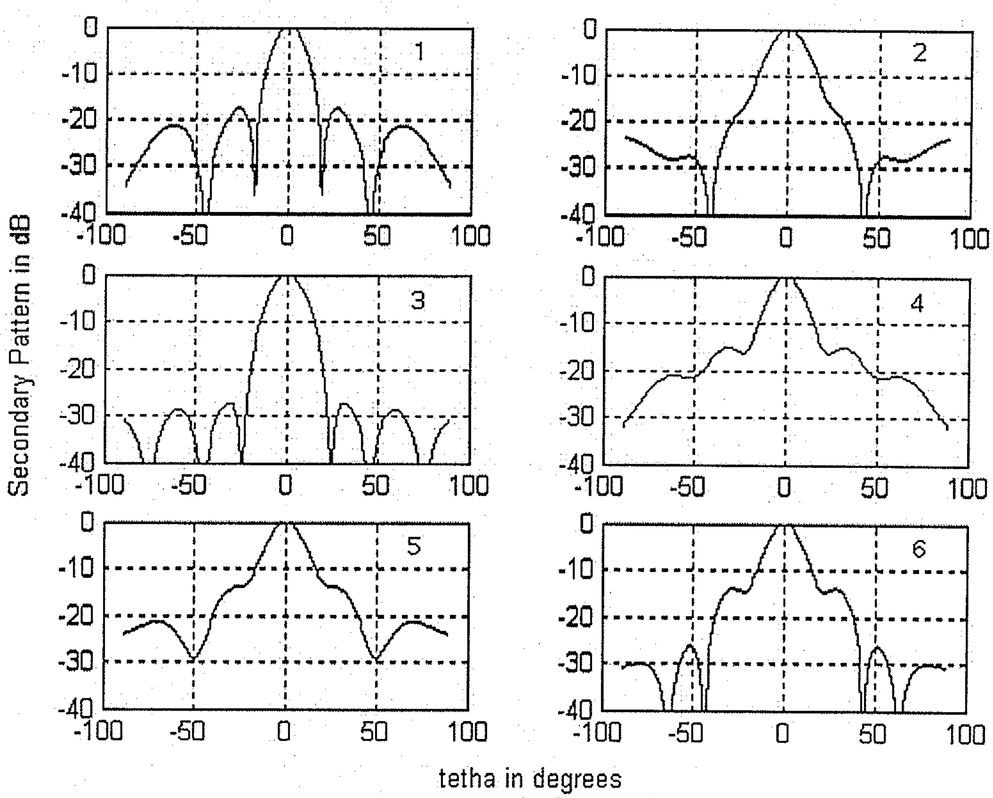

Figure 3.6: Generated Secondary Patterns for the synthesized parameters from Table2 using Three-step Staircase distribution for $\alpha1+\alpha2+\alpha3=1$, $L=5\lambda$, $A=4.7\lambda$. B, C, $\alpha1$, $\alpha2$, $\alpha3$ are variables.

The synthesized parameters of the Three-step staircase distribution are tabulated in Table 2 and their respective secondary field patterns are shown in figure 3.6. Practically the Three-step staircase distribution in the thesis design means the introduction of the four conductive plates into the horn aperture.

The secondary pattern results in Table 1 and 2 are by synthesizing the cosine distribution using Two-step and Three-step Staircase distributions. For the general case of Cosine distribution in the aperture the first sidelobe level occurs at -23 dB [Appendix A].

The maximum achieved first sidelobe level when synthesizing with the Two-step Staircase distributions is -20dB (about 3dB lesser than the cosine distribution) but for the case of Three-step Staircase distribution -27dB is obtained, an improvement of 4dB. This supports the earlier inference that for more number of step functions in the synthesis technique, improved results are achieved and are better than ideal.

Let us repeat the synthesis technique for cases when $\alpha 1+\alpha 2<1$ and $\alpha 1+\alpha 2+\alpha 3<1$. Their respective secondary patterns are tabulated from the generated synthesized parameters after synthesizing the Cosine distribution using the Two-step and Three-step Staircase distributions. The secondary pattern and the synthesized parameters for all the cases when $\alpha 1+\alpha 2<1$ and $\alpha 1+\alpha 2+\alpha 3<1$ are plotted in Table 3-6 and from figure 3.7-3.10.

Table 3: Synthesis of Cosine Distribution using Two-Step Staircase Distribution $\alpha 1+\alpha 2=0.9$, $L=5\lambda$, $A=4.7\lambda$. B, $\alpha 1$, $\alpha 2$ are variables.

Parametric values					SSL1 (dB)	SLL2 (dB)
Case	**B(λ)**	$\alpha 1$	$\alpha 2$	$\alpha 1/\alpha 2$		
1	3	0.2	0.7	0.28	-16	-20
2	3	0.3	0.6	0.5	-18	-22
3	2.5	0.4	0.5	0.8	-19	-20
4	2	0.5	0.4	1.25	-22	-16

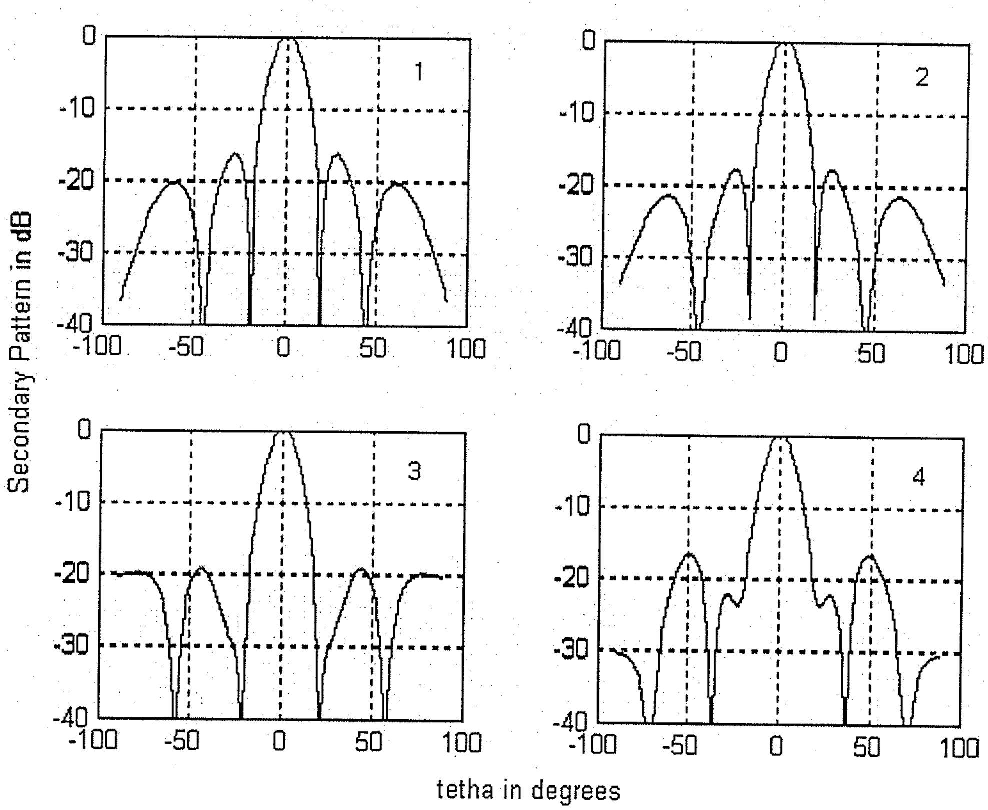

Figure 3.7: Generated Secondary Patterns for the synthesized parameters from Table 3 using Two-step Staircase distribution for $\alpha 1+\alpha 2=0.9$, $L=5\lambda$, $A=4.7\lambda$. $A=4.7\lambda$. B, $\alpha 1$, $\alpha 2$ are variables.

Table 4: Synthesis of Cosine Distribution with Three-Step Staircase Distribution $\alpha 1+\alpha 2+\alpha 3$=0.9, L=5 λ, A=4.7 λ. B, C, $\alpha 1, \alpha 2, \alpha 3$ are variables.

Parametric values						SSL1 (dB)	SLL2 (dB)
Case	**B(λ)**	**C(λ)**	$\alpha 1$	$\alpha 2$	$\alpha 3$		
1	4	1.5	0.4	0.4	0.1	-19	-19
2	3	2	0.3	0.4	0.2	-24	-28
3	2.5	1.5	0.4	0.4	0.1	-20	-24
4	2	1.5	0.5	0.3	0.1	-19	-17

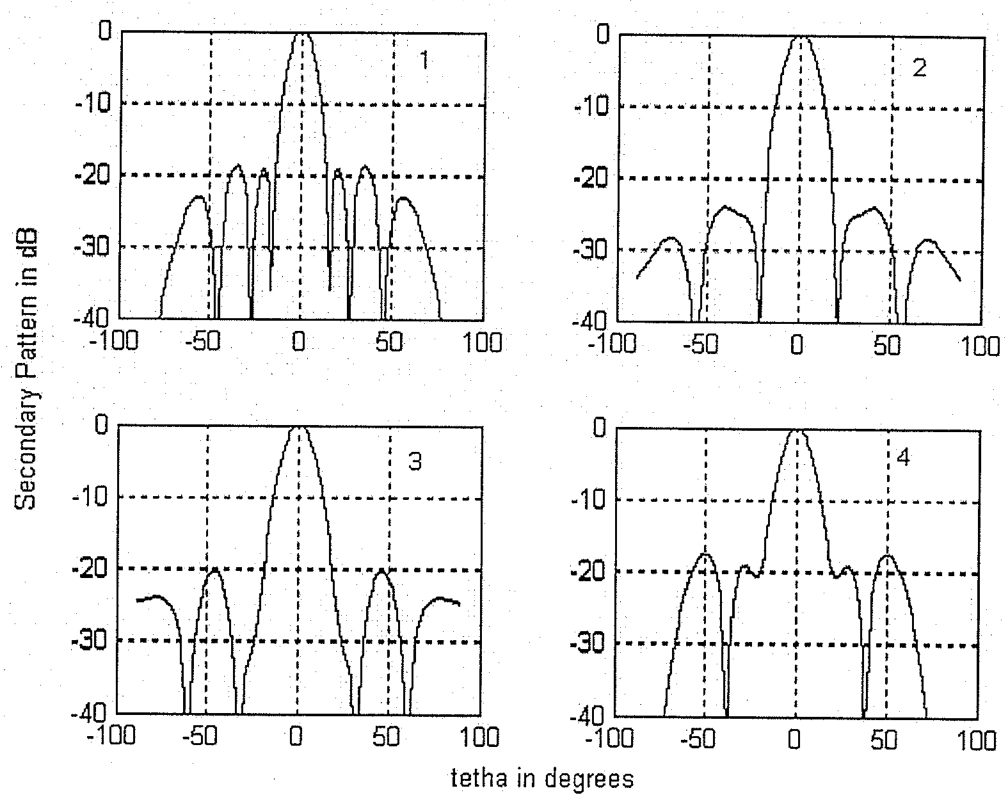

Figure 3.8: Generated Secondary Patterns for the synthesized parameters from Table 4 using Three-step Staircase distribution for $\alpha 1+\alpha 2+\alpha 3$=0.9, L=5 λ, A=4.7 λ. B, C, $\alpha 1, \alpha 2, \alpha 3$ are variables.

Table 5: Synthesis of Cosine Distribution using Two-Step Staircase Distribution $\alpha 1+\alpha 2$=0.8, L=5 λ, A=4.7 λ. B, $\alpha 1$, $\alpha 2$ are variables.

Parametric values					SSL1 (dB)	SLL2 (dB)
Case	**B(λ)**	$\alpha 1$	$\alpha 2$	$\alpha 1/\alpha 2$		
1	3	0.3	0.5	0.6	-18	-22
2	2.5	0.4	0.4	1	-30	-20
3	2	0.5	0.3	1.66	-22	-17
4	2	0.6	0.2	3	-26	-22

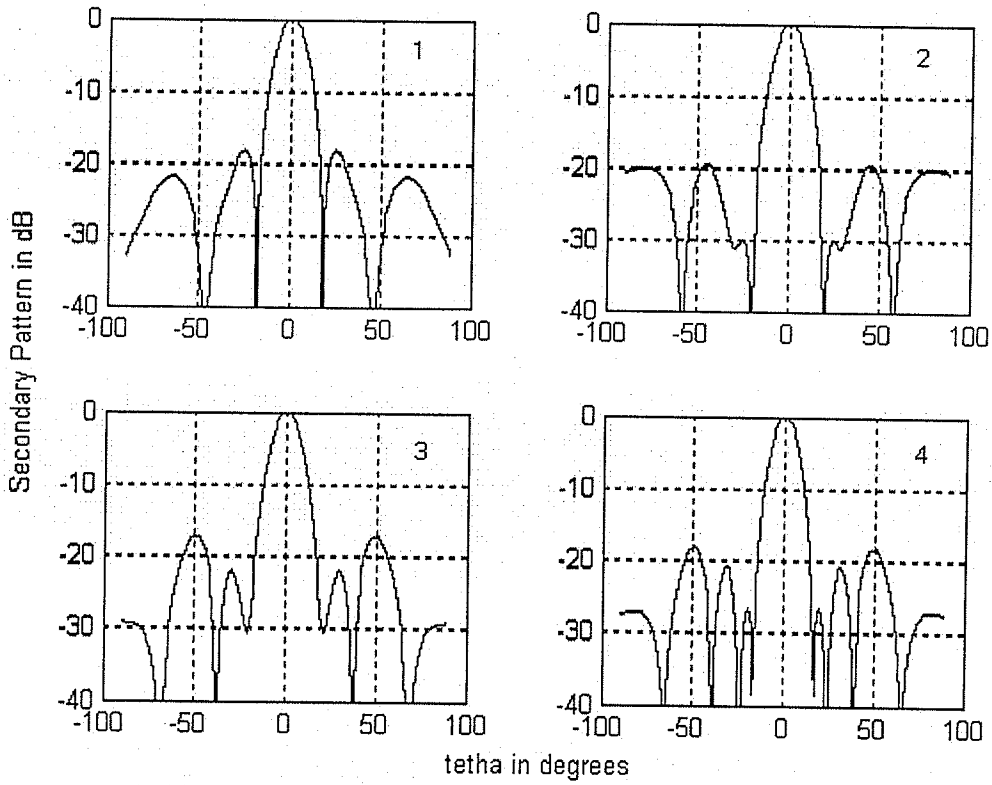

Figure 3.9: Generated Secondary Patterns for the synthesized parameters from Table5 using Two-step Staircase distribution for $\alpha 1+\alpha 2$ =0.8, L=5 λ, A=4.7 λ. A=4.7 λ. B, $\alpha 1$, $\alpha 2$ are variables.

Table 6: Synthesis of Cosine Distribution with Three-Step Staircase Distribution $\alpha1+\alpha2+\alpha3$=0.8, L=5λ, A=4.7λ.B, C, $\alpha1,\alpha2,\alpha3$ are variables.

Parametric values						SSL1 (dB)	SLL2 (dB)
Case	**B(λ)**	**C(λ)**	$\alpha1$	$\alpha2$	$\alpha3$		
1	4	1.5	0.1	0.6	0.1	-19	-19
2	3.5	2.5	0.3	0.3	0.2	-20	-38
3	3.5	2	0.2	0.5	0.1	-19	-28
4	3	1.5	0.4	0.3	0.1	-30	-34

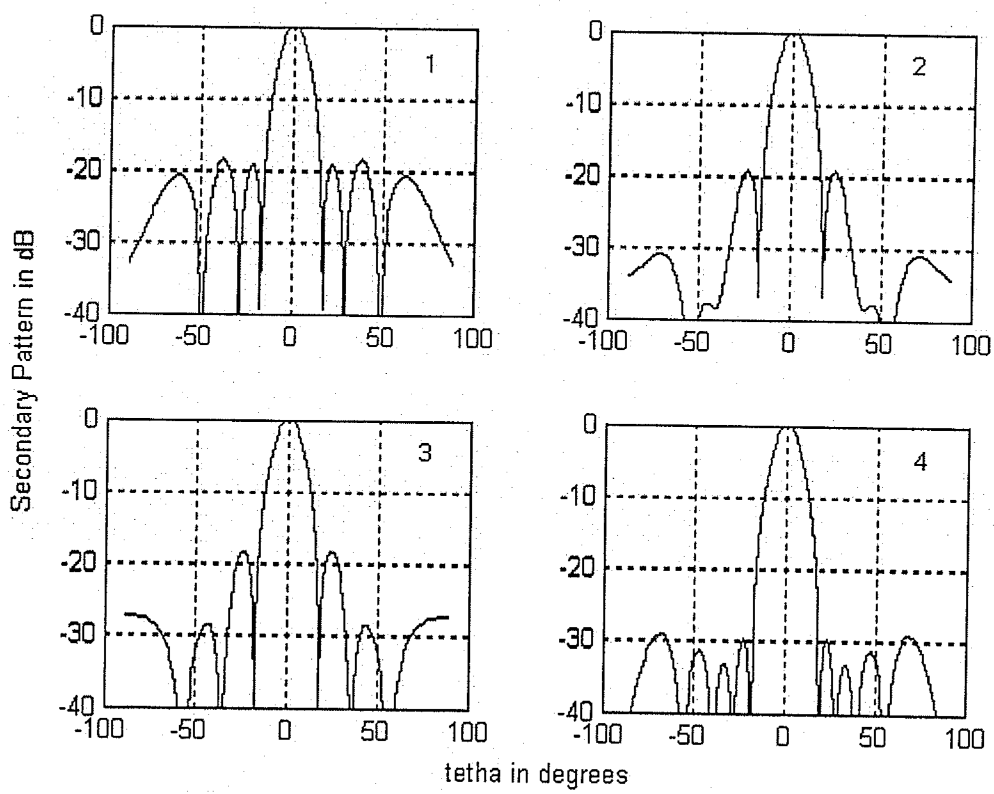

Figure 3.10: Generated Secondary Patterns for the synthesized parameters from Table 6 using Three-step Staircase distribution for $\alpha1+\alpha2+\alpha3$=0.8, L=5λ, A=4.7λ. B, C, $\alpha1,\alpha2,\alpha3$ are variables.

From the above synthesized study it is evident that when $\alpha 1+\alpha 2<1$ or $\alpha 1+\alpha 2+\alpha 3<1$, excellent results are achieved. There is considerable improvement in the generated secondary patterns from both synthesized parameters of Two-step and Three-step Staircase distributions.

The best achieved first sidelobe level in the secondary pattern is compared in Table 7 for different synthesized parameters of both Two-step and Three-step staircase distributions.

Table7: Comparison of Best achieved sidelobe characteristics from both synthesized parameters of Two-step Staircase and Three-step Staircase distributions from Cosine distribution $L=5\lambda$ and $A=4.7\lambda$.

Synthesized parameters Two-step distribution	Best Achieved Side lobe level (dB)	Synthesized parameters Three-step distribution	Best Achieved Side lobe level (dB)
$\alpha 1+\alpha 2=1$	-20	$\alpha 1+\alpha 2+\alpha 3=1$	-27
$\alpha 1+\alpha 2=0.9$	-19	$\alpha 1+\alpha 2+\alpha 3=0.9$	-24
$\alpha 1+\alpha 2=0.8$	-20	$\alpha 1+\alpha 2+\alpha 3=0.8$	-30

From the comparison in Table 7 it is evident that excellent sidelobe characteristics are achieved for the case $\alpha 1+\alpha 2+\alpha 3=0.8$ from the Three-step Staircase distribution. The first sidelobe level occurs at -30dB below the main lobe for this case. The Two-step staircase distribution has the sidelobe envelope occurring at -20dB for most of the cases. There is a huge improvement in sidelobe characteristics for the case when $\alpha 1+\alpha 2<1$ when compared to the case $\alpha 1+\alpha 2=1$. The best field pattern was achieved from the synthesized parameters of Three-step Staircase distribution for the case when $\alpha 1+\alpha 2+\alpha 3=0.8$. It is better than ideal.

3.3 Cosine-square Distribution

A similar synthesis technique is again repeated with the Cosine-square distribution as shown in figure 3.11. The different synthesized parameters and their respective secondary patterns are generated and tabulated for both Two-step and Three-step Staircase distribution cases when $\alpha 1+\alpha 2$ and $\alpha 1+\alpha 2+\alpha 3$ are varied from 1 to 0.8. For the general cosine-square distribution the first side lobe is about -32 dB [Appendix A].

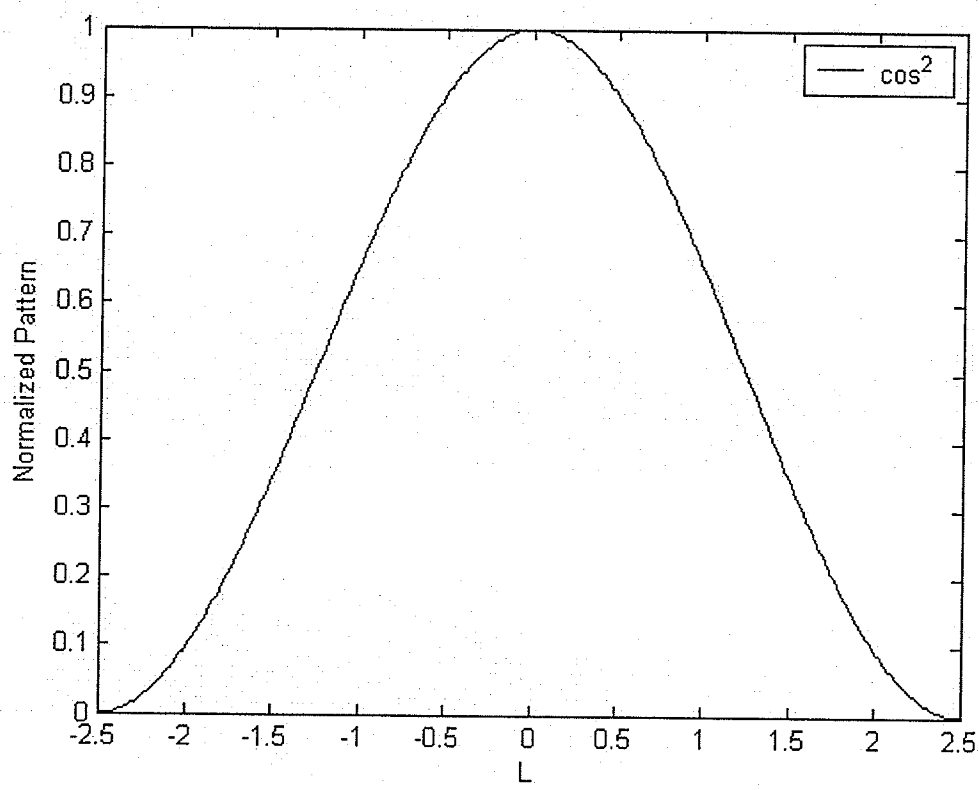

Figure 3.11: Cosine-square Distribution for L=5 λ.

Table 8: Synthesis of Cosine-square distribution with Two-Step Staircase Distribution $\alpha 1+\alpha 2=1$, $L=5\lambda$, $A=4.7\lambda$. $B, \alpha 1, \alpha 2$ are variables.

Parametric values					SSL1 (dB)	SLL2 (dB)
Case	B(λ)	$\alpha 1$	$\alpha 2$	$\alpha 1/\alpha 2$		
1	2	0.2	0.8	0.25	-14	-
2	1.5	0.3	0.7	0.43	-17	-
3	2.7	0.5	0.5	1	-23	-22
4	0.5	0.45	0.55	0.81	-5	-8

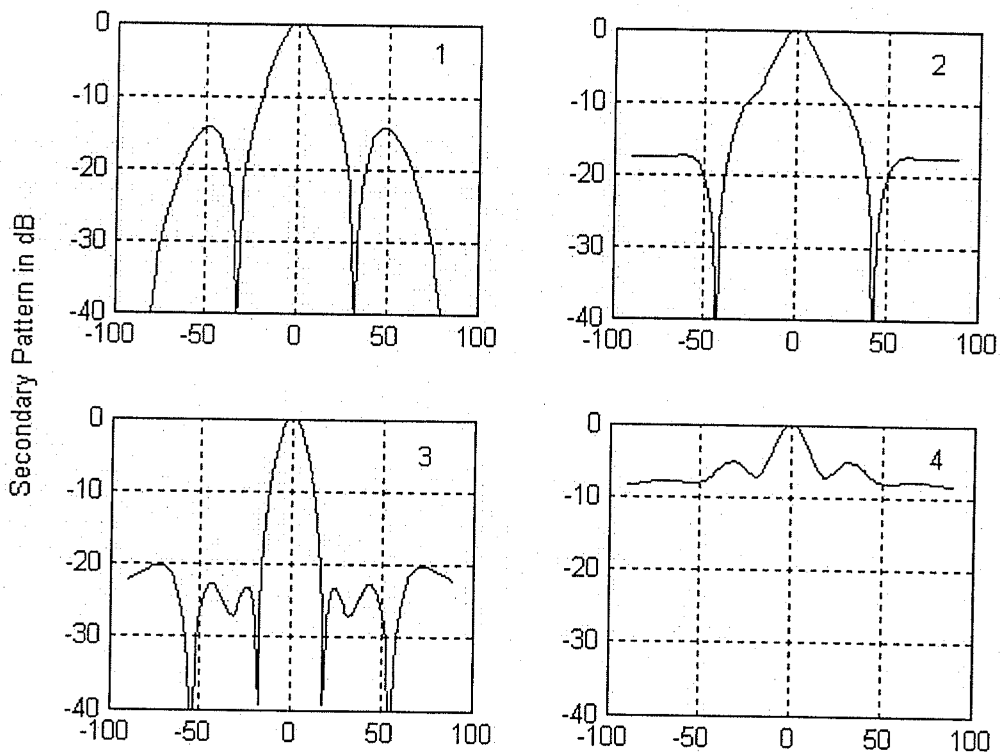

Figure 3.12: Generated Secondary Patterns for the synthesized parameters of Cosine-square from Table 8 using Two-step Staircase distribution for $\alpha 1+\alpha 2=1$, $L=5\lambda$, $A=4.7\lambda$. $A=4.7\lambda$. $B, \alpha 1, \alpha 2$ are variables.

It is interesting to note here that the synthesized secondary pattern results obtained after the synthesizing for the case when $\alpha 1+\alpha 2=1$ from Table 8 are not as efficient as the previous synthesizing results of the Cosine distribution using the Two-step Staircase distributions. The best achieved first sidelobe for this case is -20dB. Now, let us synthesize the Cosine-square distribution using the Three-step staircase distribution. The synthesized parameters and their secondary patterns are tabulated in Table 9 and plotted in figure 3.13.

Table 9: Synthesis of Cosine-square distribution with Three-Step Staircase Distribution $\alpha 1+\alpha 2+\alpha 3=1$, $L=5\lambda$, $A=4.7\lambda$. *B, C,* $\alpha 1, \alpha 2, \alpha 3$ *are variables*

Parametric values						SSL1 (dB)	SLL2 (dB)
Case	**B(λ)**	**C(λ)**	$\alpha 1$	$\alpha 2$	$\alpha 3$		
1	2.8	1.5	0.1	0.4	0.5	-27	-23
2	2.5	1.5	0.2	0.3	0.5	-21	-
3	2.5	1	0.3	0.2	0.5	-10	-20

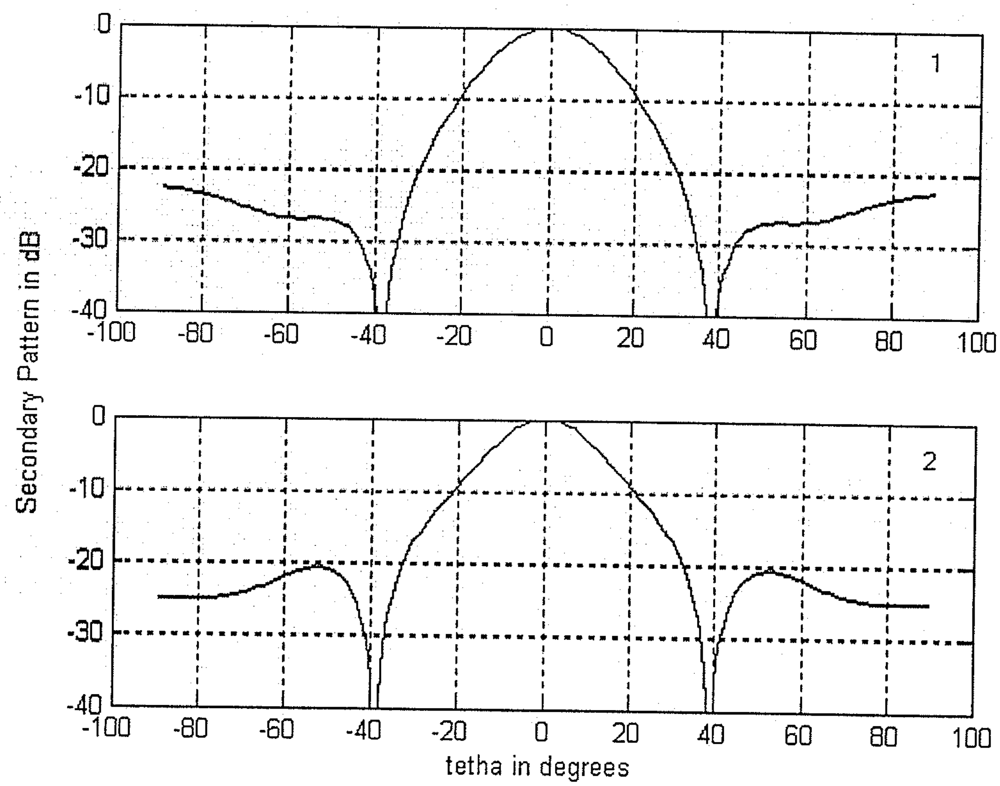

Figure 3.13: Generated Secondary Patterns for the synthesized parameters of Cosine-square from Table 9 using Three-step Staircase distribution for $\alpha 1+\alpha 2+\alpha 3=1$, $L=5\lambda$, $A=4.7\lambda$. *B, C,* $\alpha 1, \alpha 2, \alpha 3$ *are variables.*

Only two secondary patterns were plotted in figure 3.13 from the synthesized parameters in Table 9. A first side lobe level of about -27dB was achieved. Now lets us repeat the same process of synthesis for the cases when $\alpha 1+\alpha 2<1$ and $\alpha 1+\alpha 2+\alpha 3<1$.

Table 10: Synthesis of Cosine-square Distribution using Two-Step Staircase Distribution $\alpha 1+\alpha 2=0.9$, *L=5* λ, *A=4.7* λ. *B,* $\alpha 1, \alpha 2$ *are variables.*

Parametric values					SSL1 (dB)	SLL2 (dB)
Case	**B(λ)**	$\alpha 1$	$\alpha 2$	$\alpha 1/\alpha 2$		
1	2	0.2	0.7	0.28	-15	-
2	1.75	0.3	0.6	0.5	-16	-
3	1.5	0.4	0.5	0.8	-12	-19
4	0.5	0.5	0.4	1.25	-7	-9

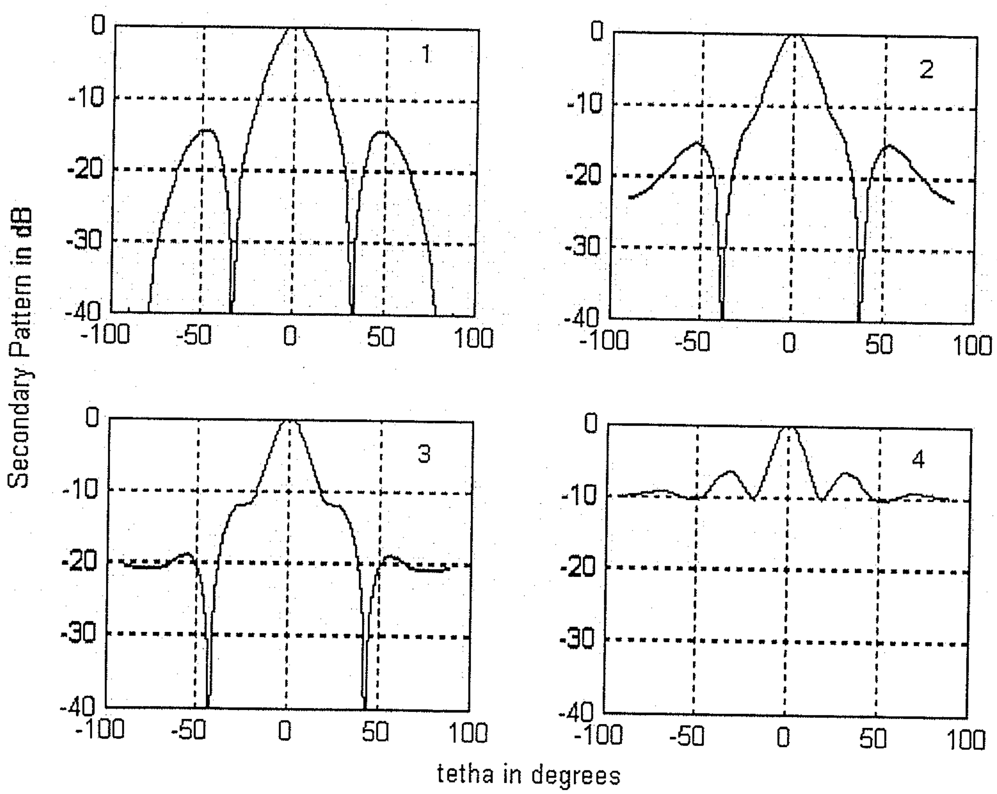

Figure 3.14: Generated Secondary Patterns for the synthesized parameters of Cosine-square from Table 10 using Two-step Staircase distribution for $\alpha 1+\alpha 2=0.9$, *L=5* λ, *A=4.7* λ. *A=4.7* λ. *B,* $\alpha 1, \alpha 2$ *are variables.*

Table 11: Synthesis of Cosine-square Distribution with Three-Step Staircase Distribution $\alpha 1+\alpha 2+\alpha 3=0.9$, $L=5\lambda$, $A=4.7\lambda$. B, C, $\alpha 1, \alpha 2, \alpha 3$ are variables

Parametric values						SSL1 (dB)	SLL2 (dB)
Case	**B(λ)**	**C(λ)**	$\alpha 1$	$\alpha 2$	$\alpha 3$		
1	3	1	0.1	0.6	0.2	-18	-
2	3	1.5	0.2	0.5	0.2	-32	-31
3	2.5	1.5	0.3	0.4	0.2	-20	-30
4	2	1	0.4	0.4	0.1	-16	-20

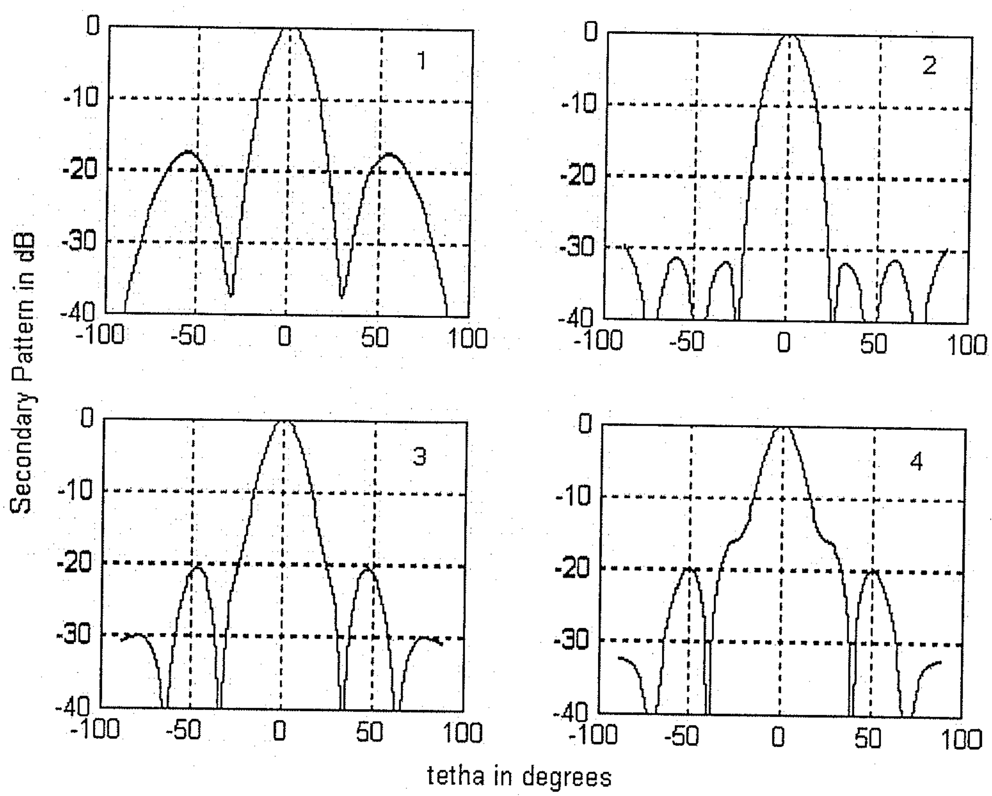

Figure 3.15: Generated Secondary Patterns for the synthesized parameters of Cosine-square from Table11 using Three-step Staircase distribution for $\alpha 1+\alpha 2+\alpha 3=0.9$, $L=5\lambda$, $A=4.7\lambda$. B, C, $\alpha 1, \alpha 2, \alpha 3$ are variables.

Table 12: Synthesis of Cosine-square Distribution using Two-Step Staircase Distribution $\alpha 1+\alpha 2=0.8$, $L=5\lambda$, $A=4.7\lambda$. $B, \alpha 1, \alpha 2$ are variables.

Parametric values					SSL1 (dB)	SLL2 (dB)
Case	**B(λ)**	$\alpha 1$	$\alpha 2$	$\alpha 1/\alpha 2$		
1	3	0.2	0.6	0.33	-17	-21
2	2.5	0.3	0.5	0.6	-18	-19
3	2	0.4	0.4	1	-22	-17
4	1.5	0.5	0.3	1.67	-14	-20

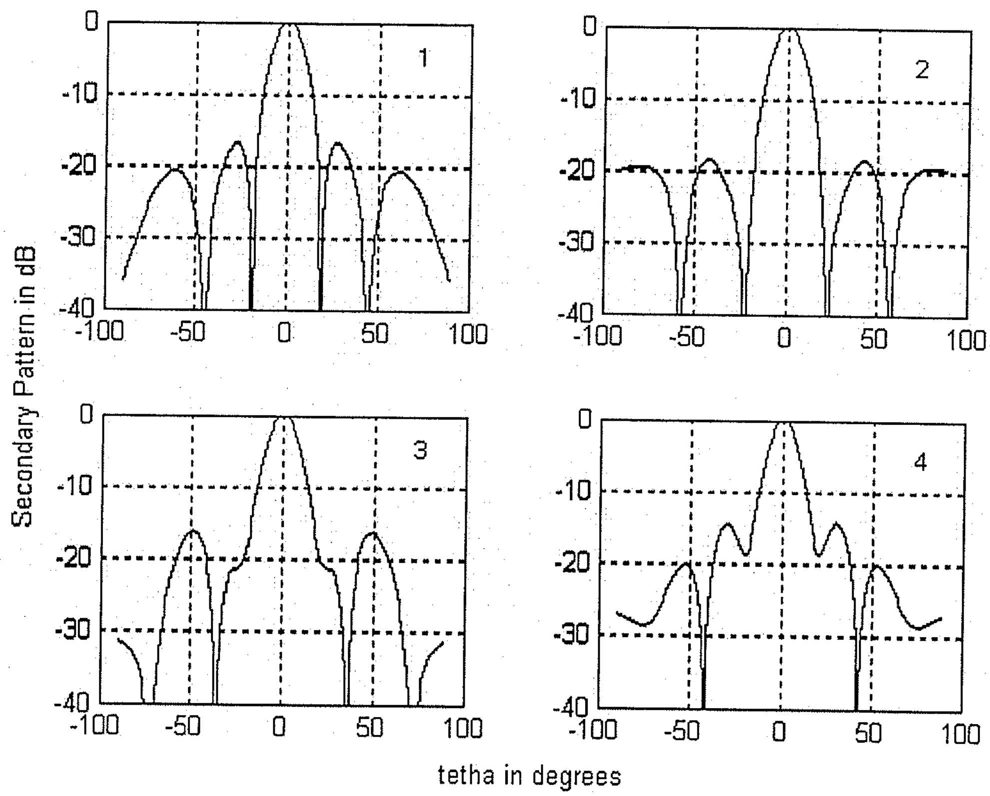

Figure 3.16: Generated Secondary Patterns for the synthesized parameters of Cosine-square from Table 12 using Two-step Staircase distribution for $\alpha 1+\alpha 2=0.8$, $L=5\lambda$, $A=4.7\lambda$. $B, \alpha 1, \alpha 2$ are variables.

Table 13: Synthesis of Cosine-square Distribution with Three-Step Staircase Distribution $\alpha 1+\alpha 2+\alpha 3=0.8$, $L=5\lambda$, $A=4.7\lambda$. B, C, $\alpha 1, \alpha 2, \alpha 3$ are variables

Parametric values						SSL1 (dB)	SLL2 (dB)	SLL3 (dB)
Case	**B(λ)**	**C(λ)**	$\alpha 1$	$\alpha 2$	$\alpha 3$			
1	4	2	0.1	0.4	0.3	-37	-33	-19
2	3.5	1	0.2	0.4	0.2	-16	-	-
3	2.5	1.5	0.3	0.4	0.1	-20	-24	-
4	2	1.5	0.4	0.3	0.1	-18	-17	-

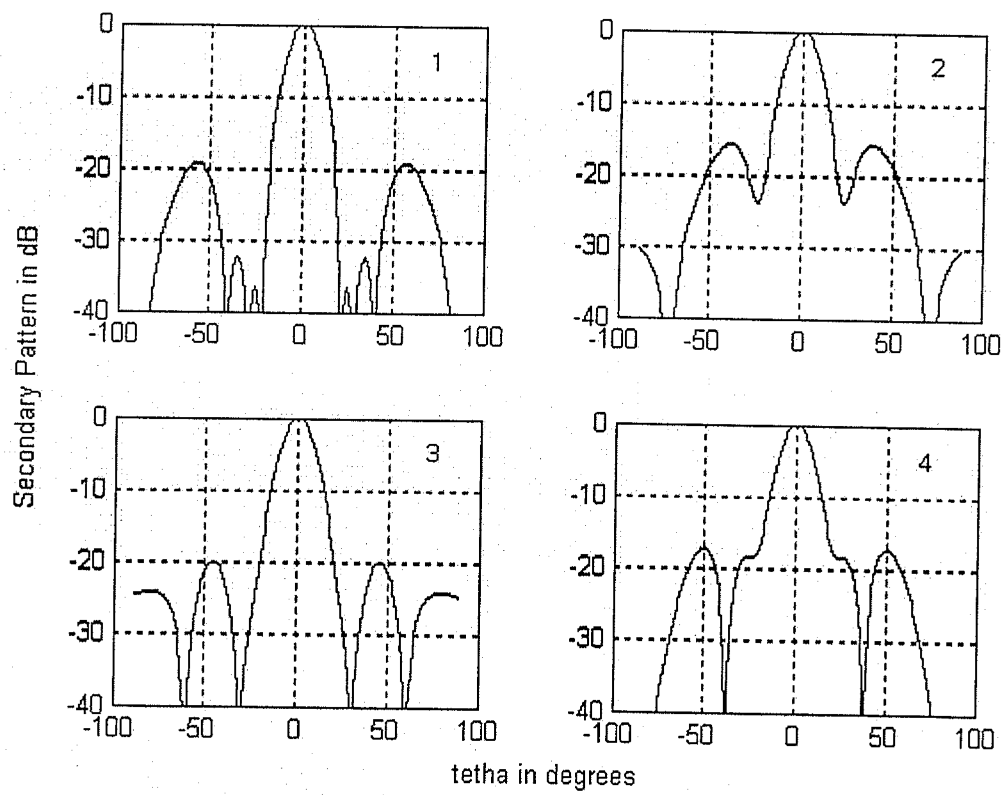

Figure 3.17: Generated Secondary Patterns for the synthesized parameters of Cosine-square from Table 13 using Three-step Staircase distribution for $\alpha 1+\alpha 2+\alpha 3=0.8$, $L=5\lambda$, $A=4.7\lambda$. B, C, $\alpha 1, \alpha 2, \alpha 3$ are variables.

The Secondary pattern results from Tables 8-13 are obtained from synthesized parameters using both Two-step and Three-step Staircase distributions for the case when $\alpha 1+\alpha 2$ and $\alpha 1+\alpha 2+\alpha 3$ are varied form 1 to 0.8. The best achieved sidelobe characteristics are tabulated in the comparison Table 14.

Table14: Comparison of Best achieved sidelobe characteristics from both synthesized parameters of Two-step and Three-step Staircase distributions from Cosine-square distribution $L=5\lambda$ and $A=4.7\lambda$.

Synthesized parameters Two-step distribution	**Best Achieved Side lobe level (dB)**	**Synthesized parameters Three-step distribution**	**Best Achieved Side lobe level (dB)**
$\alpha 1+\alpha 2=1$	-20	$\alpha 1+\alpha 2+\alpha 3=1$	-22
$\alpha 1+\alpha 2=0.9$	-16	$\alpha 1+\alpha 2+\alpha 3=0.9$	-32
$\alpha 1+\alpha 2=0.8$	-20	$\alpha 1+\alpha 2+\alpha 3=0.8$	-20

From the comparison Table 14, considerable improvement in the first sidelobe seen in the cases when $\alpha 1+\alpha 2=0.8$ and $\alpha 1+\alpha 2+\alpha 3=0.9$. The best achieved first sidelobe for the Two-step Staircase distribution synthesis case is -22dB. This is a difference of 10dB with the original Cosine-square distribution (-32dB).The cosine-square distribution is more tapered than the cosine distribution. Therefore, it is more beneficial to synthesize the Cosine than the Cosine-square distribution using the Two-step staircase distribution. Excellent sidelobe characteristics are obtained when synthesized using the Three-step Staircase distributions for the case $\alpha 1+\alpha 2+\alpha 3=0.9$. This is equivalent to the normal Cosine distribution sidelobes.

Also, it is obvious that the above synthesis of Cosine distribution that the synthesis technique when used on the cosine-cube distribution wont be very efficient for the Two-step Staircase distribution because of further tapering of the curves.

3.4 Taylor Distribution

Certain distributions which provide excellent field pattern characteristics can also be synthesized. One such distribution is the Taylor distribution shown in figure 3.18.

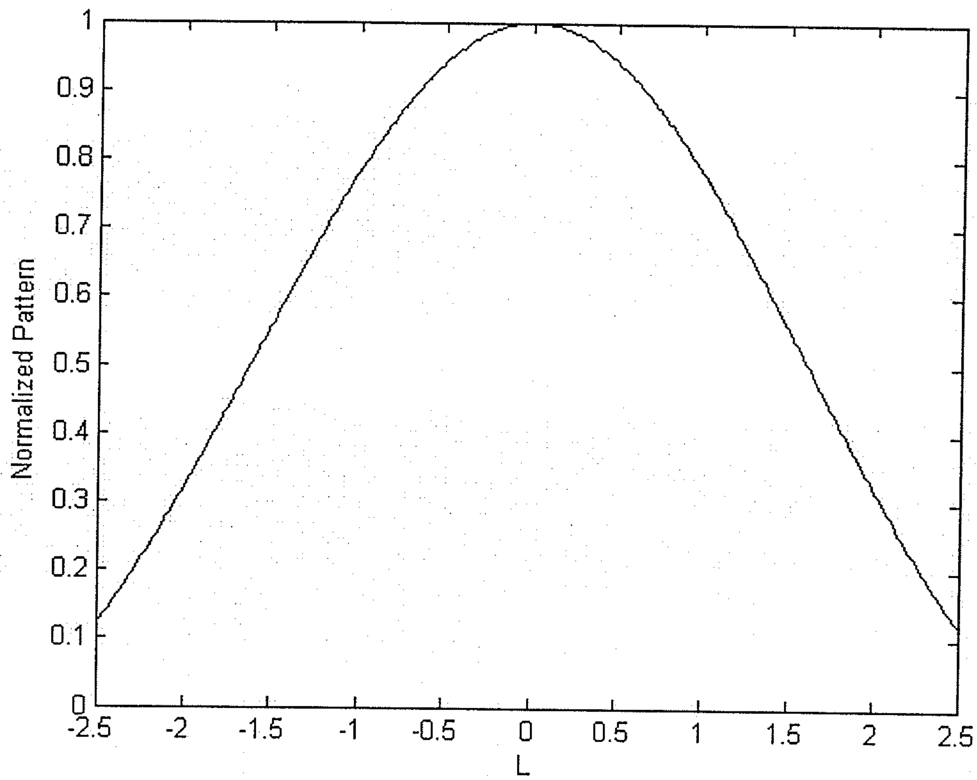

Figure 3.18: Taylor Distribution for L=5 λ

The expression for a single parameter Taylor distribution [18] is given as

$$I_n(z') = \left\{ J_o \left[j\pi B \sqrt{1 - \left(\frac{2z'}{l} \right)^2} \right] \right\} \qquad (3.1)$$

Where 'l' is the total length of the aperture and $-l/2 \leq z' \leq l/2$. J_o is the Bessel function of the first kind of order zero and B is a constant to be determined from the specified side lobe level and $J_o(e^{-j\frac{n\pi}{2}} z') = J_o(jz') = I_o(z')$ .Now from equation 3.1 J_o is formulated to I_o (x) in equation 3.2.

$$J_o \left[j \left(\pi B \sqrt{1 - \left(\frac{2z'}{l} \right)^2} \right) \right] = I_o \left(\pi B \sqrt{1 - \left(\frac{2z'}{l} \right)^2} \right) \qquad (3.2)$$

The Bessel function J_o is calculated from the polynomial approximations [15] given in equation 3.3.

$$\begin{aligned} I_o(x) &= 1 + 3.5156229t^2 + 3.0899424t^4 + \\ &1.2067492t^6 + .2659732t^8 + \\ &.0360768t^{10} + .0045813t^{12} + \varepsilon \end{aligned} \qquad (3.3)$$

To achieve a side lobe level around -25dB, B is assumed as1.0229 and $t = x/3.75$.

Also 'x' is given from equation 3.2 as.

$$x = \left(\pi B \sqrt{1 - \left(\frac{2z'}{l} \right)^2} \right)$$

and varies from $-3.75 \le x \le 3.75$.

Using these polynomial approximations, the Taylor distribution is generated across the aperture length L as shown in figure 3.18. A first side lobe at -25dB is obtained for this particular distribution.

The same synthesizing technique for the cosine and cosine-square distribution was repeated. Instead of tabulating all the generated secondary patterns again only the best cases of achieved first sidelobe when $\alpha 1+\alpha 2$ and $\alpha 1+\alpha 2+\alpha 3$ are varied from 0.8 to 1 were tabulated in the comparison Table 15.

Table15: Comparison of Different Synthesized parameters with results of the Synthesized Two-step and Three-step Staircase distributions of a Taylor distribution L=5 λ and A=4.7 λ.

Synthesized parameters Two-step distribution	**Best Achieved First Side lobe level (dB)**	**Synthesized parameters Three-step distribution**	**Best Achieved First Side lobe level (dB)**
$\alpha 1+\alpha 2=1$	-16	$\alpha 1+\alpha 2+\alpha 3=1$	-24
$\alpha 1+\alpha 2=0.9$	-18	$\alpha 1+\alpha 2+\alpha 3=0.9$	-28
$\alpha 1+\alpha 2=0.8$	-20	$\alpha 1+\alpha 2+\alpha 3=0.8$	-23

The Taylor distribution ideally was generated to achieve -25dB first sidelobes. The result in the comparison Table 15 shows similar results. As expected, there was an improvement in the first sidelobe levels from the synthesized parameters of the Three-step staircase distribution to the two-step distribution. A first sidelobe of -28dB was noted for the case when $\alpha 1+\alpha 2+\alpha 3=0.9$. The synthesized parameters for that respective case were $\alpha 1=0.4, \alpha 2=0.4, \alpha 3=0.1$, B=3 λ and C=1.5 λ. The best case when synthesizing with Two-step staircase distribution occurs when $\alpha 1+\alpha 2=0.8$. The synthesized parameters for this case were $\alpha 1=0.6, \alpha 2=0.2$ and B=2.5 λ.

The secondary patterns of the best case synthesized parameters for the cases $\alpha 1+\alpha 2=0.8$ and $\alpha 1+\alpha 2+\alpha 3=0.9$ are plotted in figure 3.19.

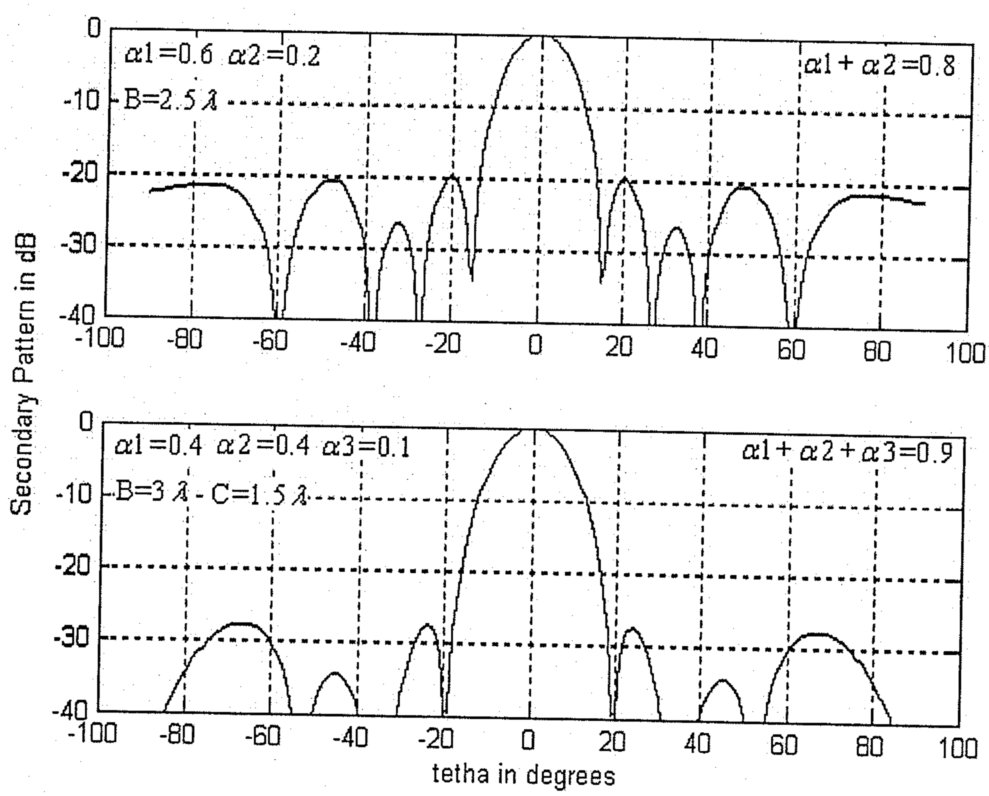

Figure 3.19: Generated Secondary Patterns for the best case synthesized parameters of Taylor Distribution from Table 15, L=5 λ, A=4.7 λ.

3.5 Complicated Distributions

The most significant advantage of synthesizing using Step functions is that it is possible to synthesize any type of distributions. Figure 3.20 is such a complicated distribution and we cannot directly synthesize this distribution with both Two-step and Three-step staircase Distributions. The major issue here is synthesizing the small ripples occurring at the end of the aperture in figure 3.20. Therefore, instead of directly using the staircase distributions we combine them with step functions or uniform distribution to synthesize such a pattern.

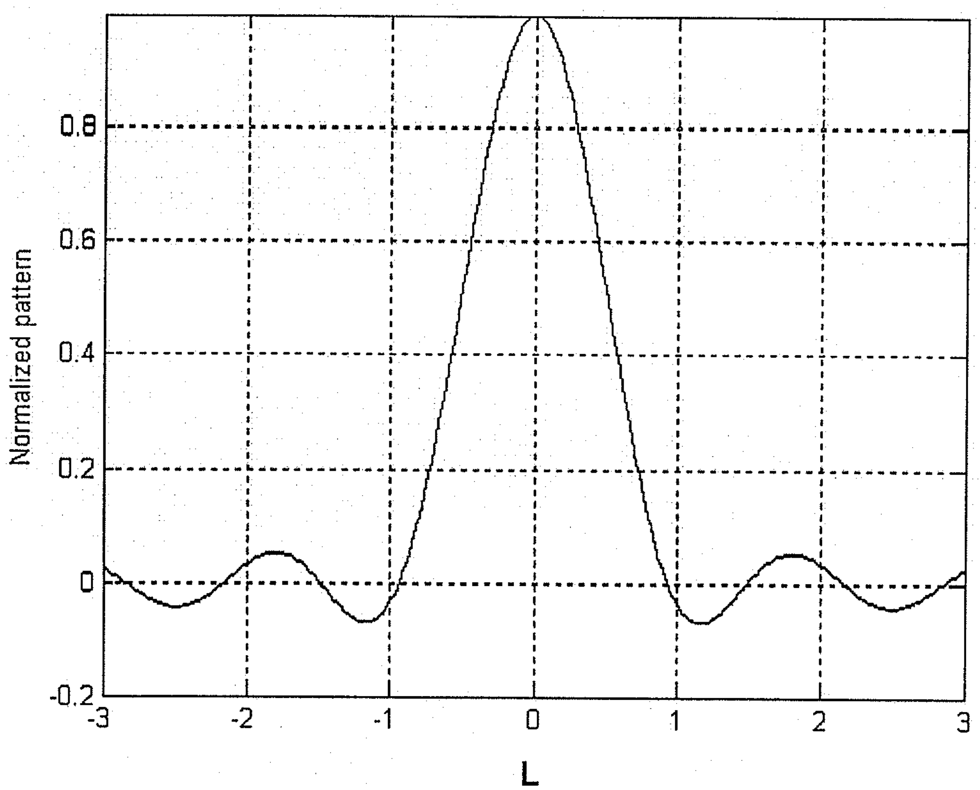

Figure 3.20: Complicated Distribution for L=6 λ

The step functions are mainly used to form the small ripples at the end of the aperture. Two step functions of different amplitudes and lengths will have to be subtracted as shown in figure 3.21 to form the ripples. The reason for using different amplitudes is to achieve the negative amplitude in the required distribution. Once these ripples are formed at the edge the Staircase distributions are added to this function to obtain the required complicated distribution as in figure 3.20.

Practically to obtain a similar distribution, extra plates will have to be applied across the aperture in the horn design. The plates will be placed near the waveguide in such a way that a 180 degree phase change will occur between the preceding plates and this causes the formation of the ripples primary pattern.

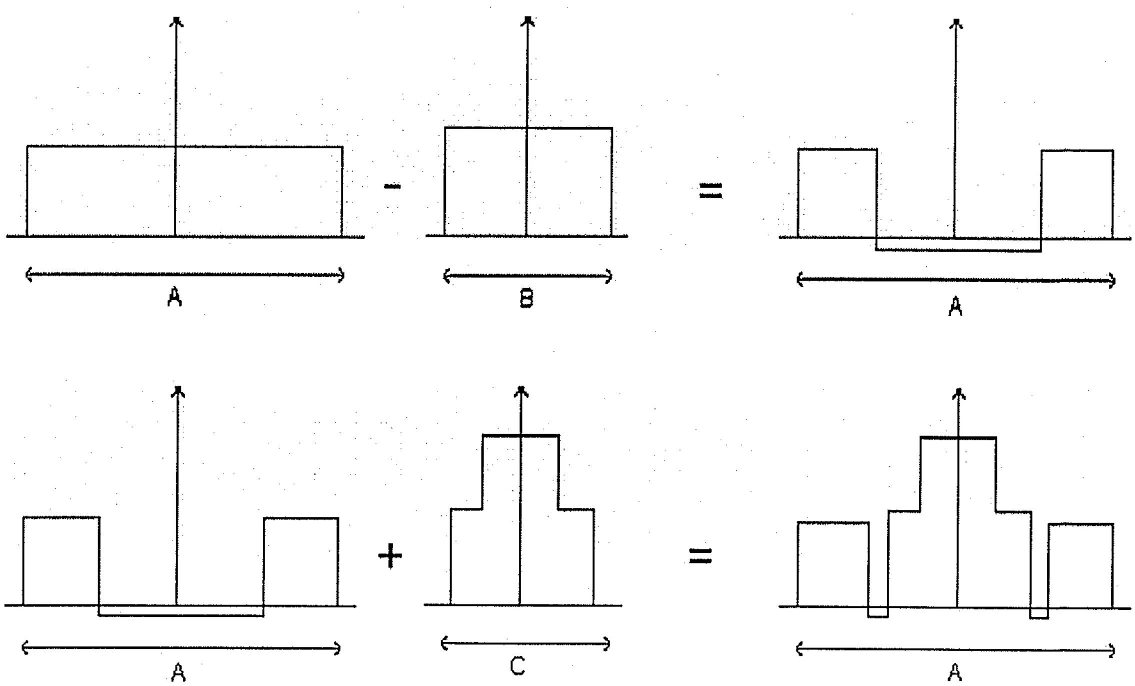

Figure 3.21: Step Functions to synthesize the complicated distribution.

3.6 Summary:

A simple synthetic technique was introduced in this chapter to synthesize beneficial distributions in the aperture. The synthesis of amplitude distributions at the rectangular aperture was carried out using both Two-step and Three-step Staircase distributions and their results were tabulated. The synthesis technique introduces a unique concept of simplifying complicated distribution using step functions. Using these synthesized parameters, it is possible to produce desirable and improved secondary patterns. These parameters can be used in the septum horn to achieve desired radiation patterns. The synthesis technique with the study of Two-step Staircase distributions in Chapter 2 enables the parametric study about the effect of the plates on the radiation pattern on a pyramidal horn to be conducted in Chapter 4.

Table16: Comparison of Different Distributions with results of the Synthesized Two-step and Three-step Staircase distributions

Distributions	**General First Side Lobe (dB)**	**Two-step distribution (dB)**	**Three-step distribution (dB)**
Cosine	-23	-20	-30
Cosine-Square	-32	-20	-32
Taylor	-25	-20	-28

The tabulated patterns evaluate the limitations and provide us sufficient information regarding the improvement in the performance of the antenna. Table 16 shows the best achieved results in the secondary pattern using the synthesis technique for both Two-step and Three-step Staircase distributions. In some cases better than ideal results are achieved.

Chapter 4

Parametric study of the Pyramidal Septum Horn Antenna and Antenna Fabrication Results

4.1 Introduction

In this chapter a detailed parametric study of the effect of the plates on a pyramidal horn antenna is carried out. From the Two-step Staircase distribution in chapter 2, it is clear that by altering the uniform amplitude distribution their results a much improved Far-Field characteristics on the antenna. This is practically achieved by introducing two conductive plate's perpendicular to the E-field and across the horns rectangular aperture. The parametric study in chapter 2 provides us valuable information regarding placement of the plates and helps us in the initial assumptions for this practical parametric study.

Ansoft's EM software HFSS is used to model and simulate the rectangular pyramidal horn with plates and to carry out the systematic parametric study. The design values of the Pyramidal rectangular horn are borrowed from Balanis [4].

Also, an E-plane horn is fabricated with two sets of conductive plates. Holes were drilled onto the horn surface so as to hold the conductive plates using screws. The diameters of the screws used were 0.21844 cm. Two sets of conductive aluminum plates were designed and fabricated.

In this chapter, the simulation results of the fabricated horn antennas are compared with their measured results obtained in the Antenna laboratory at the

University of Manitoba. The fabricated antennas were tested for the far-field radiation patterns using the equipment in the Far Field Anechoic Chamber in the Antenna Laboratory. The measured results are compared with their simulated results. It is found that a good agreement is achieved between them.

4.2 Pyramidal Horn design.

The dimensions of the horn design to be simulated are in terms of λ and are a=0.8382 λ, b=0.3725 λ, where a and b are the inner dimensions of the waveguide to the horn, a_1=6.002 λ, b_1=4.715 λ and p_e=p_h=10.005 λ, where a_1 and b_1 are the inner dimensions of the rectangular aperture. p_e and p_h are the distance between the horn aperture and waveguide from both directions (E and H-plane) respectively as shown in figure 4.1.

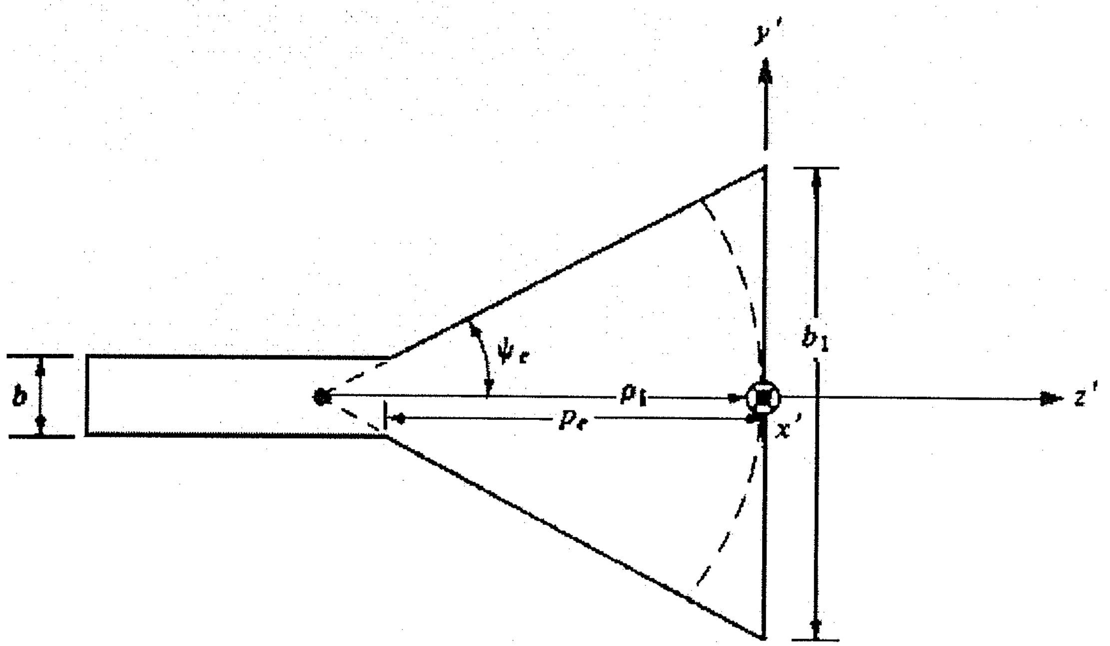

Figure 4.1: E-plane view of Rectangular Horn Antenna [4].

The design frequency for the horn is in X-band (10 GHz). Therefore, their respective wavelength λ is 3cm. Using these dimensions; the rectangular pyramidal horn was modeled and simulated in HFSS. The field accuracy in HFSS was set to 2% and convergence rate to 0.02.

The Far-field radiation pattern shown in figure 4.2 is obtained from the simulated results of the modeled Pyramidal Rectangular horn antenna. The achieved gain was about 22dB for this design. The Far-field patterns were normalized in order to closely study the sidelobe characteristics.

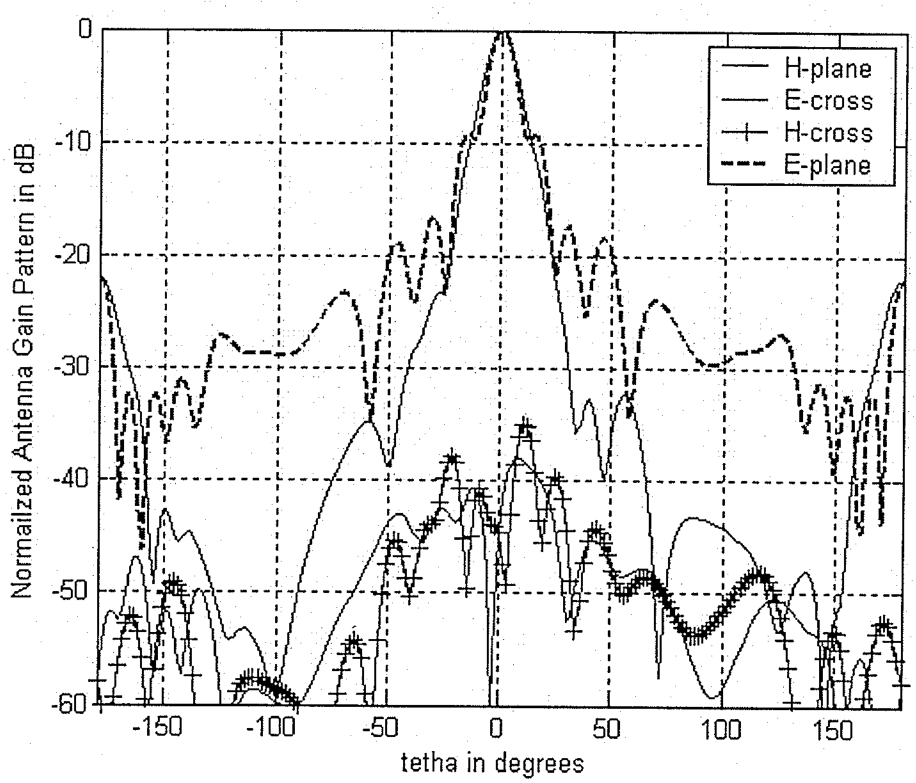

Figure 4.2: Far-Field pattern of Rectangular Horn Antenna without plates a=0.8382 λ,

$b=0.3725\lambda$, $a_1=6.002\lambda$, $b_1=4.715\lambda$ and $p_e=p_h=10.005\lambda$.

Figure 4.2 shows the first sidelobe for this design occurring at -9dB below the main lobe in the E-plane of the field pattern. As discussed in the previous chapter, for a rectangular aperture, the first side lobe generally occurs at -13dB. The reason for the loss in 4dB in the sidelobe is due to phase error in the pyramidal horn aperture. The cross-polarization is for both E and H-planes are well below -30dB.

4.3 Parametric Study

Considering, two conductive plates are symmetrically introduced across the Horn aperture to obtain the Two-step Staircase distribution in chapter 2, some important plate parameters affecting the Field patterns would be

a) Thickness of the plates (t).
b) Size of Central aperture (B).
c) Throat gap near the waveguide (d).
d) Length of the plates (l).

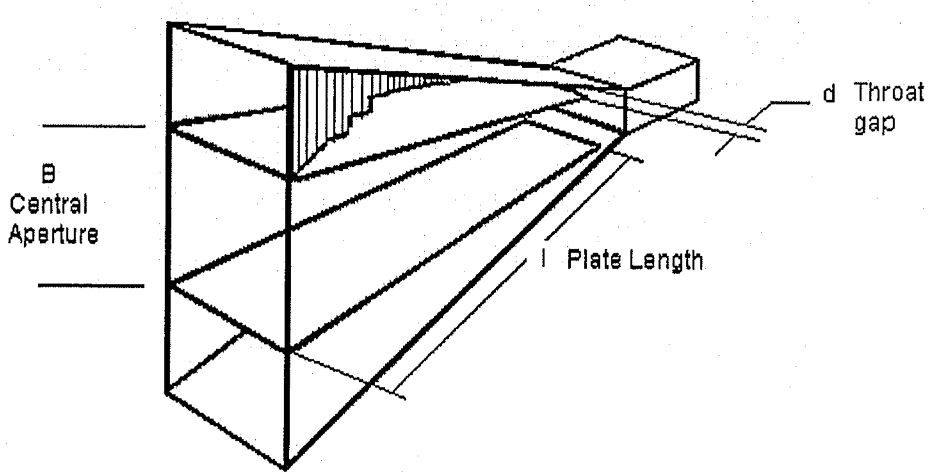

Figure 4.3: Geometry of two plate septum horn antenna

Most of the above defined parameters are related to the parameters used in the study of Two-step Staircase distribution in Chapter 2. The parameter 'B', size of the central aperture is directly similar to the parameter B used in the chapter 2 and is also represented in terms of λ . The combination of parameters 'l' and'd' will represent the ratio parameter of $\alpha 1$ and $\alpha 2$ from Chapter 2.

Therefore, by varying these parameters a systematic study is carried out on the Pyramidal horn antenna using Ansoft's HFSS. The rectangular horn has flare on both directions and therefore the conducting plates will also taper down according to the horn flare.

a) Thickness of the plate (t):

The first parameter analyzed is the thickness of the conductive plates. The horn design is the same as the one modeled earlier in this chapter except for the two plates to be introduced across the aperture. Initially, the lengths of the conductive plates are similar to the horn flares; therefore they will originate from the waveguide and move on till the aperture of the horn.

Let us place the two plates across the aperture in such a way that they divide them in a binomial distribution, i.e. the aperture of the horn is divided into three apertures and the central aperture has twice the area of the two adjacent apertures. This assumption is carried out from Chapter 2. The initial assumed value of B is 2.3575 λ. The plates are placed near the waveguide such that Throat gap d=0.05cm and l=10.005 λ.

Using these initial assumptions, the parametric study is conducted by varying the thickness of the plate. Initially, the thickness of the plate is assumed to be 0.05cm and is varied until about 3cm. The pyramidal horns with the corresponding thickness of the conductive plates are modeled and simulated using Ansoft's HFSS. The results from the simulation are shown in figure (4.4) with respect to the parametric changes in't'. The E-plane field patterns are normalized as to study the sidelobe characteristics of the horn.

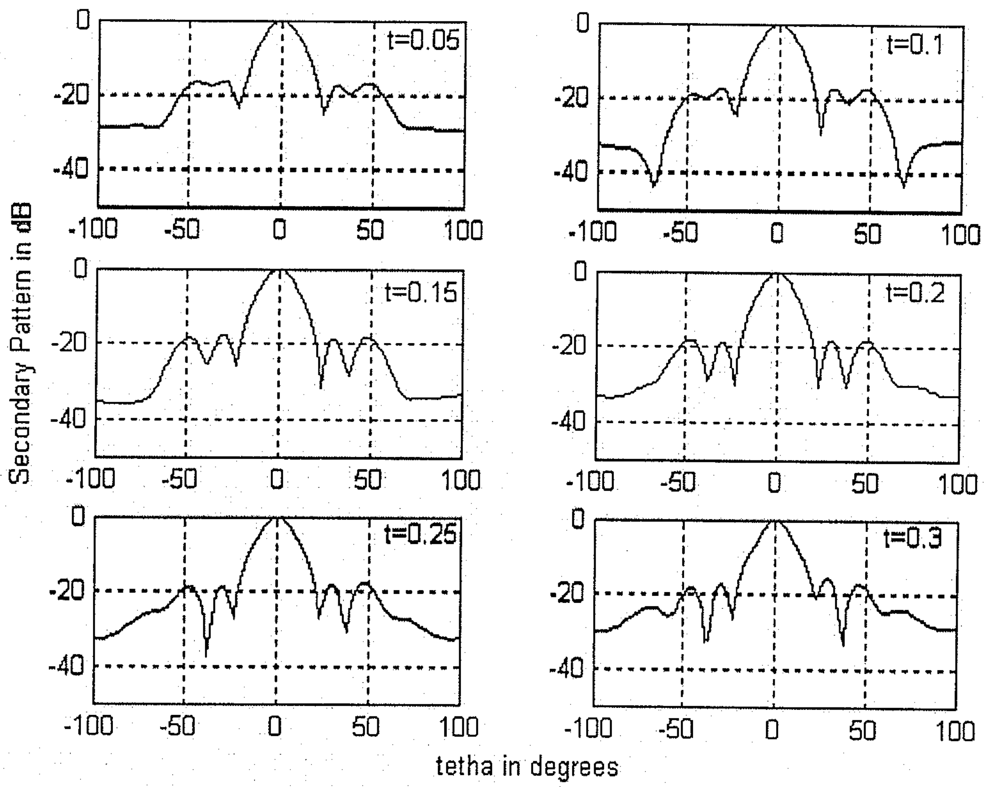

Figure 4.4: Simulated Secondary Patterns for parametric changes in't' from 0.05 to 0.3, B=2.3575 λ, l=10.005 λ and d=0.05cm.

From figure (4.4), it is evident that the thickness of the plate is not a major parameter in the influence in the Field patterns. Only after t = 0.3cm the pattern seems to detoriate, it is also important to mention here that if the plate is too thick than it will block the power flow into the horn. Therefore for the rest of the parametric studies, let us assume the thickness of the plate to be 0.1cm. Also, it is noted here that only the E-plane patterns are compared in the simulated analysis has the plates do not affect the H-plane patterns of the horn.

b) Size of Central Aperture (B):

For the next part of the parametric study, the design is modeled with plate thickness 0.1cm. In this study, we simulate different cases by moving the plates across the horn's rectangular aperture i.e. Central Aperture B. The movement of the plate is measured by the distance between the conductive plates in terms of λ. The simulated results in figure 4.5 are when parameter B is varied from 2 to 3 λ. This study is very similar to the parametric study of Two-step distribution in chapter 2 except for the exact specified values of $\alpha 1$ and $\alpha 2$. Throat gap is 0.05cm and l is 10.005 λ.

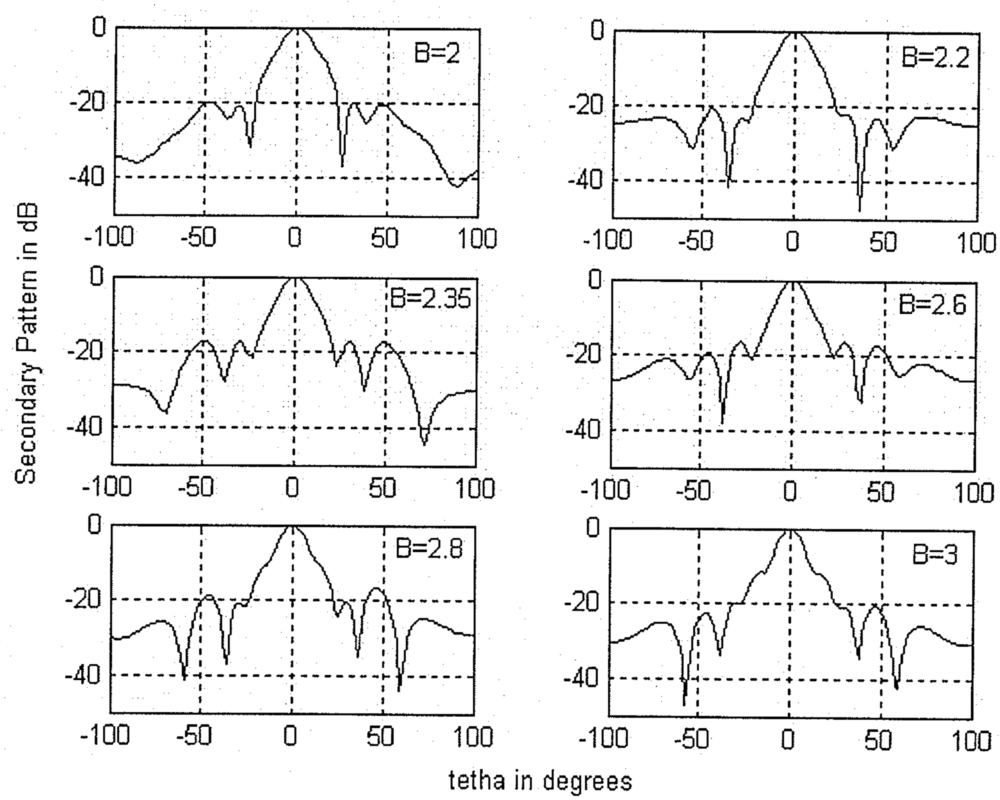

Figure 4.5: Simulated Secondary Patterns for parametric changes in 'B' from 2 to 3 λ, l=10.005 λ, d=0.05cm and t=0.1cm.

From the figure 4.5, we obtain similar results as the one from the parametric study in Chapter 2. Excellent Far-field characteristics are obtained when the plates are placed around 2.3575λ. The first side lobe occurs at around -20dB for this case and an improvement of 11dB from the general horn antenna pattern shown in figure 4.2 is achieved. There is a huge improvement of the sidelobes on the E-field pattern and also the rest of the characteristics are not drastically affected.

c) Throat gap (d):

Now let us assume B=2.3575λ , t=0.1cm and move onto the next parametric study where we vary the Throat gap (d) near the waveguide. In the earlier cases, d was assumed to be 0.05cm and therefore let us slowly increase'd' from this assumption and study its effect on the E-field pattern. This parametric study will indirectly relate to the study of the ratio parameters $\alpha 1$ and $\alpha 2$ in Chapter 2. 'l' is assumed again to be 10.005λ. Figure 4.6 shows the resultant E-field pattern when the Throat gap is varied from 0.04cm to 0.25cm.

From figure 4.6, it is obvious that when'd' is greater than 0.15cm; the resultant Far-field pattern is drastically changed. The main lobe is altered and higher sidelobes occur due to phase errors. Therefore it is not beneficial to move the plate too far away from the horn flares. This practically makes sense because when the throat gap is large, more power will flow into the two adjacent apertures rather than the central aperture. This will effect the near field distribution in the horn aperture by increasing the parameter $\alpha 2$ and uniform distribution occurs.

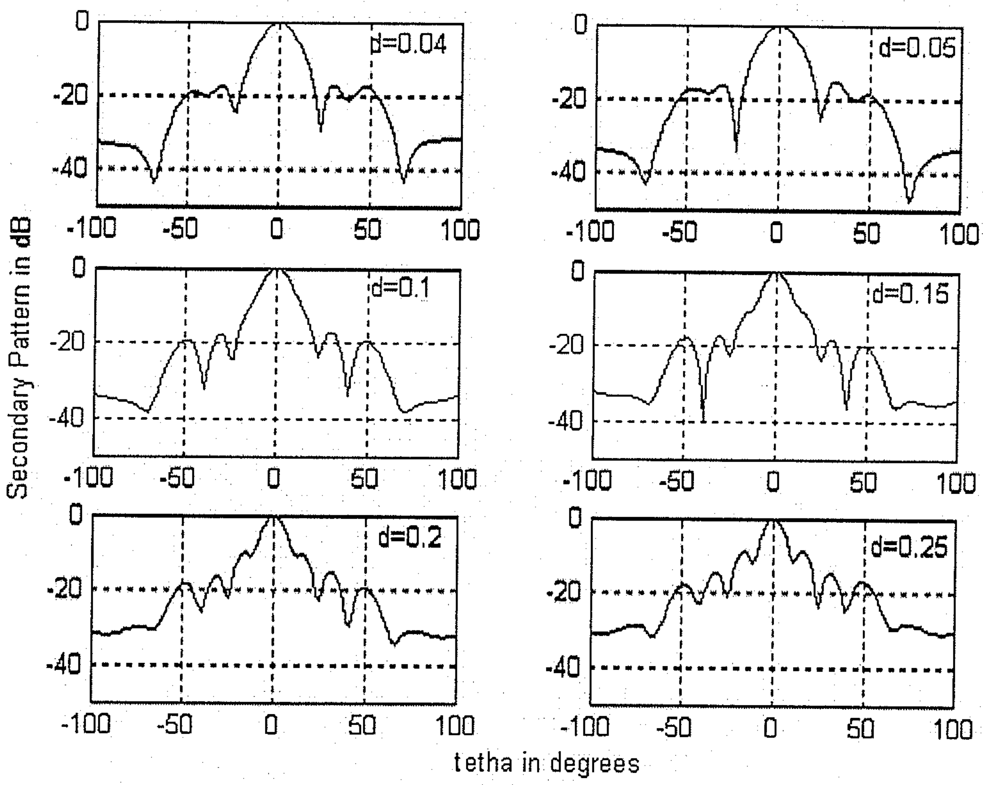

Figure 4.6: Simulated Secondary Patterns for parametric changes in 'd' from 0.04 to 0.25cm, B=2.3575λ , *l=10.005λ and t*=0.1cm.

Also, to achieve excellent characteristics the optimum ratio $\alpha 1/\alpha 2$ should be in-between 1.5 to 2.5 as discussed in Chapter 2. Therefore, let Throat gap d be approximately around 0.05cm for improved results in the E-plane Far-field.

d) Length of the plate (l):

Now, let us vary the parameter length of the plates. Its combination with Throat gap parameter d will give us the similar relation as the ratio parameters $\alpha 1/\alpha 2$.The Plate length was assumed as 10.005λ for the earlier cases i.e. they originated from the waveguide till the aperture of the horn. For this part of the study, let us decrease the length of the conductive plates in terms of λ from the waveguide end and study its effect on the Field pattern. Throat gap d is 0.05cm, t=0.1cm and B=2.3575λ for the entire study. The length of plate (l) is varied from 10.005λ to 7.505λ and its resultant simulated E-field patterns are shown in figure 4.7.

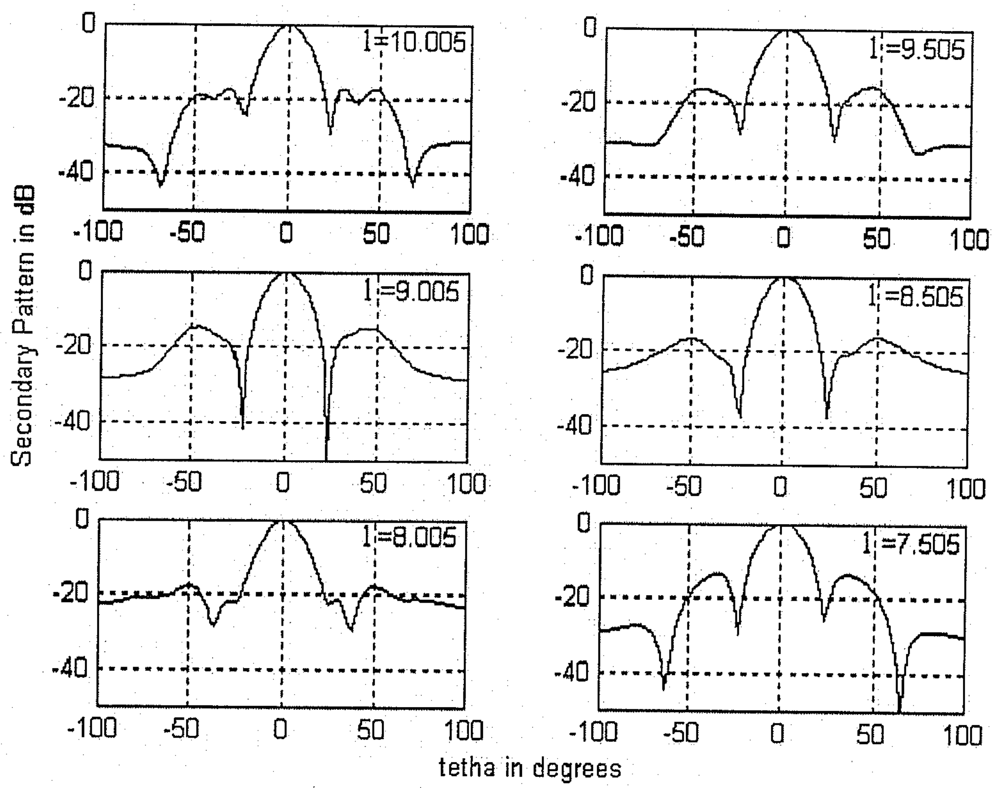

*Figure 4.7: Simulated Secondary Patterns for parametric changes in plate length l is varied from 10.005λ to 7.505λ ,B=2.3575λ ,d=0.05cm and t=*0.1cm.

The obtained patterns in figure 4.7 look promising especially when the plate lengths are around 9.005λ to 8.005λ. As established before the relationship between parameter L and parameter d would be similar to the ratio parameters of $\alpha 1/\alpha 2$.

Therefore, further investigation is necessary to study the affect of these combinational parameters to obtain an optimum result for this type of horn antenna.

Let us carry out a similar parametric study for individual cases of parameter l ranging from 9.005 λ to 8.005 λ. The only difference being that for each of these cases Throat gap d will be varied like its parametric study.

e) Varying Throat gap when l=9.005 λ:

The plate length is 9.005 λ i.e. about 1 λ reduced near the waveguide, t=0.01, B=2.3575 λ. 'd' is initially assumed to be 0.05cm and is gradually increased. The resultant simulated Field patterns in figure 4.8 are cases when d is varied from 0.05cm to 0.3cm.

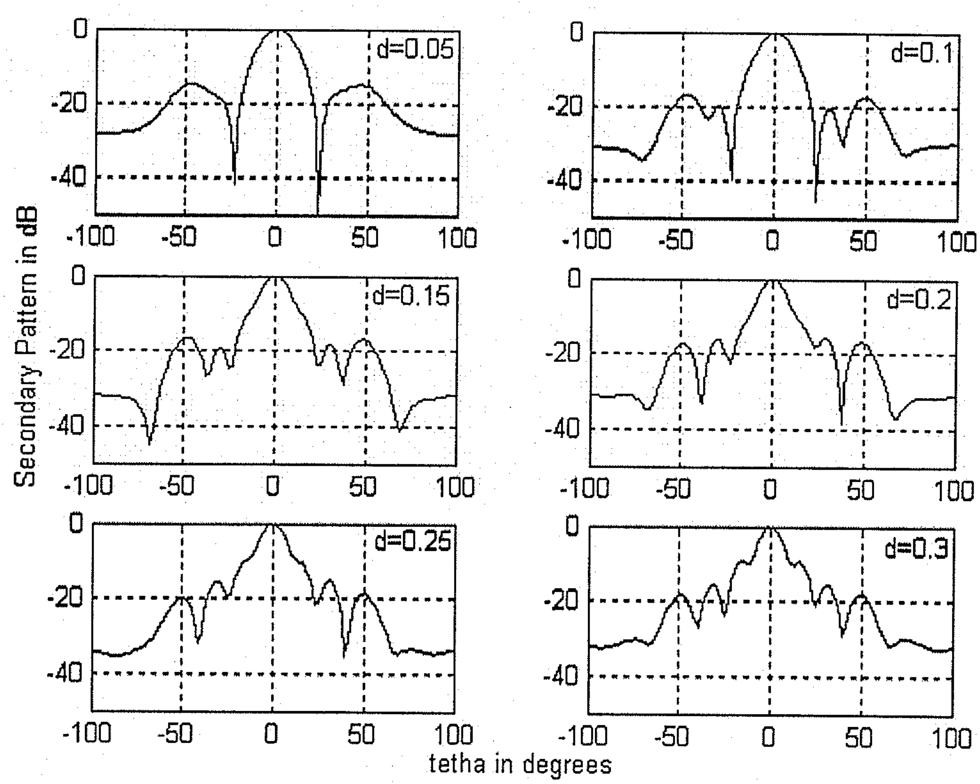

*Figure 4.8: Simulated Secondary Patterns for parametric changes in 'd' when l= 9.005 λ, B=2.3575 λ and t=*0.1cm.

Some interesting results are obtained from figure 4.8. Improved field patterns are obtained when d is in-between 0.1 and 0.15cm. The first side lobe level occurs around or below -20db for these cases. As expected when d is increased to more than 0.25cm the field patterns detoriates and higher side lobes occur.

f) Varying Throat gap when l=8.505 λ:

The same study is repeated except now the plate length is 8.505 λ i.e. about 1.5 λ reduced from the waveguide. Figure 4.9, shows the simulated resultant field pattern when Throat gap d is varied from 0.05cm to 0.3cm.

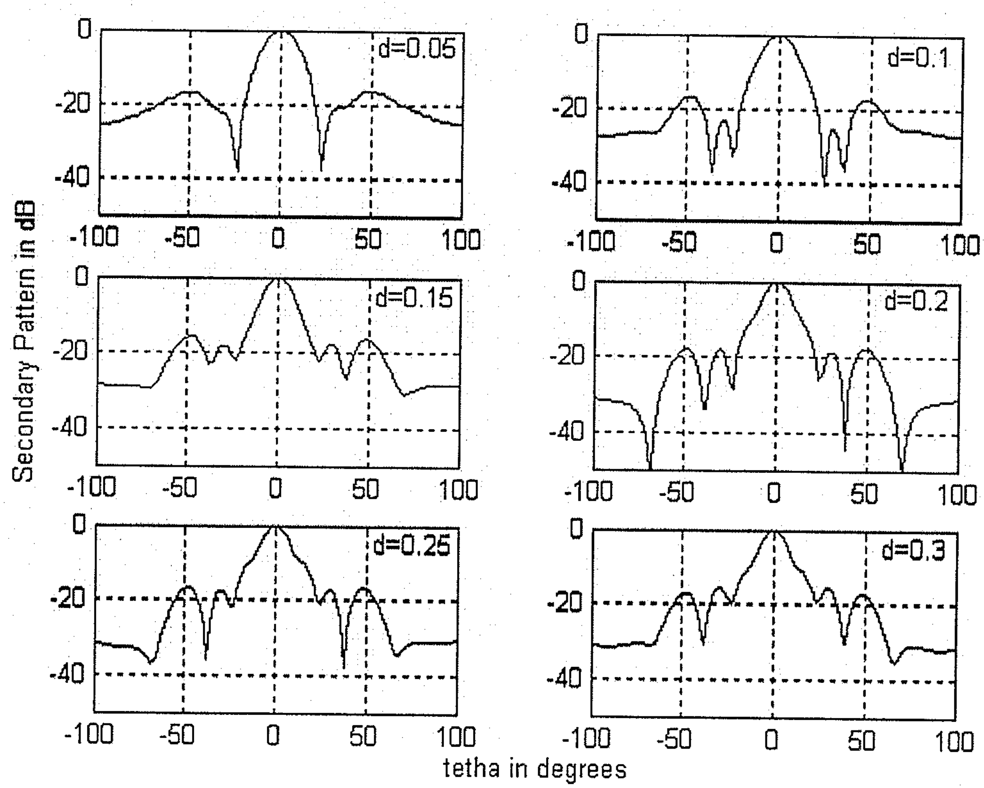

*Figure 4.9: Simulated Secondary Patterns for parametric changes in 'd' when l = 8.505 λ B=2.3575 λ and t=*0.1cm.

Improved results are achieved when d=0.1cm .The First side lobe occurs at around -25dB for this case but the second sidelobe is higher. With relation to the earlier case it is obvious that at d=0.1cm and 0.15cm, better results are obtained in this field pattern.

g) Varying Throat gap when l=8.005 λ :

The plate length is considered about 8.005 λ i.e. about 2 λ reduced near the waveguide. Similar study is repeated and 'd' is varied from 0.05cm to 0.3cm. The resultant simulated field pattern in shown figure 4.10.

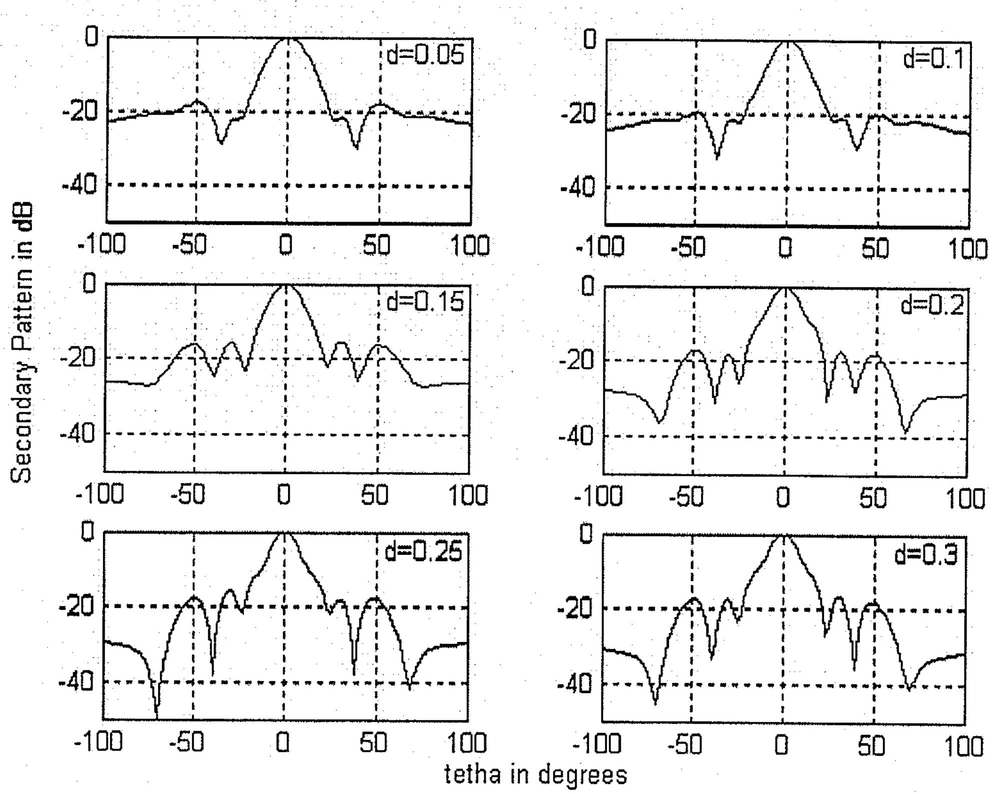

*Figure 4.10: Simulated Secondary Patterns for parametric changes in 'd' when l= 8.005 λ ,B=2.3575 λ and t=*0.1cm.

At d=0.1cm, the first side lobe is below -20db in figure 4.10. It should also be noted that at the case d=0.3cm, the side lobes do not detoriate as the initial cases for this study when l=9.005 λ. The reasoning behind this could be because of the increase in area between the lower plates has the plate length decreases. So the closer they move towards each other, the field pattern is affected drastically.

The above three systematic study gives us a better insight about the effect of the parameters l and d on the Far-field pattern. Optimum result was obtained when l=8.005 λ and d=0.1cm. The sidelobe envelope of the E-field pattern occurs below -20dB for this case. This is an improvement of 11dB from the first sidelobe level of the general pyramidal rectangular horn antenna. The results are comparable to the study of Two-step Staircase distribution in Chapter 2.

4.3 Near Field Study:

The parametric study of pyramidal horn with conductive plates has provided us valuable information regarding the working principle for this type of antenna and verified the aperture theory study in Chapter 2. The far-field characteristics and their side lobe characteristics were extensively analyzed in this study for a pyramidal rectangular Horn antenna.

It is important to look into the Near-field patterns of the modeled antenna to support the Two-step Staircase distributions and its parameters in Chapter 2. The Near-field patterns across the aperture of the antenna can be generated using Ansoft's HFSS.

Only few of the above analyzed cases are considered to discuss the Near-field to verify the theory from Chapter 2.

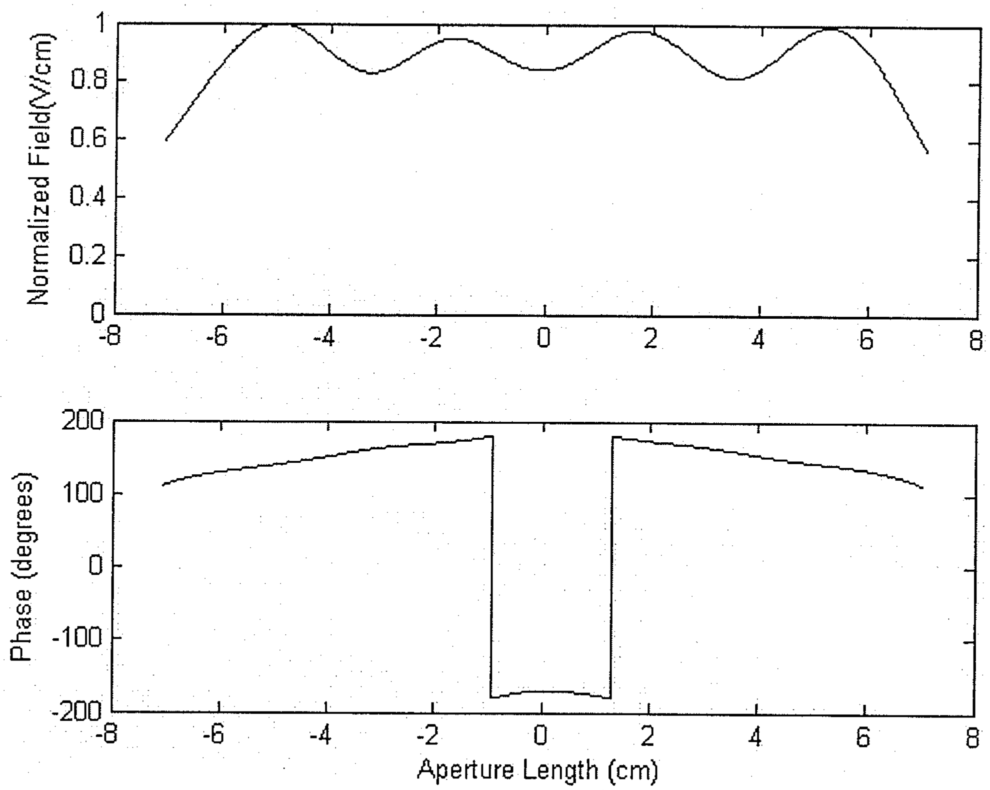

Figure 4.11: Near-Field pattern (Magnitude and Phase) of Pyramidal Horn Antenna without plates.

Figure 4.11 shows the magnitude and phase pattern of the antenna without any plates. The patterns are plotted with respect to the aperture dimension in cm (4.715λ=14.145cm). It is obvious to note from the normalized magnitude pattern that uniform field distribution occurs throughout the aperture. The uniform field across the aperture causes the higher sidelobes in the E-field of the horn. The field in figure 4.11 has some minor ripples instead of total uniformity and some asymmetry. This may be caused due to the error percentage in the simulations using HFSS. The field accuracy was set to 2% and with a convergence rate of 0.02., Even with the increase in accuracy and convergence rate, similar results were achieved.

The phase plot in figure 4.11 has the phase at -170 at the center of aperture and around 110 near the ends of the aperture. The phase jumps from -180 to 180 in the plot because of the phase cycle. Therefore, between the edges to the centre of the aperture there is a phase change of 80°.

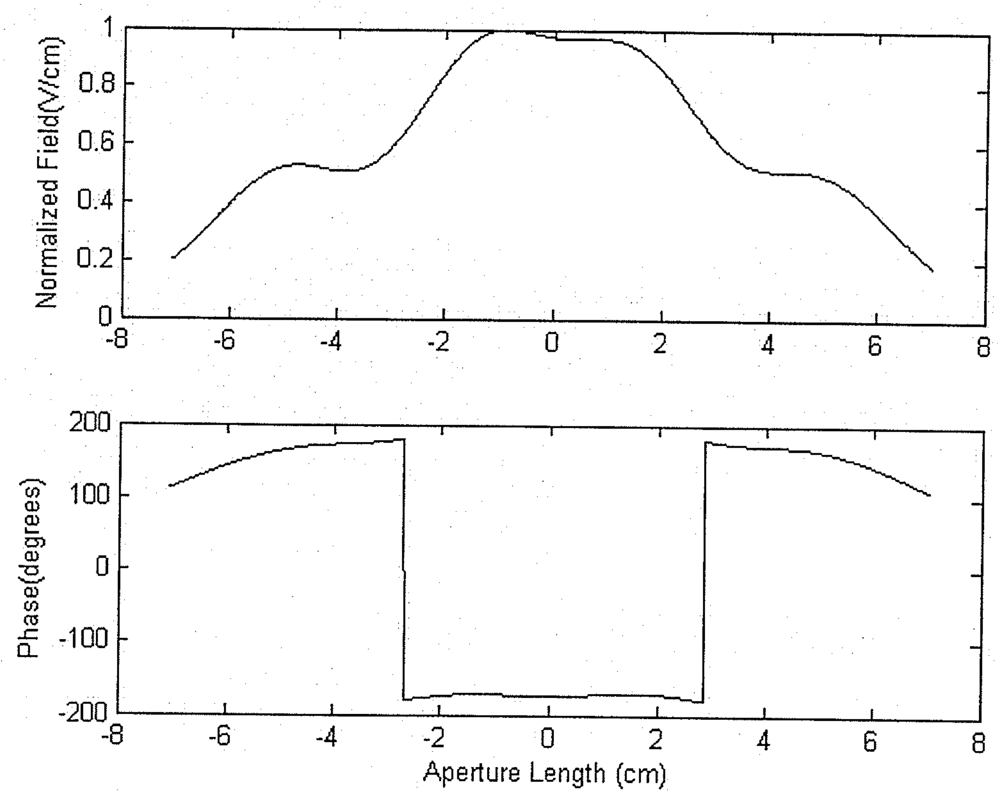

Figure 4.12: Near-Field pattern (Magnitude and Phase) of Horn Antenna with two conductive plates (B=2.3575λ, d=0.01cm, l=8.005λ)

The magnitude and phase pattern of the antenna with two conductive plates with parameters B=2.35λ, d=0.01cm, l=8.005λ is shown in figure 4.12. This design resulted in one of the best achieved patterns. As seen the magnitude plot there exists some asymmetry and this could be caused due to the simulation error in the software. The magnitude plot is similar to a Two-step Staircase distribution defined in Chapter 2. The change in the field distribution is exactly similar to the parameter B (2.35λ=7.0725cm). The field plot confirms the theory that the conductive plates alter the uniform distribution to a two-step distribution, hence resulting in improved results at the Far-field pattern of the antenna.

The phase plot is very similar to the previous case and the phase change between the edges to the centre is about 75°.The plot is broader than the previous discussed case.

The near-field study confirms the theory about the effect of the plates on the uniform field at the aperture. The field obtained in figure 4.12 is very similar to the Two-step Staircase distribution introduced in Chapter 2. This validates the parameters established in the parametric study of Chapter 2.

4.4 Septum Horn Antenna with four conductive plates:

In chapter 3, Cosine and Cosine-square distribution was synthesized using Two and Three-step Staircase distributions. The Three-step Staircase distribution means practically four conductive plates have to be introduced into the horn aperture. The only limitation of introducing four or more plates into the aperture will results in impedance problems near the waveguide.

From the synthesis of Cosine-square distribution in chapter 3, an optimum result was obtained when $B=3\lambda$, $C=1.5\lambda, \alpha1=0.2, \alpha2=0.5, \alpha3=0.2$. C will be the distance between the two new conductive plates introduced in the aperture. The throat gap parameter d was assumed as 0.1cm and the similar parameter for the new plate was assumed as 0.2cm. Using these design parameters, four conductive plates were introduced and the antenna was modeled in HFSS.

Figure 4.13 shows the far-field characteristics for the antenna with four conductive plates. A first sidelobe around -22dB is achieved. This result is not very similar to the first sidelobe of -32 dB achieved in the synthesis of Cosine-square distribution due to phase errors in the horn antenna design. This antenna design has excellent characteristics with low-cross polarization.

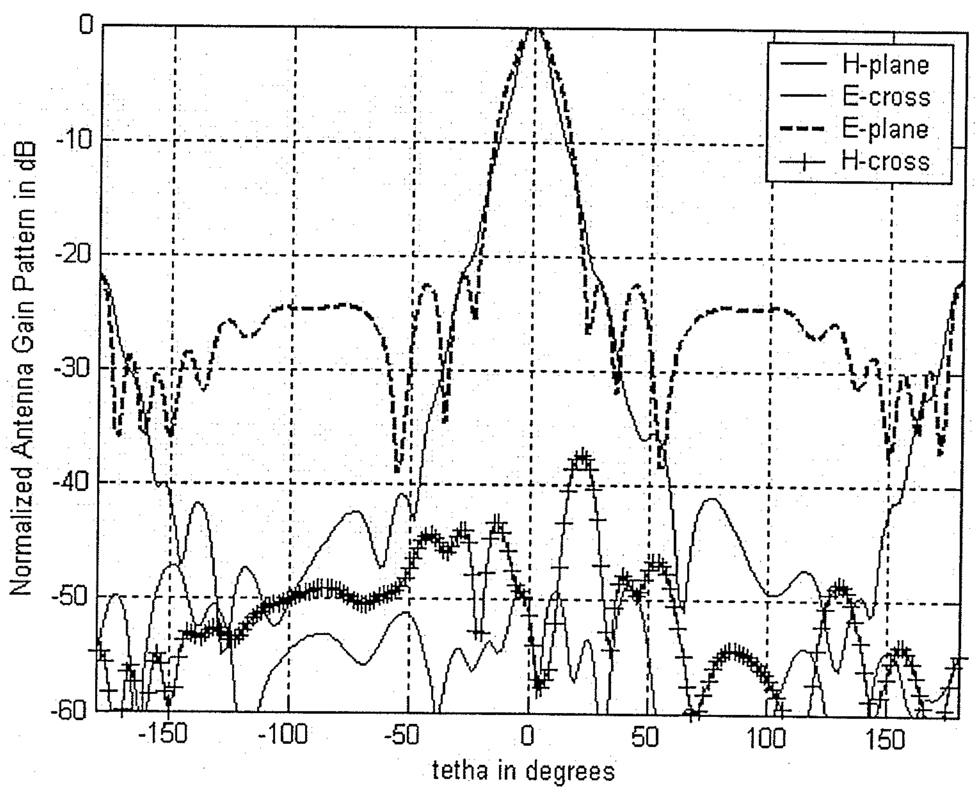

Figure 4.13: Far-Field pattern of Rectangular Horn Antenna with four conductive plates A=4.7 λ, $B=3\lambda$, $C=1.5\lambda$, $\alpha 1=0.2$, $\alpha 2=0.5$, $\alpha 3=0.2$.

4.5 Antenna Measurement Results:

An E-plane horn antenna with two sets of conductive plates was designed and fabricated at the University of Manitoba. The dimensions of the horn are: a=2.286cm, b=1.016cm (waveguide WR90), a_1=2.286cm, b_1= 3.81cm, p_e=10.16cm (E-plane). Copper was used to fabricate the horn. Multiple holes were drilled in the horn flare to hold the conductive plates. The holes were drilled to hold a screw of diameter 0.21844 cm. The design frequency was 10 GHz. The dimensions are different than the one discussed in the previous pyramidal horn design.

Two sets of conductive aluminum plates were fabricated. The length of one pair of the plates was L_1=10.16cm. The other pair had the length L_2 =7.62cm (3/4 L_1). Holes were drilled in the plates on both the sides and near the edges to hold the screws. The designed plates had a thickness of 0.3175cm. The thickness of the plates used in the parametric study of pyramidal horn was 0.1cm. The reason for using a thicker plate was because of the availability and time considerations to make the thinner design. When the thickness of the plates was greater than 0.3 cm, the simulated results were not desirable. Therefore, to limit the thickness the plates were sharpened at the edges. The plates were exactly filed from 0.635cm to the tip. The thicknesses of the tips were 0.1397cm in all the plates and on both sides.

The holes were drilled in such a way that for both the plates d =0.1cm. Multiple holes were drilled near the horn radiation aperture so as to vary the length between the plates (B).

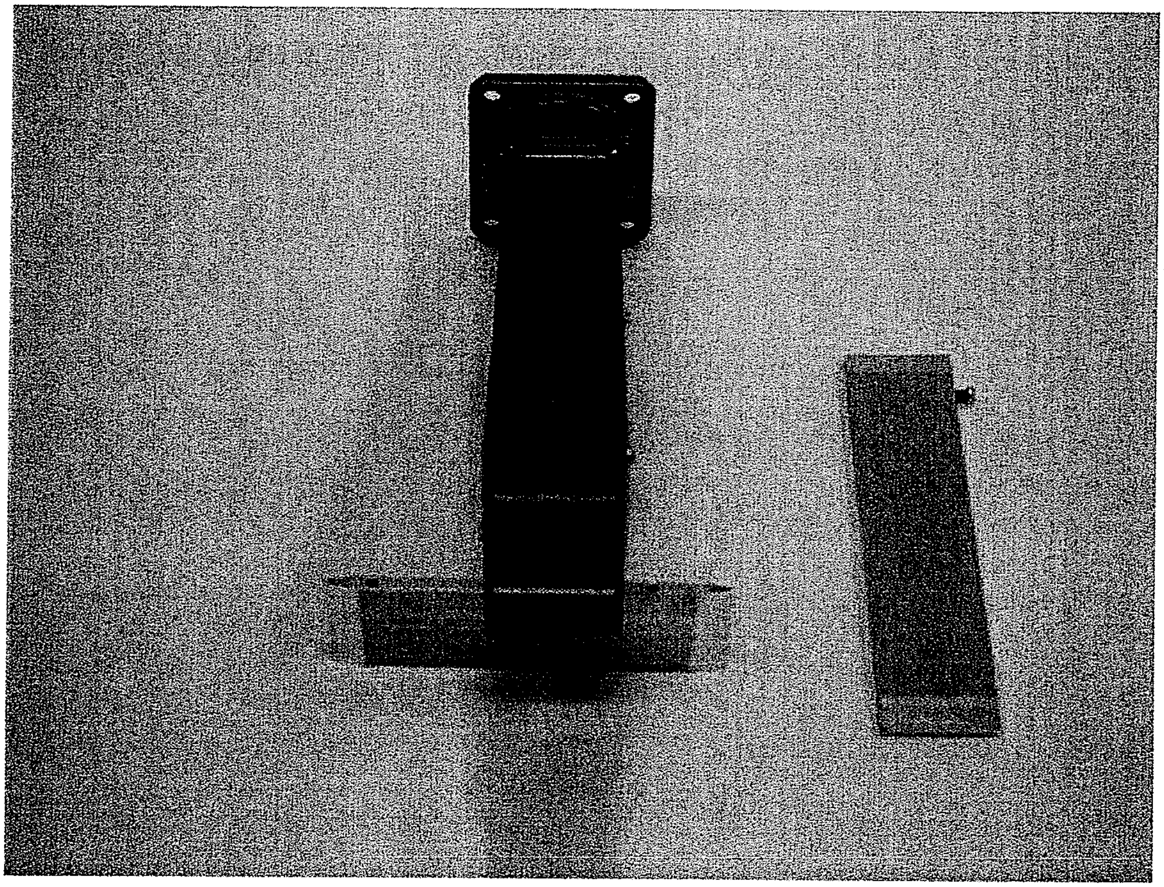

Figure 4.14: Fabricated E-plane Horn Antenna with 2sets of Aluminum plates

a=2.286cm, b=1.016cm, a_1= 2.286cm, b_1=3.81cm, p_e=10.16cm.

The fabricated antennas with plates placed across the aperture were tested for far-field radiation pattern using the equipment in the Far Field Anechoic Chamber in the Antenna laboratory. Many cases were tested but primarily three measured results for the far field radiation patterns are discussed in the following sections. The three cases are

1. E-plane Horn without any plates
2. E-plane horn with two aluminum full plates (L_1=10.16cm ,d=0.1cm,B=1.76cm)
3. E-plane horn with two aluminum ¾ plates (L_2 =7.62cm ,d=0.1cm,B=1.76cm)

Their measured results are compared with their simulation results. The E–plane horn was also modeled and simulated using HFSS for all the above discussed cases. It is found that a good agreement is achieved between them. The measured results validate the simulated results.

a) Case 1: E-plane Horn without any plates

The E-plane horn is tested without any plates in the aperture. The measured E-fields with comparison to its respective simulated results are shown in figure 4.14. The measured and simulated E-field plots have good agreement. There is a small noticeable shift of 1.5 dB at the first sidelobe between them. Both have typical characteristics of uniform distribution with -13dB sidelobes.

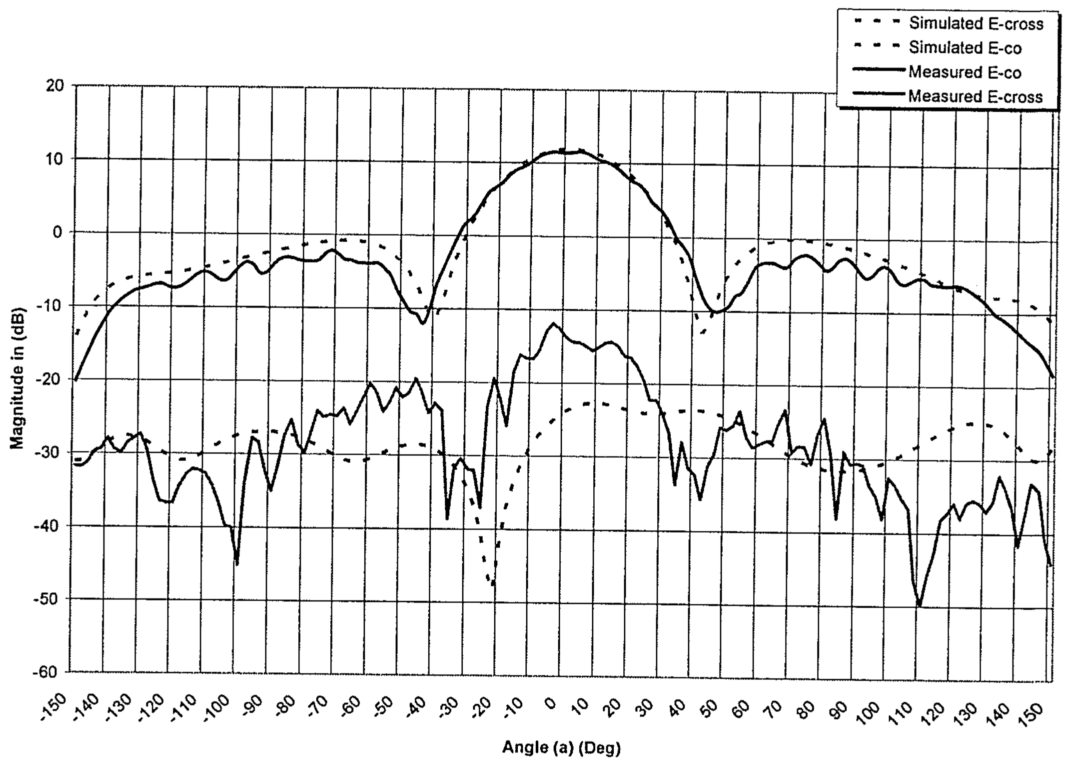

Figure 4.15: Comparison of Simulated and Measured E-co and E-cross pattern for the Fabricated E-plane Horn Antenna without any plates a=2.286cm, b=1.016cm, a_1= 2.286cm, b_1=3.81cm, p_e=10.16cm.

The cross-pol pattern for the measured data shows about 23.25dB below the main lobe of the E-plane pattern. The simulated data shows better results. Another important factor to note is the non-existence of any kind of ripples in the simulated E-field pattern. The convergence was set to 0.02 and field accuracy to 2% during the simulation. There wasn't any change in the sidelobes for lower convergence and accuracy values. There is a small increase in first sidelobe level in the simulate pattern when compared to the measured pattern in the E-plane.

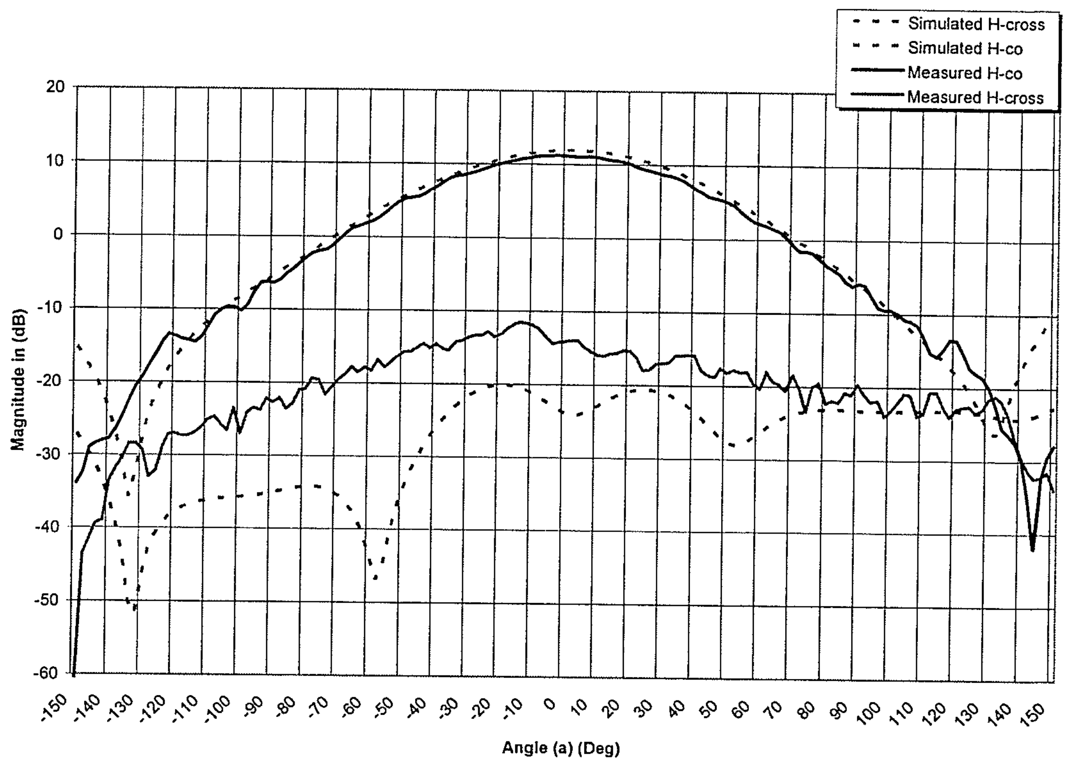

Figure 4.16: Comparison of Simulated and Measured H-co and H-cross pattern for the Fabricated E- Horn Antenna plates a=2.286cm, b=1.016cm, 2.286cm, b_1=3.81cm, p_e=10.16cm.

The measured H-field results with comparison to its respective simulated fields are given in figure 4.15. The measure cross-pol is 22.5 dB below the measured H-plane.

The H-plane simulated results have good agreement with the measured results with approximately 1dB increase at the peak. The measured S11 and Return loss for this antenna for a frequency bandwidth of 9.5-10.5 GHz is shown in figure 4.17. The respective E-co pattern is shown in figure 4.18.

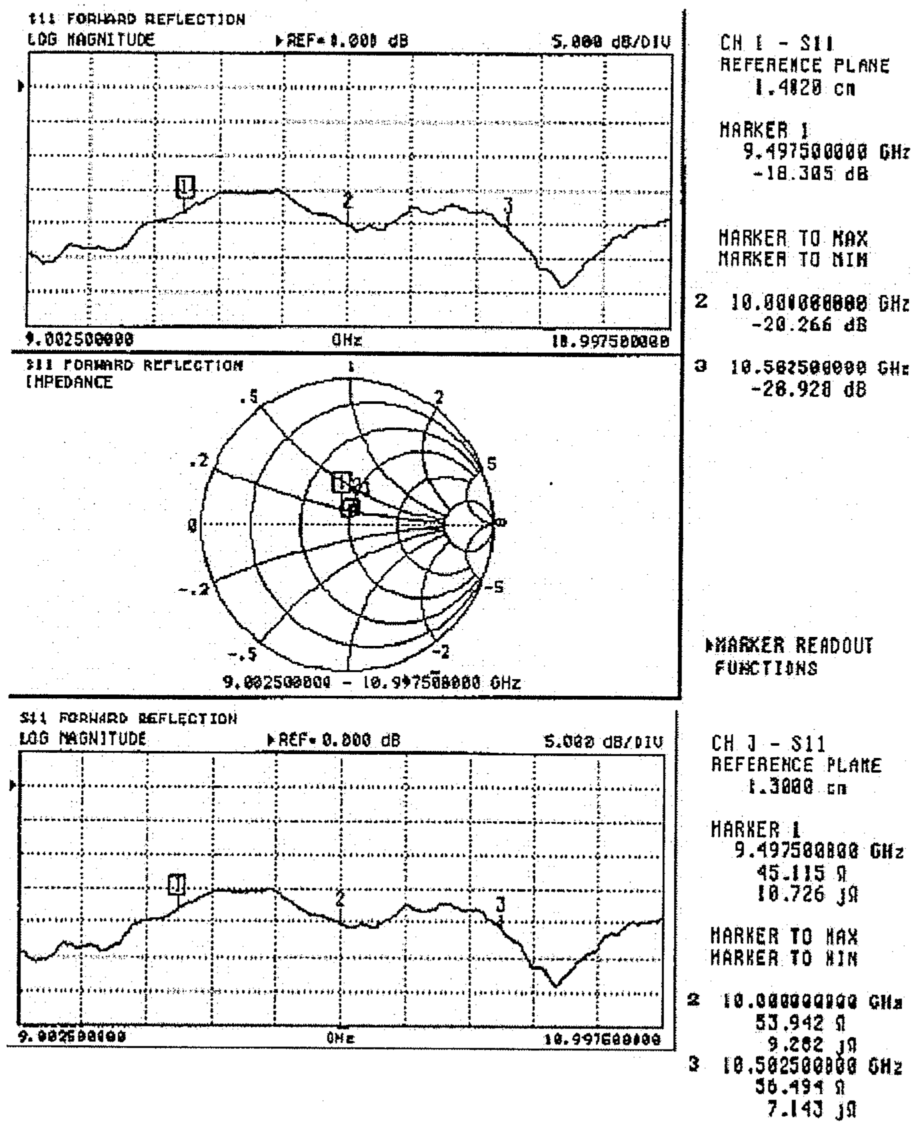

Figure 4.17: Measured S11 and Return loss Fabricated E- Horn Antenna without plates for (9.5 to 10.5 GHz) a=2.286cm, b=1.016cm, 2.286cm, b_1=3.81cm, p_e=10.16cm.

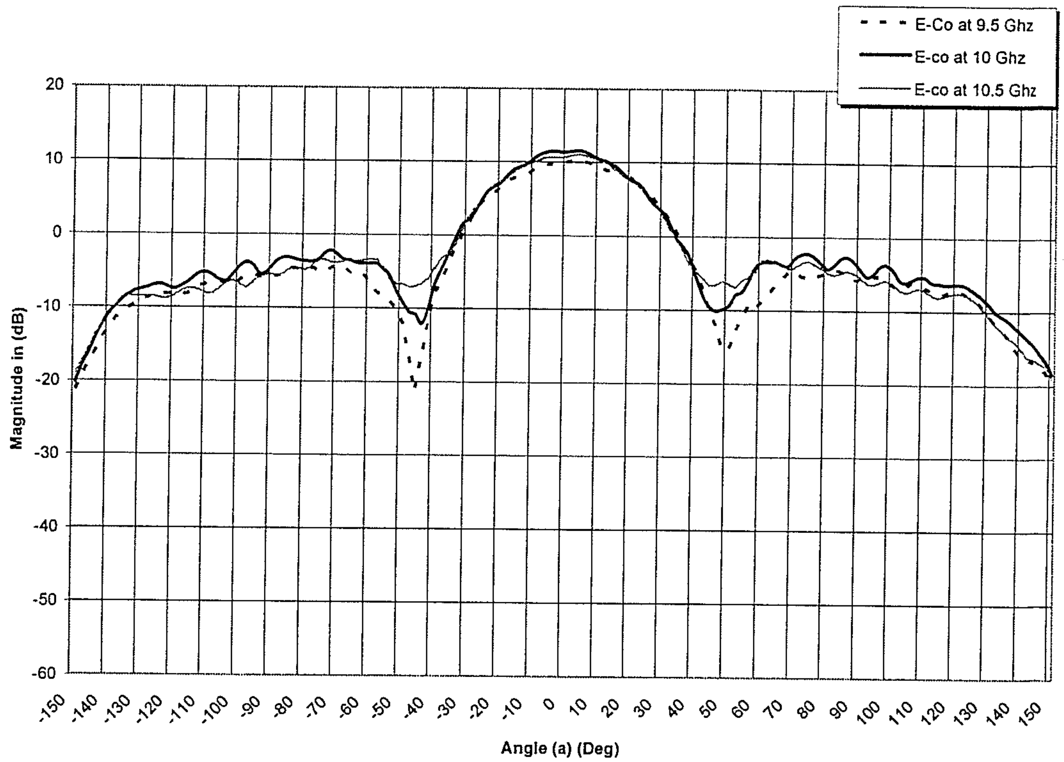

Figure 4.18: Measured E-co pattern for Fabricated E- Horn Antenna without plates for (9.5 to 10.5 GHz) a=2.286cm, b=1.016cm, 2.286cm, b_1=3.81cm, p_e=10.16cm.

b) **Case 2: E-plane horn with two plates (L_1=10.16cm, d=0.1cm, B=1.76cm)**

The E-plane horn is tested with two conductive aluminum plates. The plates are arranged in such a way that they have a throat gap of 0.1cm and separate the horn aperture exactly by 1.76cm. From figure 4.16, it is obvious that there is a shift in the simulated E-co pattern. The peak does not occur at 0° and there exists considerable asymmetry in the measured results.

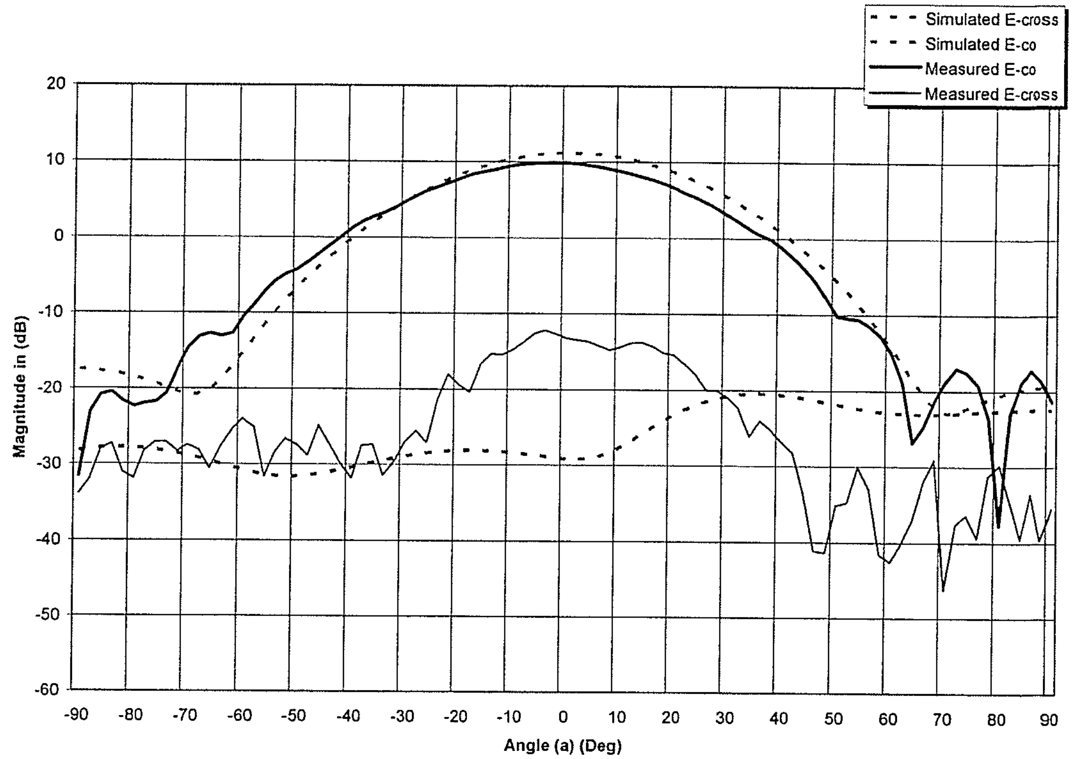

Figure 4.19: Comparison of Simulated and Measured E-co and E-cross pattern for the Fabricated E- Horn Antenna with two full length conductive plates a=2.286cm, b=1.016cm, 2.286cm, b_1=3.81cm, p_e=10.16cm, L_1=10.16cm, d=0.1cm and B=1.76cm

The sidelobe formulation is ambiguous. The simulated E-co pattern has a first sidelobe of -28dB occurring around 90°. The measured E-co pattern is more complicated has it looks like the first side lobe has merged with main lobe at around 60°. But if we consider the first sidelobe with respect to the Simulated E-co pattern, than we can consider the first sidelobe near 75°. This will give a first sidelobe of about -28dB exactly similar to the simulated result. The Measured and simulated H-cross pattern are well below 20dB to the H-plane pattern.

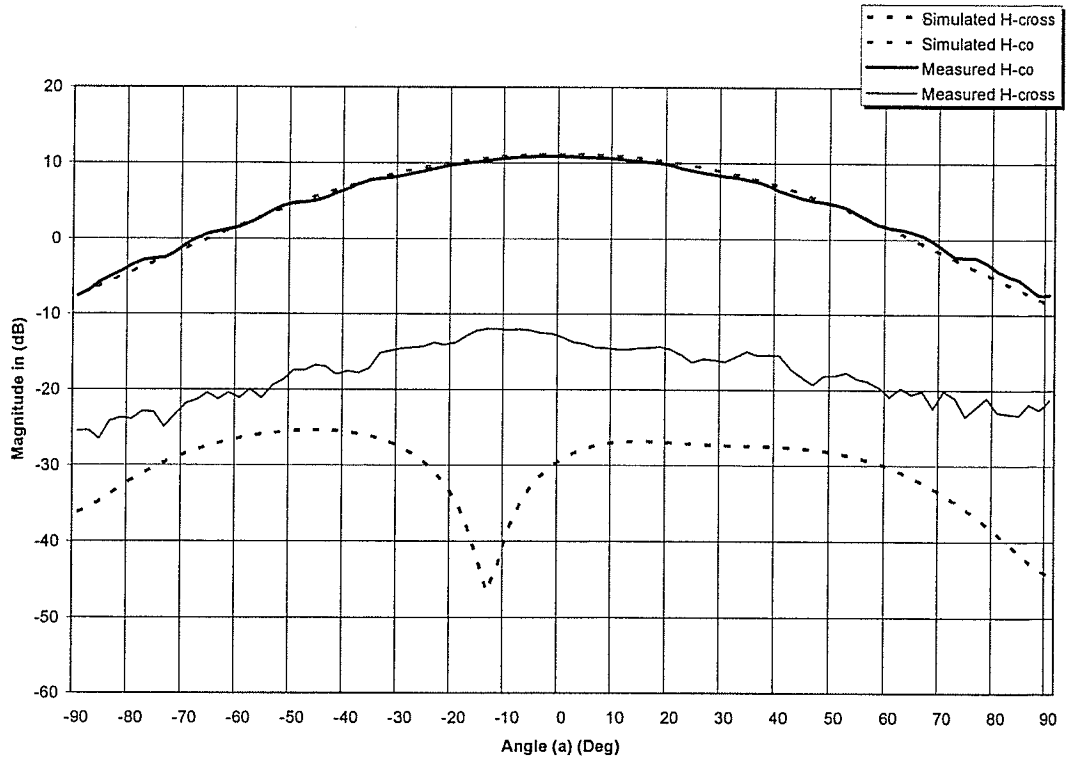

Figure 4.20: Comparison of Simulated and Measured H-co and H-cross pattern for the Fabricated E- Horn Antenna with two full-length conductive plates a=2.286cm, b=1.016cm, 2.286cm, b_1=3.81cm, p_e=10.16cm, L_1=10.16cm, d=0.1cm and B=1.76cm.

The H- co measured pattern looks very similar to the H-co simulated pattern. The cross patterns are also well below 20dB than their respective H-co patterns for both the measured and simulated cases. The measured S11 and Return loss for this case for a frequency bandwidth of 9.5-10.5 GHz is shown in figure 4.21. The respective E-co pattern is shown in figure 4.22. There is a shift in the E-co pattern for different cases of the patter.

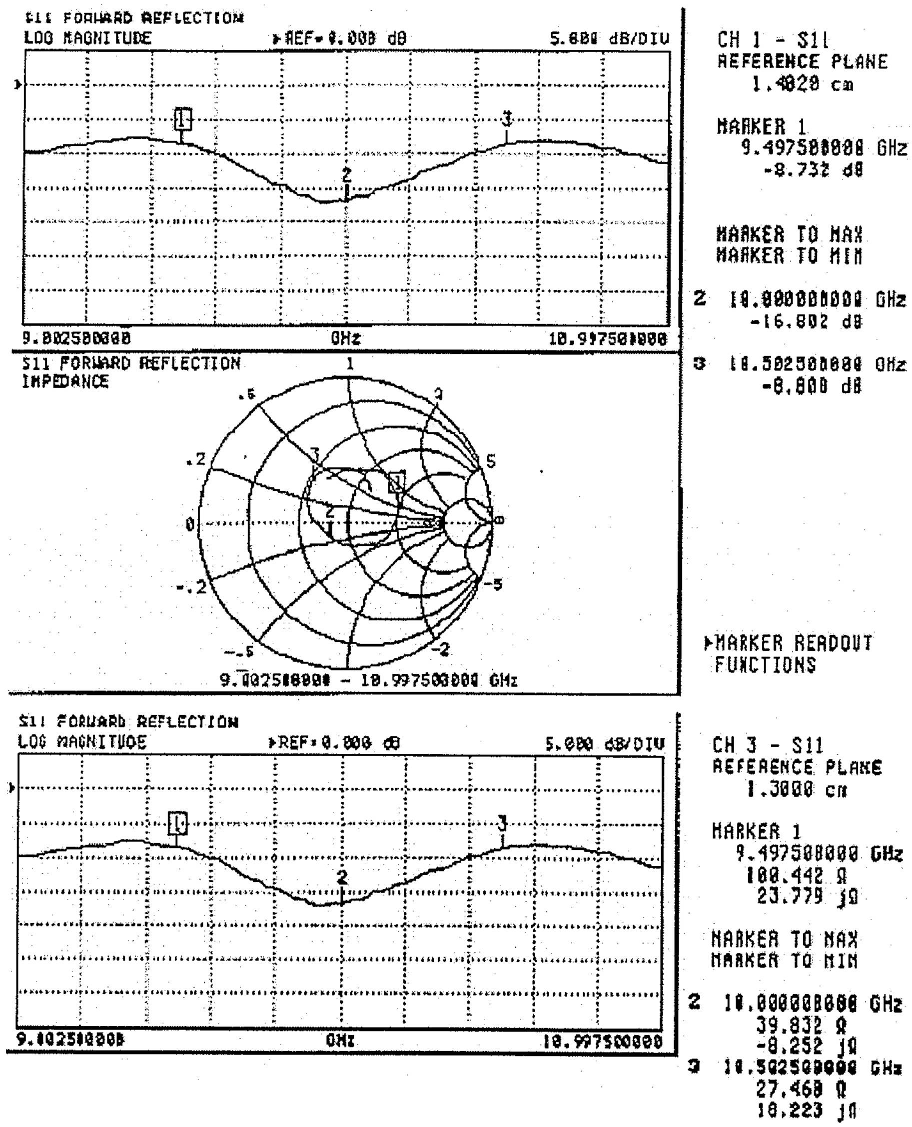

Figure 4.21: Measured S11 and Return loss Fabricated E- Horn Antenna with full plates for (9.5 to 10.5 GHz) a=2.286cm, b=1.016cm, 2.286cm, b_1=3.81cm, p_e=10.16cm, L_1=10.16cm, d=0.1cm and B=1.76cm.

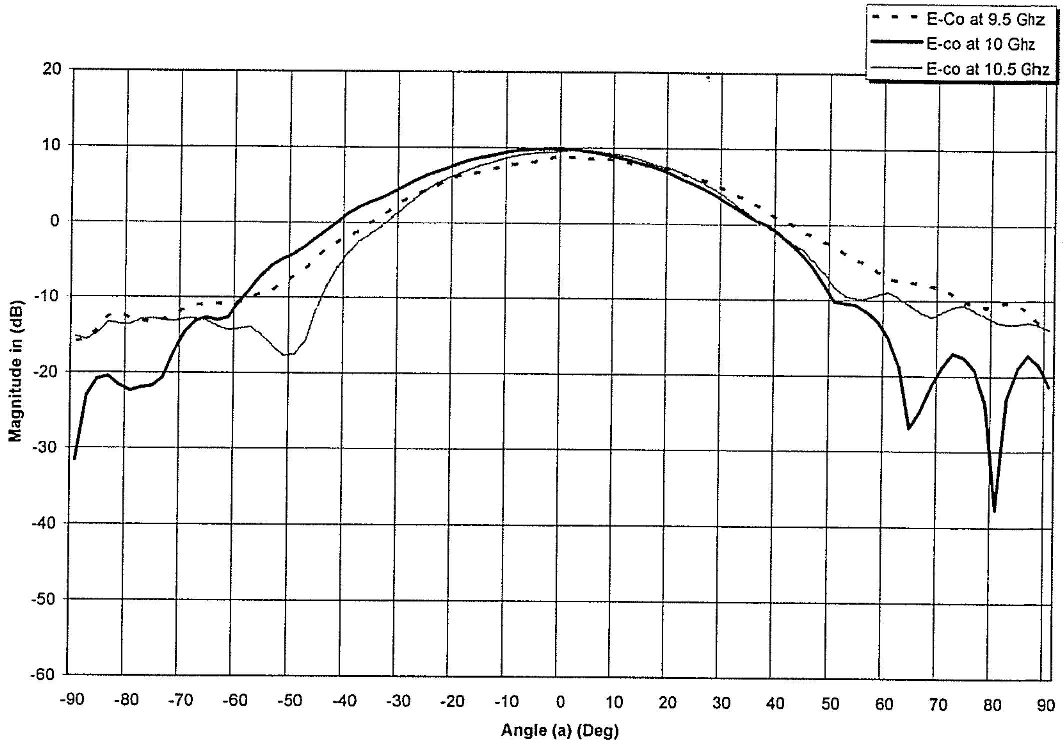

Figure 4.22: Measured E-co pattern for (9.5-10.5 GHz) Fabricated E- Horn Antenna with full plates for (9.5 to 10.5 GHz) a=2.286cm, b=1.016cm, 2.286cm, b_1=3.81cm, p_e=10.16cm L_1=10.16cm, d=0.1cm and B=1.76cm.

c) **Case 3: E-plane horn with two plates (L_2 =7.62cm, d=0.1cm, B=1.76cm)**

The E-plane horn is tested with two conductive plates with length 7.62 cm placed across its aperture symmetrically. The throat gap is set by the holes drilled in such a way that the plates are placed 0.1cm from the horn flare.

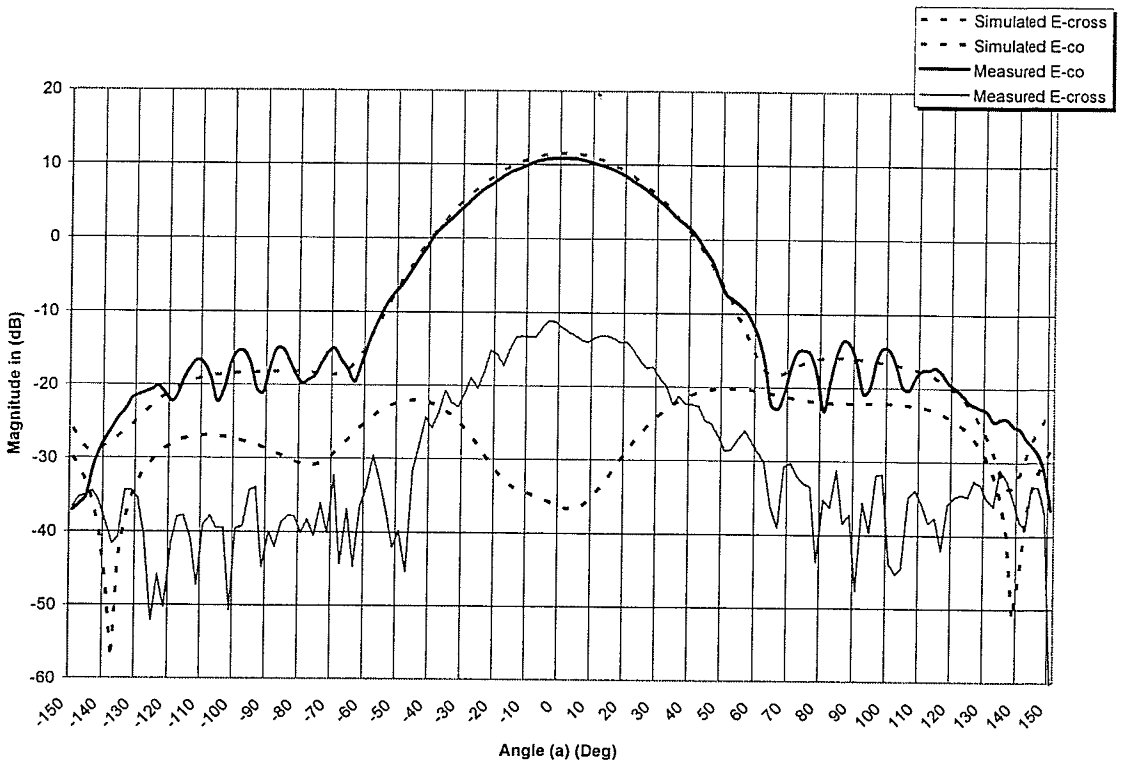

Figure 4.23: Comparison of Simulated and Measured E-co and E-cross pattern for the Fabricated E- Horn Antenna with two ¾ length conductive plates a=2.286cm, b=1.016cm, 2.286cm, b_1=3.81cm, p_e=10.16cm, L_2 =7.62cm, d=0.1cm and B=1.76cm.

Both the simulated and measured results have excellent agreement in the E-co pattern. They are almost similar except for the sidelobe ripples in the measured data. The first sidelobe level occurs -25dB below the main lobe. E-cross below 20dB is achieved from the main E-co plot.

The simulated H-co plot is slightly higher at the peak value than the measured E-co plot. But the case reverses as we move away from the centre. The H-cross plot is below 20dB to the H-co for both the plots.

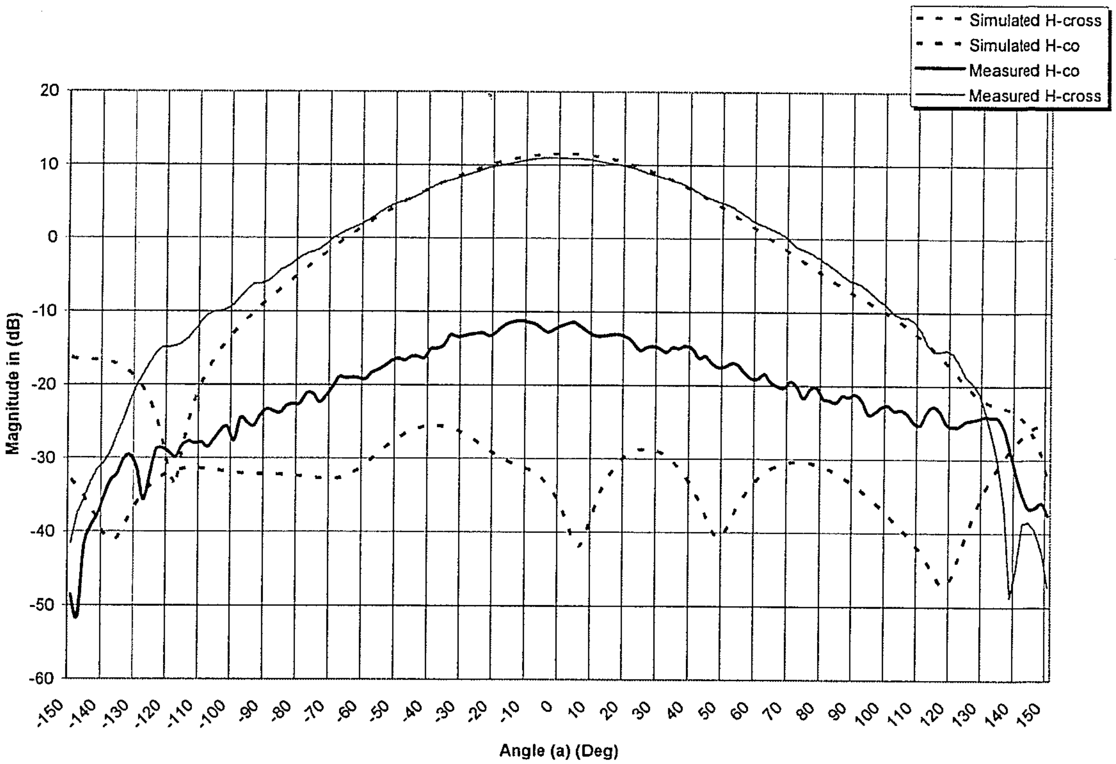

Figure 4.24: Comparison of Simulated and Measured H-co and H-cross pattern for the Fabricated E- Horn Antenna with two ¾ length conductive plates a=2.286cm, b=1.016cm, 2.286cm, b_1=3.81cm, p_e=10.16cm, L_2 =7.62cm, d=0.1cm and B=1.76cm.

The comparison of simulated E and H-cross and measured E and H-cross is difficult in most of the cases as they are both well below 30dB and the accuracy of the software is 2%. Therefore, the error increases in plots below 20dB considerably. It is also noted that case 2 was measured for an angle of rotation between -90° to 90°.In the plots of the measured results where the angle is between -150° to 150°, the measured data after -120° till -150° and 120° till 150° will have major drop off or inaccurate values. This occurs because the design antenna which works as a receiver in the anechoic chamber moves out of range from the transmitting antenna range.

The measured S11 and Return loss for this case for a frequency bandwidth of 9.5-10.5 GHz is shown in figure 4.25. The respective E-co pattern for this range is shown in figure 4.26.

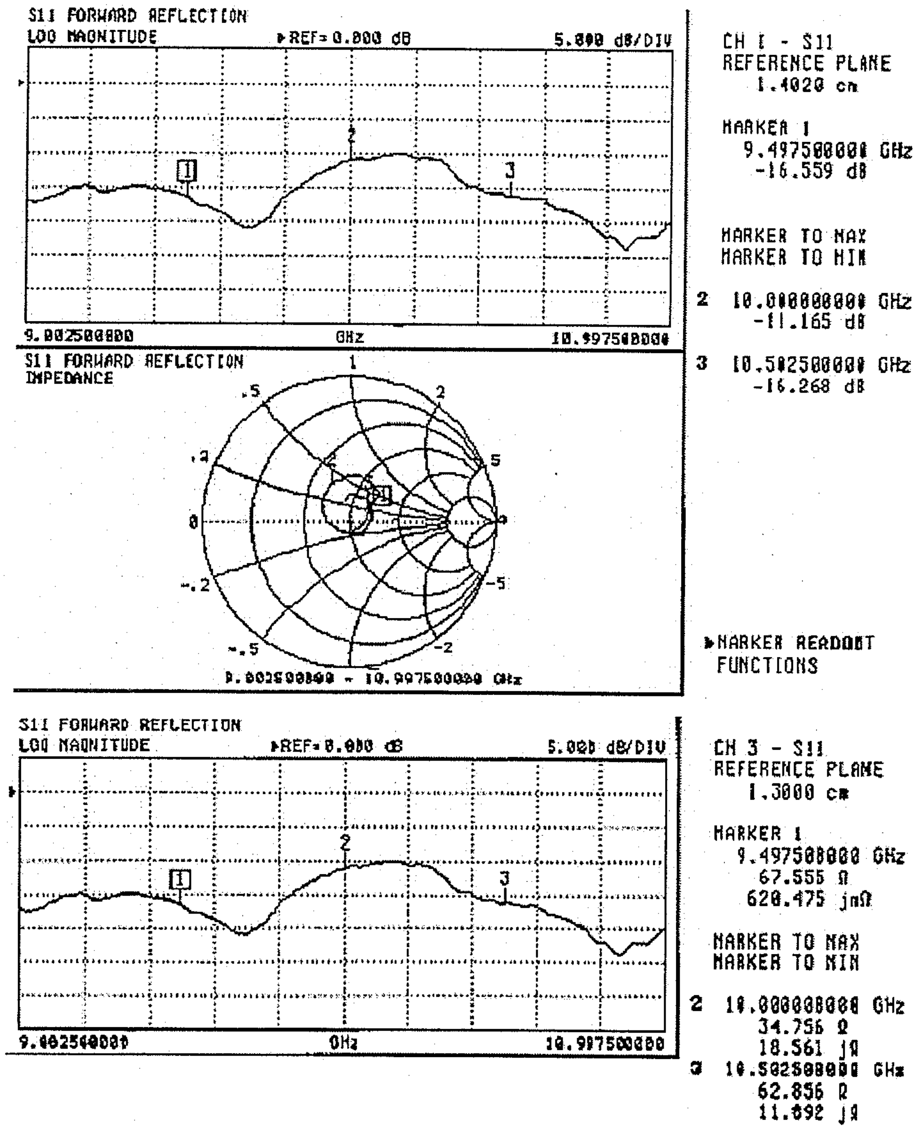

Figure 4.25: Measured Return loss Fabricated E- Horn Antenna with full plates for (9.5 to 10.5 GHz) a=2.286cm, b=1.016cm, 2.286cm, b_1=3.81cm, p_e=10.16cm, L_2 =7.62cm, d=0.1cm and B=1.76cm.

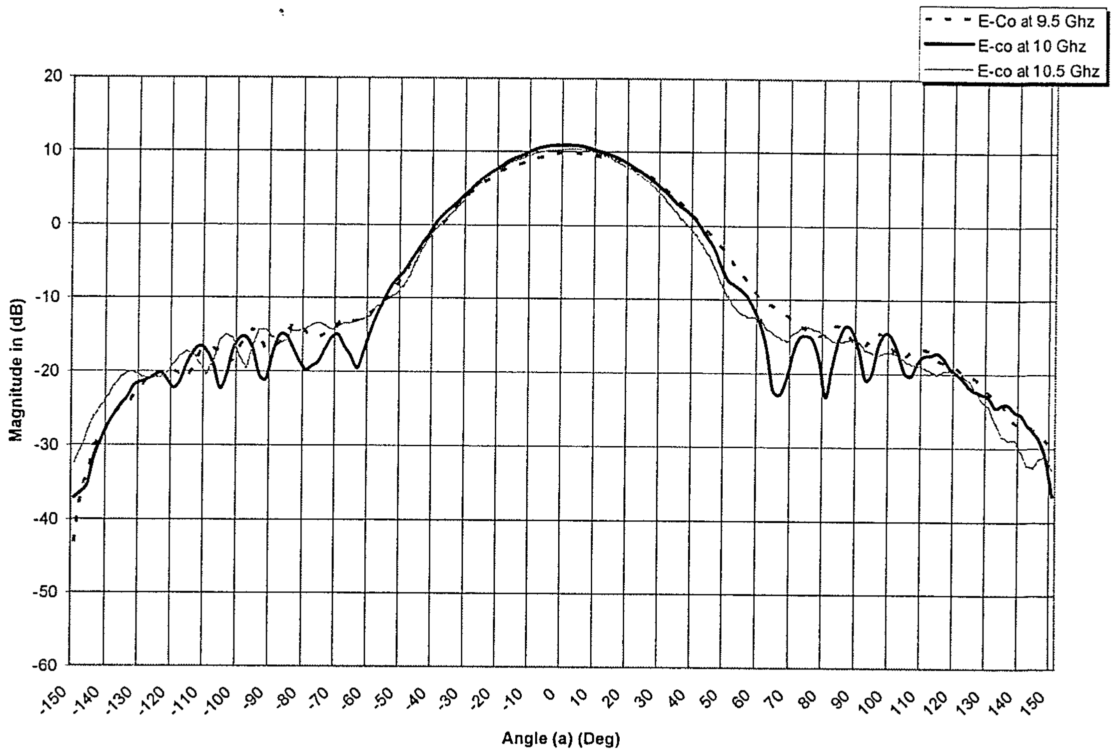

Figure 4.26: Measured E-co pattern for 9.5-10.5 GHz

Fabricated E- Horn Antenna with two ¾ length conductive plates a=2.286cm, b=1.016cm, 2.286cm, b_1=3.81cm, p_e=10.16cm, L_2 =7.62cm, d=0.1cm and B=1.76cm.

4.6 Summary

Chapter 4 discussed in detail a parametric study of the pyramidal septum horn using Ansoft HFSS. This study was conducted using the theory from Chapter 2 and the introduction of Two-step Staircase Distributions. From this study, the effect of the parametric changes in the plates on the field characteristics was investigated and the optimum parametric values were noted. For the pyramidal horn design, the optimum ranges of the plate's parameter are.

- Throat gap =0.05-0.15cm
- Central Aperture=2.3 λ -2.4 λ
- Length of plate= 8.005 λ -9.505 λ
- Thickness of plate = 0.05-1.5cm

The Field characteristics of the rectangular pyramidal antenna were studied with respect to these parameters and a first sidelobe of -20dB was obtained. This is an improvement of 11dB from the pyramidal horn without any plates. Also, the near field was generated for a few cases from HFSS and was compared with the Two-step staircase distribution from Chapter 2. The theory of step function amplitude distributions introduced in Chapter 2 was validated by this comparison. The parameters established in Two-step Staircase distribution were verified. Therefore, using the study and parameters in chapter 2 it is possible to achieve the desired radiation pattern on the septum horn antenna. The synthesized parameters from the Cosine-square distribution were used to model a four plate pyramidal septum horn. A first side lobe of -22dB was achieved for this case

An E-plane horn was designed and fabricated in University of Manitoba. The antenna was tested in the antenna laboratory and its measured results were compared to the simulated results. This comparison also verifies the accuracy of the simulation software. A good agreement between the simulated and measured results was obtained.

Chapter 5

Conclusion

In this thesis the performance of pyramidal septum horn was investigated. A detailed parametric study was conducted on the effect of the plates on the horn antenna and on its far field characteristics. This study provided optimum parameters and a better insight into its working principle. Using the aperture theory, uniform amplitude distributions across the aperture were studied and simplified equations were deduced for generating the secondary patterns. The effect of the plates on the uniform distribution across the horn aperture was deduced and a Two-step Staircase distribution was introduced.

A correlation was achieved between the parameters from the Two-step Staircase distributions and the physical parameters of the plates introduced into the pyramidal horn (septum horn). Using aperture theory, an extensive study about the effects of the parameters from the Two-step Staircase distribution on the secondary pattern was carried out. This study provides the optimum parameters in the Two-step Staircase distribution which will enhance the respective field distribution of the antenna. Therefore, we can directly characterize the position or type of plates in the horn aperture and its effect on the radiation properties.

Also, many desirable distributions like Cosine, Cosine-square and Taylor with enhanced field characteristics were synthesized using the Two-step and Three-step Staircase distributions and their parameters were used in the pyramidal septum horn to achieve improved field patterns. This synthesis technique provides the range of parameters for enhancing the field characteristics of the septum horn, but more importantly it is a simple technique which can be used to synthesize any other distribution to acquire its desirable properties.

The optimum parameters from the Two-step Staircase distribution study were used as initial assumptions in the parametric simulation study of the septum pyramidal horn. The simulations were carried out using Ansoft's HFSS. The computed results from the simulation were comparable to the results from the amplitude distribution study. The simulation systematic study imposed the actual range of parameters for optimum characteristics. The optimum parameters provided significant improvements in the sidelobes of the respective antenna secondary patterns. A first sidelobe of -20dB was achieved for the case when B=2.3575 λ, L=8.005 λ and d=0.1cm in the septum horn with two symmetric plates across its aperture. This is an improvement of 11dB compared to the first sidelobe level achieved by the pyramidal horn without any plates.

The synthesized parameters from the Cosine-square distribution using Three-Step staircase method were introduced in a 4-plate pyramidal septum horn. Using HFSS, a first sidelobe of -22 dB was achieved compared to the actual -32 dB from the synthesis.

Furthermore an E-plane horn was fabricated and measured from the Antenna Laboratory. The measured Far-field results were compared with the simulated Ansoft HFSS computations; the measured results showed good agreement with the corresponding simulation results. This validates the accuracy of the simulation software.

References

[1]G.M. Peace and E.E.Swartz, "Amplitude Compensated Horn Antenna," Microwave Journal, 7, 66-68 February 1964.

[2]R.T.Nash, "Stepped-Amplitude Distributions," IEEE Trans. Antennas and Propagation, AP-12, July 1964.

[3]Samuel Silver "Microwave Antenna Theory and Design", Peter Peregrinus Ltd., London, UK, 1984.

[4]Constantine A. Balanis, "ANTENNA THEORY: Analysis and Design", John Wiley & Sons, Inc., New York, 1997.

[5]A.W. Love, "Electromagnetic Horn Antennas", IEEE Press, New York, 1976.

[6]T.S. Chu and R.A. Semplak, "Gain of Electromagnetic Horns", Bell System. Tech. J., Vol.44, pp. 527-537, Mar. 1965.

[7]E.H. Braun, "Some data for the design of Electromagnetic Horns", IEEE Trans. Antennas and Propagation, Vol. AP-4, pp.29-31, Jan.1956.

[8]E.V.Jull, "Finite-Range Gain of Sectoral and Pyramidal Horns", Electronics Letters, Oct.1970.

[9]John D. Kraus "ANTENNAS", second edition, McGraw-Hill, Inc,1997.

[10]K.L.Walton and V.C. Sundberg, "Broadband Ridged Horn Design", Microwave Journal, 7, 96-101 March 1964.

[11]R.E. Lawrie and L. Peters, Jr, "Modifications of Horn Antennas for Low Sidelobe Levels", IEEE Trans Antennas and Propagation, Vol. AP-14, pp.605-610, Sept.1966.

[12]A.W. Love, "The Diagonal Horn Antenna", "Microwave Journal, 5, 117-122 March.1962.

[13]Page653, Constantine A. Balanis, “ANTENNA THEORY: Analysis and Design”, John Wiley & Sons, Inc., New York, 1997.

[14]Warren L.Stutzmann, “Polarization in Electromagnetic Systems”, Artech House Publishers, 1992.

[15]Harold Mott. “Polarization in Antennas and Radar”, John Wiley & Sons, Inc., New York, 1986.

[16]Milton Abramowitz, “Handbook of Mathematical Functions with Formulas, Graphs and Mathematical Tables “(National Bureau of Standards Applied Mat).

[17]Page583, Constantine A. Balanis, “ANTENNA THEORY: Analysis and Design”, John Wiley & Sons, Inc., New York, 1997.

[18]Page363, Constantine A. Balanis, “ANTENNA THEORY: Analysis and Design”, John Wiley & Sons, Inc., New York, 1997.

APPENDIX A

Secondary Pattern Characteristics produced by Various Types of Aperture Distributions [3]

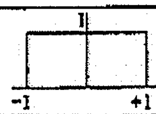	$f(x) = 1 \quad \lvert x\rvert > 1$; $= 0 \quad \lvert x\rvert > 1$			$g(u) = \frac{\sin u}{u}$
	Gain factor $\mathcal{G}_n$	Full width at half power Θ, radians	Angular position θ of first zero	Intensity of first side lobe; db below peak intensity
	1	$0.88 \frac{\lambda}{a}$	$\frac{\lambda}{a}$	13.2
	$f(x) = 1 - (1 - \Delta)x^2, \lvert x\rvert < 1$; $g(u) = a\left[\frac{\sin u}{u} + (1 - \Delta)\frac{d^2}{du^2}\left(\frac{\sin u}{u}\right)\right]$; $\mathcal{G}(\Delta) = \frac{(2 + \Delta)^2}{9[1 - \frac{2}{3}(1 - \Delta) + \frac{1}{5}(1 - \Delta)^2]}$			
$\Delta = 1.0$	1	$0.88 \frac{\lambda}{a}$	$\frac{\lambda}{a}$	13.2
0.8	0.994	$0.92 \frac{\lambda}{a}$	$1.06 \frac{\lambda}{a}$	15.8
0.5	0.970	$0.97 \frac{\lambda}{a}$	$1.14 \frac{\lambda}{a}$	17.1
0.0	0.833	$1.15 \frac{\lambda}{a}$	$1.43 \frac{\lambda}{a}$	20.6
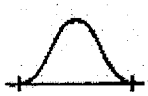	$f(x) = \cos^n \frac{\pi x}{2} \quad \lvert x\rvert < 1$; $g(u) = \frac{2a}{\pi} \frac{n! \cos u}{\prod_{k=0}^{\frac{n-1}{2}}\left[(2k + 1)^2 - \frac{4u^2}{\pi^2}\right]}$ n, odd; $g(u) = a \frac{n!}{\prod_{k=1}^{\frac{n}{2}}\left[(2k)^2 - \frac{4u^2}{\pi^2}\right]} \cdot \frac{\sin u}{u}$ n, even; $\mathcal{G}_n = \frac{4}{\pi^2}\left[\frac{2 \cdot 4 \cdot 6 \cdots (n-1)}{1 \cdot 3 \cdot 5 \cdots n}\right]^2 \left(\frac{2 \cdot 4 \cdot 6 \cdots 2n}{1 \cdot 3 \cdot 5 \cdots 2n-1}\right)$ n, odd; $\mathcal{G}_n = \left[\frac{1 \cdot 3 \cdot 5 \cdots (n-1)}{2 \cdot 4 \cdot 6 \cdots n}\right]\left[\frac{(n+2)(n+4) \cdots 2n}{(n+1)(n+3) \cdots 2n-1}\right]$ n, even			
$n = 0$	1	$0.88 \frac{\lambda}{a}$	$\frac{\lambda}{a}$	13.2
1	0.810	$1.2 \frac{\lambda}{a}$	$1.5 \frac{\lambda}{a}$	23
2	0.667	$1.45 \frac{\lambda}{a}$	$2 \frac{\lambda}{a}$	32
3	0.575	$1.66 \frac{\lambda}{a}$	$2.5 \frac{\lambda}{a}$	40
4	0.515	$1.93 \frac{\lambda}{a}$	$3 \frac{\lambda}{a}$	48

APPENDIX B

List of Notations

x', y', z'	Rectangular Coordinates
r, θ, ϕ	Spherical Coordinates
$\mathbf{a_1}, \mathbf{b_1}$	Dimensions of Rectangular Aperture
C(x)	Cosine Fresnel Integral
S(x)	Sine Fresnel Integral
$\mathbf{J_s}$, **Ms**	Current and Magnetic Source
A, F	Current and Magnetic Vector Potential
$\hat{n}$	Outward Normal to the Aperture
k	Wavenumber
$\boldsymbol{\lambda}$	Wavelength
$F(x', y')$	Field over the Aperture
$g(\theta, \phi)$	Secondary Pattern
g_{res}	Resultant Secondary Pattern
$\psi(x)$	Phase error term in x direction
A, B, $\alpha 1, \alpha 2$	Parameters of Two-step Staircase distribution
A, B, C, $\alpha 1, \alpha 2, \alpha 3$	Parameters of Three-step Staircase distribution